Rapid Modeling of Nonlinearities in Heat Transfer

Jillian Chodak Free

Dissertation submitted to the faculty of the Virginia Polytechnic Institute and State University in partial fulfillment of the requirements for the degree of

Doctor of Philosophy
In
Mechanical Engineering

Brian Y. Lattimer
Thomas E. Diller
Srinath Ekkad
Scott T. Huxtable
Anne E. Staples

December 15th, 2016
Blacksburg, VA

Keywords: heat transfer, nonlinearities, material properties, radiation, source heating, reduced order model, proper orthogonal decomposition

Rapid Modeling of Nonlinearities in Heat Transfer

Jillian Chodak Free

ABSTRACT

Heat transfer systems contain many sources of nonlinearity including temperature dependent material properties, radiation boundary conditions, and internal source terms. Despite progress in numerical simulations, producing accurate models that can predict these complex behaviors are still encumbered by lengthy processing times. Accurate models can be produced quickly by utilizing projection Reduced Order Modeling (ROM) techniques. For discretized systems, the Singular Value Decomposition technique is the preferred approach but has had limited success on treating nonlinearities. In this research, the treatment of nonlinear temperature dependent material properties was incorporated into a ROM. Additional sources of nonlinearities such as radiation boundary conditions, temperature dependent source heating terms, and complex geometry were also integrated. From the results, low conductivity, highly nonlinear material properties were predicted by the ROM within 1% of full order models, and additional nonlinearities were predicted within 8%. A study was then done to identify initial snapshots for use in developing a ROM that can accurately predict results across a wide range of inputs. From this, a step function was identified as being the most accurate and computationally efficient. The ROM was further investigated by a discretization study to assess computational gains in both 1D and 3D models as a function of mesh density. The lower mesh densities in the 1D and 3D ROMs resulted in moderate computational times (up to 40 times faster). However, highly discretized systems such as 5000 nodes in 1D and 125000 nodes in 3D resulted in computational gains on the order of 2000 to 3000 times faster than the full order model.

Rapid Modeling of Nonlinearities in Heat Transfer

Jillian Chodak Free

General Audience Abstract

Heat transfer systems contain many sources of nonlinearity including temperature dependent material properties, radiation boundary conditions, and internal source terms. Despite progress in numerical simulations, producing accurate models that can predict these complex behaviors are still limited by the time it takes to compute meaningful results. Accurate models can be produced quickly by utilizing some mathematical techniques whereby the original problem is projected into a smaller sub-space and solved with fewer variables. The full space results are then determined by undoing the projection on the results. This is one approach from a larger knowledge base called Reduced Order Modeling (ROM) techniques. For discretized systems, the Singular Value Decomposition technique is the preferred approach but has had limited success on treating nonlinearities. In this research, the treatment of nonlinear temperature dependent material properties was incorporated using the projection approach, tailored to treat the specific material property nonlinearity as well as radiation boundary conditions, temperature dependent source heating terms, and complex geometry. While the approach presented here is specific to the heat transfer application, other problems of a similar form can be handled in the same manner. From the results, low conductivity, highly nonlinear material properties were predicted by the ROM within 1% of full order models, and additional nonlinearities were predicted within 8%. A study was then done to identify initial snapshots for use in developing a ROM that can accurately predict results across a wide range of inputs. From this, a step function was identified as being the most accurate and computationally efficient. The ROM was further investigated by a discretization study to assess computational gains in both 1D and 3D models as a function of mesh density. The lower mesh densities in the 1D and 3D ROMs resulted in moderate computational times (up to 40 times faster). However, highly discretized systems such as 5000 nodes in 1D and 125000 nodes in 3D resulted in computational gains on the order of 2000 to 3000 times faster than the full order model.

Dedication

This work is dedicated to my family, immediate and extended. Their continuous support during my graduate experience helped see me through to the finish.

Jackson and Weston

I hope you are inspired by your parents to pursue your dreams, whatever those may be.

Josh

Thank you for always lifting me up during this process. Love you.

Acknowledgements

I would like to acknowledge my advisor Dr. Brian Lattimer for his continued support during my Masters and PhD work. The struggles have been worth the reward. I am grateful to have been on this journey with you.

Thank you to Dr. Alan Lattimer for several discussions on POD. Your insight provided clarity and you were a great resource, especially in the early stages of this work.

Thank you to my committee members Dr. Ekkad, Dr. Diller, Dr. Huxtable, and Dr. Staples for their continued encouragement.

I would not have been able to continue down this path without my network of friends, family and neighbors to cheer me on, listen to my gripes, and lend a helping hand when needed.

I would like to especially acknowledge my mom for always sending positive, inspiring, and humorous text messages to me in the middle of the night. Sometimes, they were just the words I needed to hear.

Last, my husband Josh has continued to be my biggest champion, even sometimes beyond what I can imagine. Thank you for your support and love, and for always setting the bar high.

Table of Contents

ABSTRACT ii
General Audience Abstract iii
Dedication iv
Acknowledgements v
Table of Contents vi
List of Figures ix
List of Tables xii
Nomenclature xiii
1 Introduction 1
1.1 Motivation 1
1.2 ROM Background 2
1.3 Previous Related Work 3
1.3.1 POD-FEM 6
1.3.2 POD and Meshless Techniques 8
1.3.3 Nonlinearity Treatments and Identification 8
1.3.4 POD-DEIM Combination 10
1.3.5 Multi-Physics Models 11
1.4 Research Objectives 12
1.5 Paper Organization 12
2 Reduced Order Model Development 14
2.1 One-Dimensional Heat Transfer Model 14
2.1.1 Governing Equations 14
2.1.2 Finite Difference Model 15
2.2 Basic ROM Development 16
2.3 Temperature Dependent Properties Effects 19
2.3.1 Finite Difference Model 19
2.3.2 Average Nodal Temperature ROM for Nonlinear Materials 20
2.3.3 Unique Nodal Temperature ROM for Nonlinear Materials 20
2.4 Boundary Condition Effects 22
2.4.1 Governing Equations 22

2.4.2 Finite Difference Model – Snapshot Generation 22
2.4.3 Radiation Boundary Condition ROM 23
2.5 Source Term Effects 23
2.5.1 Governing Equations 23
2.5.2 Finite Difference Model – Snapshot Generation 23
2.5.3 Nonlinear Source Term ROM 24
2.5.4 DEIM Algorithm 24
2.6 Three-Dimensional Transient Heat Transfer 26
2.6.1 Governing Equations 26
2.6.2 Commercial Code – Snapshot Generation 26
2.6.3 3D ROM Development 27
3 Nonlinear Material Property Results 29
3.1 Nonlinear Material Property Introduction 29
3.2 Full Order Model Verification 29
3.3 ROM Rank selection 31
3.4 Average Nodal and Unique Nodal ROMs 33
3.4.1 AA 5083-H116 33
3.4.2 Unifrax Ceramic Board 38
3.5 Increased Spatial Discretization 42
3.6 Estimated Heat Flux Results 45
3.7 Summary 46
4 Nonlinear Boundary Conditions Results 48
4.1 Full Order Model Verification 48
4.2 POD Rank selection 51
4.3 ROM with Radiation 53
4.3.1 AA 5083 Results 53
4.3.2 Unifrax Ceramic Board Results 55
4.4 Modal Energy Analysis 57
4.4.1 AA 5083 Modal Energy Analysis 58
4.4.2 Unifrax Modal Energy Analysis 59
4.5 Summary 61
5 Nonlinear Source Heating Results 63

5.1 Nonlinear Source Heating Introduction 63
5.2 Full Order Model Verification 63
5.3 Simulation Case and Full Order Model Solutions 64
5.4 ROM Rank Selection 66
5.4 DEIM Algorithm 66
5.5 Nonlinear Source ROM 67
5.5.1 AA 5083 Results 68
5.5.2 Unifrax Ceramic Board Results 69
5.6 Summary 70
6 Complex Geometry Results 71
6.1 Complex Geometry Introduction 71
6.2 Full Order Model Verification 71
6.3 ROM Rank Selection 73
6.4 3D Transient ROM 76
6.4.1 AA 5083 Results 76
6.4.2 Stainless Steel 302 77
6.4.3 Unifrax Results 79
6.4.3 Increased Spatial Discretization 80
6.5 Summary 81
7 Conclusions 82
7.1 Conclusions 82
7.2 Future Work 83
References 85
Appendix A 94
Appendix B 97

List of Figures

Figure 1. Heat transfer model for 1D heat transfer with multiple sources of nonlinearities 1
Figure 2. Homogeneous 1D slab with boundary conditions (Lefebre [34]) 5
Figure 3. Discrete Empirical Interpolation Method (DEIM) algorithm for nonlinear model reduction (Chaturantabut [108]) 25
Figure 4. Example material property functions as determined for AA6082-T651 – thermal conductivities and specific heats were given (left), and thermal diffusivity and the inverse volumetric heat capacity were determined (right) 31
Figure 5. Example output of eigenvalues from Singular Value Decomposition as a function of rank number 31
Figure 6. Example output of energy content from Singular Value Decomposition as a function of rank number 32
Figure 7. Example plot of relative error as a function of rank 32
Figure 8. Plots of AA 5083-H113 using the Average ROM (a) Ratio of FOM vs. ROM solution times and (b) Relative Error using the average nodal ROM model 34
Figure 9. Average Nodal Temperature ROM results for the discretization study on AA 5083-H116 (a) solution time ratio, (b) POD generation time, and (c) Relative Error plotted as a function of increasing discretization using 35
Figure 10. Plots of AA 5083-H113 from Unique Nodal Temperature ROM (a) ratio of snapshot solution times vs. ROM solution times and (b) Relative Error using the Unique Nodal ROM model 36
Figure 11. Full solution snapshots for AA 5083-H116 36
Figure 12. Plots of re-expanded ROM solutions (a) Average and (b) Unique Nodal, errors for ROM solution surfaces (c) Average and (d) Unique Nodal, unexposed surface ROM (red) vs snapshot (blue) solutions for (e) Average and (f) Unique Nodal, and unexposed surface ROM solutions errors for (g) Average and (h) Unique Nodal. 38
Figure 13. Full solution snapshots for Unifrax 39
Figure 14. Plots of Unifrax rank results from the Average Nodal Temperature ROM (a) ratio of snapshot solution times vs. ROM solution times and (b) Relative Error using the Unique Nodal ROM model 40
Figure 15. Output of energy content from Singular Value Decomposition as a function of rank number for Unifrax. 40
Figure 16. Plots of re-expanded ROM solutions for Unifrax material (a) Average and (b) Unique Nodal, errors for ROM solution surfaces (c) Average and (d) Unique Nodal, unexposed surface ROM (red) vs snapshot (blue) solutions for (e) Average and (f) Unique Nodal. 41
Figure 17. Plots of re-expanded ROM solutions for Unifrax material unexposed surface ROM solutions errors for (a) Average and (b) Unique Nodal. 42
Figure 18. Plots of advanced discretization results for AA 5083 material using Unique Nodal Temperature ROMs (a) ratio of snapshot solution times vs. ROM solution times, (b) POD generation times, (c) Relative Error, (d) surface errors for 50 nodes, and (e) surface errors for 5000 nodes. 43
Figure 19. Plots of advanced discretization results for Unifrax material using Unique Nodal Temperature ROMs (a) ratio of snapshot solution times vs. ROM solution times, (b) POD

generation times and (c) Relative Error, (d) surface errors for 50 nodes, and (e) surface errors for 5000 nodes. 44
Figure 20. Relative errors for each ROM shown for estimated heat flux values. 46
Figure 21. Computational re-use times for ROMs developed from various input conditions used to estimate unknown Heat Flux Boundary Conditions. 46
Figure 22. Abaqus 3D model used for verification on 1D finite difference model. 49
Figure 23. Results from full order finite difference model (symbols) and Abaqus model (lines) using radiation boundary conditions. 49
Figure 24. Full order model solutions for AA 5083 with convection boundary conditions only (left) and with convection and radiation boundary conditions (right). 50
Figure 25. Full order model solutions for Unifrax with convection boundary conditions only (left) and with convection and radiation boundary conditions (right). 51
Figure 26. Eigenvalues for AA 5083 POD with convection only (diamond) and with convection and radiation boundary conditions (circle) 52
Figure 27. Eigenvalues for Unifrax POD with convection only (diamond) and with convection and radiation boundary conditions (circle) 53
Figure 28. Solution error as a function of rank for AA 5083 material with radiation at boundaries *(left) and r*atio of solution times *(right)*. 54
Figure 29. ROM with AA 5083 material properties and radiation boundary conditions (a) absolute error, (b) maximum relative error at x = 0, (c) maximum relative error at x = L/2, and (d) maximum relative error at x = L. 55
Figure 30. Solution error as a function of rank for Unifrax material with radiation at boundaries (left) and ratio of solution times (right). 56
Figure 31. ROM with Unifrax material properties and radiation boundary conditions (a) absolute error, (b) maximum relative error at x = 0, (c) maximum relative error at x = L/2, and (d) maximum relative error at x = L. 57
Figure 32. First 5 contributing energy modes for AA 5083 with convection only (a) – (e) and with radiation applied (f) – (j). 59
Figure 33 – First 5 contributing energy modes for Unifrax with convection only (a) – (e) and with radiation applied (f) – (j). 61
Figure 34. Steady state results for temperature-dependent source term Full Order Model (blue) against known solution (orange). 64
Figure 35. Full order model solutions for AA 5083 without source heating term (left) and with nonlinear source heating term (right). 65
Figure 36. Full order model solutions for Unifrax without source heating term (left) and with nonlinear source heating term (right). 65
Figure 37. Eigenvalues for AA 5083 POD (left) and Unifrax POD (right) without source heating (diamond) and with nonlinear source heating (circle). 66
Figure 38. Eigenvalues for AA 5083 nonlinear source POD-DEIM term (left) and for Unifrax nonlinear source POD-DEIM term (right). 67
Figure 39. Solution error as a function of rank (left) and ratio of solution times for the ROM (right) for AA 5083 material with nonlinear source heating 68

Figure 40. Absolute error (left) and maximum relative error at boundary each node (right) from ROM using AA 5083 and nonlinear source heating 69
Figure 41 - Solution error as a function of rank (left) and ratio of solution times for the ROM (right) for Unifrax material with nonlinear source heating 69
Figure 42 - Absolute error (left) and maximum relative error at boundary each node (right) from ROM using Unifrax and nonlinear source heating 70
Figure 43. Abaqus 3D model and results used for model validation and snapshot generation in the 3D ROM. 72
Figure 44. Full order model MATLAB solution (left) and errors across the sample domain (right) arranged by node number. 72
Figure 45. Steady state Abaqus 3D model solutions for Stainless Steel 302 (left) and Unifrax (right) used for snapshot generation in the 3D ROM. 73
Figure 46. Eigenvalues for AA 5083 POD with convection only 1D model (diamond) and 3D model (circle). 74
Figure 47. Eigenvalues for Stainless Steel 302 POD with convection only 1D model (diamond) and 3D model (circle) 75
Figure 48. Eigenvalues for Unifrax POD with convection only 1D model (diamond) and 3D model (circle) 76
Figure 49. Solution error as a function of rank for AA 5083 material (left) and ratio of solution times for the ROM using AA 5083 material properties (right) 77
Figure 50. Absolute error (left) and maximum relative error at boundary each node (right) from 3D ROM using AA 5083 material properties. 77
Figure 51. Solution error as a function of rank for Stainless Steel 302 material (left) and ratio of solution times for the ROM using Stainless Steel 302 material properties (right). 78
Figure 52. Absolute error (left) and maximum relative error at boundary each node (right) from 3D ROM using Stainless Steel 302 material properties 78
Figure 53. Solution error as a function of rank for Unifrax material (left) and ratio of solution times for the ROM using Unifrax material properties (right). 79
Figure 54. Absolute error (left) and maximum relative error at boundary each node (right) from 3D ROM using Unifrax material properties. 80
Figure 55. Plots of advanced discretization results for AA 5083 material using the 3D transient ROM (a) ratio of snapshot solution times vs. ROM solution times and (b) Relative Error 81

List of Tables

Table 1. Materials and properties for use in model 30
Table 2. Comparison between the two ROMs for AA 5083-H116 36
Table 3. Comparison between the two ROMs for Unifrax 40
Table 4. Table of Initial Heat Flux values used to create a ROM and the associated heat flux values that are investigated by the ROM 45

Nomenclature

SYMBOL	DESCRIPTION	UNITS
c_p	specific heat	J/kg-K
E	emissivity	-
h	convective heat transfer coefficient	W/m^2-K
k	thermal conductivity	W/m-K
L	thickness of domain	m
Q''	surface heat flux	W/m^2
S	source heating term	J/kg
t	time	s
T	temperature	°C or K
^{T}	matrix transpose	-
u(t)	applied heat flux	W/m^2
x	through thickness direction	m
y	through thickness direction	m
z	through thickness direction	m

Greek

α	thermal diffusivity	m^2/s
Δ	change in parameter	-
ρ	density	kg/m^3
Σ	diagonal matrix of singular values	-
φ	projection matrix	-

Subscripts

BC	boundary conditions
conv	convection
diff	diffusion
i	nodal index/spatial
j	nodal index/spatial
k	nodal index/spatial
Inf or ∞	ambient
r	reduced
rad	radiation
p	nodal index/temporal
source	source heating

1 Introduction

1.1 Motivation

Materials are known to respond in a variety of ways under thermal load. Whether its thermal expansion, degradation in yield strength properties, off gassing, or initiating combustion, all of these are complex and dynamic design concerns that affect safety. In practice, not every scenario can be tested. Models are increasingly being used to predict behavior and understand thermal response of materials as they represent a cost effective alternative to experimental testing. Model accuracy depends on including realistic physical attributes which are typically nonlinear such as material properties, radiation boundary conditions, generalized source terms, and complex physical geometry. A 1D representation of a heating scenario with nonlinearities is shown in Figure 1.

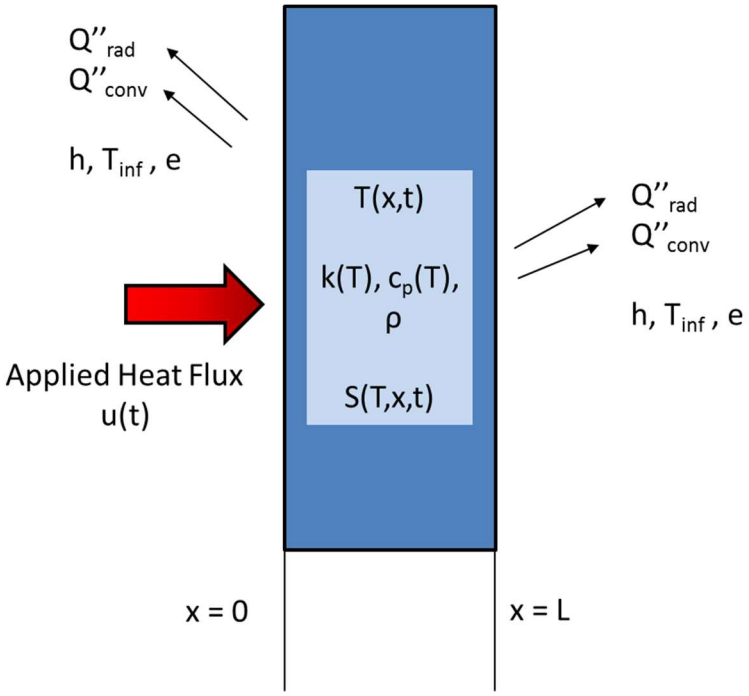

Figure 1. Heat transfer model for 1D heat transfer with multiple sources of nonlinearities

Exact solutions not likely to exist and are difficult to resolve using numerical simulation techniques such as Finite Difference or Finite Element. For simple cases, hand analytical solutions can be estimated by using average quantities. However, there is a loss of accuracy over large temperature ranges. For more complex systems, numerical techniques are used to approximate solutions. Traditionally, discretized models are created to tackle complex physical phenomenon such as transient heat transfer. Despite progress in computational science, in order to simulate the full extent of physical behavior in these systems, result fidelity depends on increasing discretization and therefore increases computational time, particularly in the case of

three-dimensional problems. A fast method to model 3D heat transfer with multiple nonlinearities is highly desirable.

One approach is to consider an effective projection-based computational method that builds a low-dimensional model accommodating a variety of physical attributes. The projection method can be used to study physical phenomenon by constructing a suitable algebraic model and projecting a solution using a known selected basis. An optimized Reduced Order Model (ROM) can quickly and accurately assess various heating scenarios including nonlinear effects.

1.2 ROM Background

Developed from well-established mathematical theories and robust numerical algorithms, ROMs are recognized as very efficient approaches for reducing the simulation time of large-scale systems (Antoulas [1]). Through model order reduction, a small system with a reduced number of equations is derived. The reduced model is simulated instead of the full scale approach, and the solution of the original equation can then be recovered from the solution of the reduced model with a high degree of accuracy. As a result, the simulation time of the original large-scale system can be shortened by several orders of magnitude. In addition, the developed reduced model can replace the original system and be reused to investigate multiple inputs, which can further save time.

A variety of methods have been developed to reduce the order of large-scale dynamical systems. Basic approximation methods are generally divided into Krylov methods and Singular Value Decomposition (SVD) methods. The Krylov method concept is based on using the Krylov subspace which is defined as a linear subspace spanned by the images of b, an n-vector, under the first r powers of 'A' a real n x n matrix.

$$\mathrm{K_r}(\mathrm{A}, \mathrm{b}) = \mathrm{span}(\mathrm{b}, \mathrm{Ab}, \mathrm{A^2b}, \dots, \mathrm{A^{r-1}b}) \qquad \text{Equation 1}$$

An iterative algorithm is applied to determine the Krylov subspaces. A sequence of vectors is constructed that converges to the eigenvector corresponding to the largest eigenvalue. Several approaches have been developed to keep and use the information provided by the sequence of vectors. Various Krylov type methods have been developed including Realization, Interpolation, Lanszos and Arnoldi. (Antoulas [1]) However, several issues exist with this method. The 'A' matrix of interest has to be square. The convergence rate for the Krylov algorithm can be slow. Krylov methods are limited to linear systems, Ax = b, for cases where 'A' is large and sparse. In addition, when a matrix is singular, Krylov methods can fail as the solution may not lie in a Krylov space at all. (Ipsen and Meyer [2]).

SVD methods are based on using the singular value decomposition which is a method of factorization of an m x n matrix, 'M,' which can be real or complex. The SVD is a factorization method that decomposes the 'M' matrix into 3 separate matrices that each contain different information.

$$\mathrm{M} = \mathrm{U\Sigma V^T} \qquad \text{Equation 2}$$

The ‘U’ matrix is an m x m unitary matrix of the orthonormal eigenvectors of MM^T (left-singular vectors). The ‘V’ matrix is an n x n unitary matrix of the orthonormal eigenvectors of M^TM (right-singular vectors). ‘Σ’ is a diagonal matrix of the square roots of the eigenvalues determined from both matrices, in descending order. These values are nonnegative real numbers and are also known as the singular values. Applications that employ the SVD include computing the pseudoinverse, least squares fitting of data, multivariable control, matrix approximation, and determining the rank, range and null space of a matrix. (Antoulas [1]) SVD ROM Methods include Balanced Model Reduction, Approximate Balanced Reduction, Singular Perturbation, Hankel Norm Approximation, Moment matching, and Balanced Truncation.

One type of SVD based method is called Proper Orthogonal Decomposition, which is an application of the SVD to approximate general dynamical systems. POD combines the SVD along with a Galerkin projection to generate a reduced model. The POD approach is used to satisfy a balanced representation. For order reduction on models with parametric dependence, Proper Orthogonal Decomposition (POD) is the preferred method of analysis. (Antoulas [1]) Using the SVD allows POD to handle any size M matrix, real or complex. In addition, POD is suited to tackle linear and nonlinear systems. Solutions obtained from this approach can be used to perform the analysis of the model in explicit form. Inverse problems and control problems are also more easily analyzed within low-dimensional models. This research explores the use of POD to reduce the computation time for large, nonlinear heat transfer problems.

1.3 Previous Related Work

Progress in computer engineering has allowed for the development of models capable of capturing complex behavior, however solution times for these complex models continues to be a limiting factor. This has driven an increasing interest in techniques for reducing model order to achieve fast and accurate simulations. Several MOR techniques are being investigated, along with utilizing the properties of Proper Orthogonal Decomposition in a variety of ways.

The use of POD is not new, but it is finding new uses when combined with advances in computational processing. The POD was developed by several people (among the first was Kosambi [3]), and goes by several names such as Principal Component Analysis, the Karhunen–Loéve Decomposition, and the single value decomposition. Since then, it has been used as a tool for processing statistical data [4–6], pattern recognition, e.g., characterization of human faces [7], and control theory [8]. Another important area of application of POD technique is in turbulence, where this method has been used to detect large-scale organized spatial motions [9]. In acoustical and random signal decomposition, POD has been applied to extract information about the modes and energy of the signals under consideration [10]. This feature is very useful in applications that involve compression and storage of stochastic signals [11]. The analysis of the activity of the visual cortex in a turtle brain [12] is an example of application of POD in bioengineering. POD has also been successfully applied to inverse problems [13] exhibiting strong regularization properties. As an a posteriori, data dependent method it does not need a priori knowledge of the system behavior and can also be used to analyze patterns in data. The main advantage of POD lies in the fact that it requires only standard matrix computations, despite its application to

nonlinear problems. Although projecting only onto linear or affine subspaces the overall nonlinear dynamics is preserved, since the surrogate model is still nonlinear.

Research has been done to compare a variety of ROM techniques for various physical phenomena. Work by Gugercin and Antoulas [14] compared seven model reduction algorithms by applying them to four different dynamical systems. Four SVD based methods and three moment matching based methods were used to investigate a structural model, a heat transfer model using a plate with 2 heating sources and measured at 2 points, a clamped beam model, and a low pass butterworth filter model. The results illustrate that overall, balanced reduction and approximate balanced reduction are the best when considered along the whole frequency range. Moment matching methods always lead to higher error norms than SVD based methods due to their local nature; but they are numerically more efficient. The authors found that the rational Krylov algorithm gave the best results due to the flexibility of the selection of interpolation points. However, the selection of the points which determines the reduced model is not an automated process and has to be specified by the user unlike the other methods which can be defined by a given tolerance value.

Blinov et al [15] studied POD vs MPS (Method of Polyargumental Systems) for thermal conductivity problems with strongly localized heat source. These problems utilized constant material properties and were in annular systems. The authors note it is possible to construct a dynamic model of the process from by approximation of the results of direct numerical simulation of a studied process with POD method at any single set of control parameters, by means of obtained empiric basis and on the base of Galerkin method [16 - 20]. In this case, the authors are replicating previously known results by use of a ROM.

Research by Hekmati, Ricot, and Druault [21] used a technique called Extended POD (EPOD) in order to analyze the correlated events between two domains, in this case automotive ventilation outlet and the associated sound pressure field. The aim of this particular research was to further understand noise production mechanisms. The EPOD procedure was used to establish a correlation between the flow contributions and the far-field acoustic pressure. The authors were able to represent 2D coherent energetic structures within the flow.

Yu and Chakravorty [22] developed a randomized version of snapshot POD referred to as RPOD. There has been great interest in the Systems and Control community over the past several years in tractable randomized techniques to solve computationally difficult systems and control design problems [23-28]. The snapshot proper orthogonal decomposition (POD) technique, followed by a Galerkin projection has been used extensively in the Fluids community to produce reduced order models (ROMs) of fluid physics phenomenon such as turbulence and fluid structure interaction [29-31]. Previously, the authors had introduced an iterative POD method (I-POD) in [32], [33] that obtained eigenfunctions of a linear operator using the individual input/output trajectories of the system. Their work showed that randomization of the procedure to choose a small subset of the input/output ensemble is sufficient to extract all the relevant modes while increasing the accuracy and number of the extracted modes. A Hankel matrix was constructed and decomposed using SVD where left and right projection matrices were created. The RPOD algorithm was then used to create a reduced sized Hankel matrix.

The authors identified that in some cases, it may be impossible to solve the SVD problem resulting from balanced POD also called BPOD. They give the example of a 17640× 80000 SVD problem for BPOD, which is not solvable in MATLAB. RPOD leads to a 8000×5000 SVD problem, which is a relatively small problem. Thus, in problems where there are a large numbers of actuators/sensors, the savings can be very significant. This implies that experimenters can reduce the scale of the instrumentation required to get the data required to form a ROM by orders of magnitude without losing significant information that can be extracted from the resulting data, which can result in significant cost savings.

Lefebvre [34] used POD to investigate 1D heat transfer through a homogeneous slab. The approach developed in this work was an expansion of the purely dynamic part of the temperature field, $\alpha \frac{\partial^2 T}{\partial x^2}$, as an infinite set of eigenfunctions where the solution was the Helmholtz equation. The solution splits into two terms, and is now referred to as a split modal model. A space sampling and reduction of eigen basis creates the model. In this work, a finite set of eigenfunctions were selected for truncation. In this case, there were no internal heat sources, constant material properties were used, and general boundary conditions were applied.

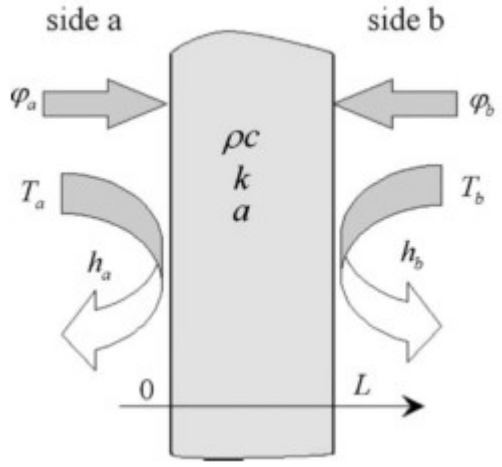

Figure 2. Homogeneous 1D slab with boundary conditions (Lefebre [34])

Baur et al [35] presented a comparison of several approaches for parametric model order reduction. In this work, the authors discussed multiple methods, error determination, and computational times offline and online while walking through benchmark problems from literature. As an enhancement to global POD, the POD-Greedy method is detailed. This is an approach for use in large SVD problems. The size of the SVD problem of the global POD can be prohibitive, which is circumvented by a greedy procedure that incrementally constructs a basis V by several small POD computations. This POD-Greedy algorithm [36, 37] meanwhile is standard in Reduced Basis Methods [38, 39, 40] and has provable quasi-optimal convergence rates [41]. Adaptive techniques of selecting parameters or snapshots for reducing the complexity of the reduced basis generation have been proposed for example in [42]. Overall, the POD-

Greedy algorithm is expected to be more computationally expensive than a global POD, as it requires many iterations of solving small PODs.

In addition, the authors discuss Interpolatory Methods such as moment-matching, the iterative rational Krylov algorithm (IRKA) [43] and balanced truncation (BT). These (deterministic) MOR methods are used to reduce the order of the system at a certain number of fixed parameter values p1, . . . , pK, i.e., model order reduction is applied K-times on the systems with transfer functions. Matrix Interpolation uses a weighted matrix reduction. Transfer Function Interpolation is based on Lagrange basis polynomials. This method does not allow a reconstruction of the state in the required form $x \approx V \hat{x}$, and also does not provide a reduced-order model in parameterized state-space form for more than one parameter. Piecewise H2 tangential interpolation is a method which uses IRKA. The generalization of moment matching MOR called multi- (parameter) moment matching or multivariate Pade' approximation was first considered in [44, 45]. This method is based on a multivariate Taylor expansion with expansion points in frequency and parameter space. Empirical cross Gramian used a snapshot-based method to compute the cross Gramian, which is only applicable to square systems. The authors noted that in general, POD seems to give the best results for state-space approximations. However, it may not be feasible if the number of training parameters or the dimension of the state is too large. According to the authors, the POD-Greedy should then be the preferred approach.

Wang et al [46] compared POD interpolation and POD projection methods in heat transfer problems. The POD interpolation method calculates amplitudes by interpolation of scattered data while the POD projection method calculates amplitudes by projecting continuous governing equations onto the low- dimensional space spanned by eigenfunctions. Both of the two methods have their own advantages and disadvantages. The POD projection method is suitable for either steady or unsteady problems, linear or nonlinear. However, a continuous function is necessary. The POD interpolation method is accurate even for strongly nonlinear problems [47] though it is commonly used for steady state problems. Results from this research indicate that the POD projection method performs better as it is more robust.

1.3.1 POD-FEM

Research on POD has expanded in the direction of coupling it more directly with Finite Difference/ Finite Element Methods. Fic, Bialecki, and Kassab [48] then furthered the ROM research by developing a POD-FEM technique that could be applied to linear and nonlinear problems. Linear problems were solved analytically or via time stepping, while nonlinear problems were solved via time stepping only. This article proposes a technique for accelerating the POD-FEM assembly process designed for the case when the entire stiffness matrix needs to be recomputed at every time step. The crucial point of the procedure is the evaluation of the POD set. A few snapshots were generated, the covariance matrix was determined, and the Galerkin method was applied to reduce the equations using POD basis vectors. This research explored a heat transfer problem with variable thermal conductivity, 20 to 40 W/m K, determined by averaging. The work was an extension of previous work [49, 50] in which the

POD-FEM combination has been used for solving transient linear heat conduction problems using modal analysis.

This article describes a variant of the POD known as the snapshot method, which was developed by Sirovich [51]. An alternative approach is to use the singular value decomposition technique to construct the POD basis. Liang, et al [52] showed the equivalence of three different POD variants: principal component analysis, Karhunen-Loeve decomposition, and singular value decomposition. The technique is also known under several other names, such as Hotteling transformation, quasiharmonic modes, empirical orthogonal functions, etc. POD as used in this research has been reinvented several times and used in many fields of science and technology, and has thusly been called by a few different names. The idea of using POD in the context of time-dependent numerical solution (primarily the finite-element method, FEM) is not new. It has been exploited in the literature in structural dynamics [53] and in aeroelastic [54] and fluid dynamics [55]. Standard time-stepping procedure has been used in all these articles.

Research by Guha and Nabi [56] focused on FEM discretization. The authors proposed a nonlinear control law which transfers arbitrary initial temperature profile to another desired one, using POD. This work takes into account complex geometry. The authors previously developed a control law for a nonlinear heat conduction problem on nontrivial domains using FEM [57] where k(T) is created and solved at each time step. In order to analyze the system, the size of the model must be reduced. So, model reduction is necessary [58, 59]. The authors state that the POD method is mostly used to reduce of size of nonlinear systems [60, 62]. Here, the authors neglected any convective and radiative heat transfer for the sake of simplicity. In addition, the input f = 0 is chosen as there is no body heating. Carbon steel material properties were used and its thermal conductivity is nonlinearly dependent on temperature, taken as proportional to T^4. At each time-step, matrix K (which is $\alpha \frac{\partial^2 T}{\partial x^2}$) is dependent on temperature, and the resulting nonlinear algebraic equation system is solved using the Newton-Raphson method.

Ding [63] applied the POD method to establish the reduced order model for the on-line control of glass thickness and heat transfer inverse problems. He introduced two branches of POD, i.e., projection and interpolation methods. POD projection method was applied to solve a one-dimensional unsteady non-linear heat conduction problem. Then, he extended the POD interpolation and projection methods to two real application problems, i.e., quality control of glass production and inverse problem of heat convection in pipe. The POD projection method is suitable for either steady or unsteady problems, no matter which are linear or nonlinear. However, this method is not adopted for the problems which cannot be described in the form of continuous functions. Nevertheless, the POD interpolation method is accurate even for strong nonlinear situation [47] though it is commonly suitable for steady problems.

Ostrowski, Białecki, and Kassab [64] developed an approach to solve inverse problems of steady state and transient heat conduction. From a previously developed model that uses radial basis functions as the interpolation functions [65], the authors developed a stable solution using a trained POD-RBF network. However, because the snapshots describe a behavior of a specific physical object, in practice the approximation holds also for arbitrary snapshots output by this

object. This approach was used to determine unknown material parameters. In this work, there was no restriction on the number of parameters and could therefore be used to predict a series of material values with time. While there is no formal proof that the model converges to the full heat transfer model, the quality of the approximation can be checked a-posteriori.

1.3.2 POD and Meshless Techniques

POD is also being coupled with techniques that do not rely on generating a mesh for use in FEM. Research by Zhang and Xiang [66] focused on a fast, meshless method using POD with Galerkin for transient heat conduction problems. Notably, mesh generation is time consuming for complex shapes. Therefore, there is a strong interest in meshless methods. Approximations are based on nodes and there is no predefined nodal connectivity, therefore removal and addition of nodes is easily done. For more details of these meshless methods, refer to [67–69]. In general for meshless methods, nodes are defined and at each node, a weight function and shape function is defined on a small domain. Several meshless methods have been proposed in literatures, such as smoothed particle hydrodynamics (SPH) [70], element free Galerkin (EFG) method [71,72], meshless local Petrov Galerkin (MLPG) method [73], reproducing kernel particle method (RKPM) [74], radial point interpolation method (RPIM) [75] and so on. Chen and Liew [76] developed a meshless local Petrov–Galerkin approach to solve transient heat conduction problems in 2-D and 3-D spaces. Khosravifard et al. [75] presented an improved meshless RPIM for nonlinear transient heat conduction problems and implemented the method to analyze the functionally graded materials with non-homogenous and temperature-dependent heat sources. In this work data was collected, and the SVD was used to find a POD basis. The POD was then used with a meshless method to generate a reduced model. The results proved to be accurate and fast. Although meshless methods have a lot of advantages over FEM, they also have some disadvantages. For example, the implementation of essential boundary condition is complicated and the computational time is more than that of FEM. Especially it has high computational cost for transient problems as compared to FEM, which limits its application seriously. Consequently, the authors noted that any contribution to reduce the computational cost of meshless method can be regarded as an important progress [75].

1.3.3 Nonlinearity Treatments and Identification

POD has been effectively used to capture known nonlinear behaviors, but there is growing interest in identifying nonlinearities unknown a priori as well as being able to estimate results with the ROM using new system inputs. The previously developed POD/Galerkin approach is explained in detail by Chatterjee [60]. This work explains the data analysis aspects of utilizing POD including mode shape investigations, projections, zero center point cloud, and modal analysis particularly for use in identifying nonlinearities. The POD has been used to obtain approximate, low-dimensional descriptions of many nonlinear phenomenon such as turbulent fluid flows [78], structural vibrations [79, 80], and insect gait [81], and has been used for damage detection [82], to name a few applications in dynamic systems.

Pinnau [83] used POD-Galerkin projection to treat radiative heat transfer given by the Rosseland model [84]. This problem contains two nonlinearities: one in the heat conductivity which models volume radiation and one in the boundary condition which adds additional surface radiation to the standard Newton cooling law. In this work, material properties were treated as constant, boundary conditions were separated out, and 4^{th} order power terms were calculated directly. The result was a 1^{st} order ODE. The inner products for global basis functions have to be computed, which is time consuming, and in this case the subspace was chosen by energy content. The ROM was solved with implicit Euler method, and results for this case were within 1%.

Walters [85] used POD to show how spectral content of a decomposed snapshot matrix can indicate the presence of nonlinear behavior in a structure. Also in this work, the authors identified patterns in the system responses. This aided in creating a ROM for arbitrary loading conditions. Nonlinear damping was modeled as a function of x^3. Results were compared for both linear and nonlinear models. In this work, the authors looked at various mode shapes from the data to see if nonlinear behavior was present using different inputs. From their results, they were able to show differences that indicated the presence of nonlinearity. Previous work [86] suggests that further work with the POD may yield algorithms capable of predicting the system response at any arbitrary set of operating conditions.

Galbally et al [87] investigated a model reduction approach for large-scale statistical inverse problems. Nonlinear terms were approximated by using a subset of interpolation points. The authors note that efficient non-linear model reduction has been previously addressed by several authors. If the problem under consideration is weakly non-linear, efficient reduced models can be obtained by retaining low-order terms in the Taylor series expansion of non-linear terms [88]. Another approach is to use the trajectory piecewise-linear scheme, which employs a weighted combination of various linear models, obtained by linearizing the non-linear system at selected points along a state trajectory [89]. Other approaches propose approximating the non-linear term through selective sampling of a subset of the original equations [90–93]. In this case, a highly non-linear combustion problem was investigated for input estimation with an Arrhenius type reaction term. A Bayesian approach was used whereby a conditional probability was updated iteratively, re-forming the problem into statistical inference. The nonlinear term was evaluated at select interpolation points. Steady state multi-dimensional solutions were estimated.

Several approaches have been proposed to address the general problem of reducing the complexity of evaluating the nonlinear term of the POD reduced model in the context of finite difference (FD) and finite volume (FV) discretization as well as differential- algebraic equations (e.g., in circuit simulation). Missing point estimation (MPE) was originally proposed in [94] to improve the complexity of the POD-Galerkin reduced system from FV discretization, by solving only a subset of equations of the original model. Alternatively, techniques for approximating a nonlinear function can be used in conjunction with the POD-Galerkin projection method to overcome this computational inefficiency. There are a number of examples that use MOR approaches with nonlinear approximation based on precomputation of coefficients defining multilinear forms of polynomial nonlinearities followed by POD-Galerkin projection [95 – 100].

One of these approaches was found in the trajectory piecewise-linear (TPWL) approximation [101, 102], which is based on approximating a nonlinear function by a weighted sum of linearized models at selected points along a state trajectory. However, there are still many nonlinear functions that may not be approximated well by using low degree piecewise polynomials unless there are very many constituent polynomials.

Feng, Rudnyi, and Korvink [103] developed an approach for a compact thermal model that is independent of the thermal boundary conditions. A conventional model order reduction method can only deal with systems when material properties are fixed using a Lagrangian transform method. In other words, the basis generated for a particular thermal conductivity k0 can be used just for a small range of k. In this work, the heat transfer equation was shown with convection boundary conditions only and thermal conductivity k was constant and uniform in space. The authors here used a ROM to create a parametric model reduction (on k) in order to find a projection subspace that allows results to be generated from a reduced model for wide range of k values by using a scaling factor to produce lowest error results. A projection matrix was defined a bit differently in this work, almost like a Krylov space, but with an additional tuning variable (μ) added to scale a matrix. The authors admit that the choice of the tuning variable requires additional research. The basis was generated without using k directly. Results were generated using single reduced model (5% error) and then three reduced models (1% error). The research was done in an empiric fashion with an expectation that some theoretical explanation will be offered in future work.

1.3.4 POD-DEIM Combination

Research had led to success in treating nonlinear source terms by combining POD with a technique called DEIM. This is the preferred method for treating nonlinear source terms in ODEs and PDEs for use in a ROM.

In the finite element context, inefficiency arises from the high computational complexity in repeatedly calculating the inner products required to evaluate the weak form of the nonlinearities as discussed in [104-106]. Nguyen and Peraire [107] discuss the limitations of such approaches and give a number of examples of equations involving nonpolynomial nonlinearities. Specifically, they study linear elliptic equations with nonaffine parameter dependence, nonlinear elliptic equations, and nonlinear time dependent convection-diffusion equations. They demonstrate for these examples that the standard POD-Galerkin approach does not allow the sort of precomputation that is possible with polynomial nonlinearities. They propose a reduced basis method with a best-points interpolation method (BPIM) to selecting interpolation points [107].

Research by Chaturanatabut [108] lead to the development of the DEIM algorithm, which is the POD-Galerkin ROM mixed with DEIM to reduce the complexity of nonlinear terms. This approach readily extends to nonlinear ODEs with minor modification. The DEIM approach proposed by the author approximates a nonlinear function by combining projection with interpolation. The POD-DEIM approach is also closely related to the approach called interpolation of function snapshots suggested in [109] as an alternative to missing point estimation (MPE) for constructing a reduced system for a nonlinear circuit model. The authors

were motivated to develop this DEIM variant to apply to arbitrary systems of ODEs regardless of their origin. The procedure presented in their research can also be applied to general nonlinear ODEs, including a FV discretized system.

1.3.5 Multi-Physics Models

POD techniques have been sought to treat complex multi-physics models that include heat and mass transfer, momentum, and fluid-structural interactions.

The POD was examined by Ly and Tran [110] for flow and control in a horizontal CVD reactor. Compressible viscous flow was coupled with the energy and species equations. The POD was used to control uniform vapor deposition. CVD reactor models are represented by systems of nonlinear partial differential equations, where the full system was solved numerically. The approach was restricted to a 2D reactor model, and steady state solutions used to drive transient solutions. In this work, the author claims to be using the thermophysical properties as temperature dependent, but the properties were evaluated at the steady state temperature. The number of basis vectors chosen was based on capturing 99.9% of characteristics (energy), and was not error driven. The overall problem was reduced by determining the covariant matrix instead of using SVD, which is now more standard approach. Good approximations were achieved based on one flow input condition. Results were extended to two other similar input conditions and resulted in fairly good approximations.

Klimanek, Bialecki, and Ostrowski [111] developed a 2D multi-phase CFD two-scale model of a wet natural draft cooling tower. In this research, the fill of the tower was modeled as porous medium. The equation set was solved using fourth order Runge Kutta solver with adaptive step control [112]. The ODEs solver is invoked iteratively for every vertical conduit and every step of the iterative loop of exchanging data between the CFD solver and the model of the fill. Preliminary calculations revealed that, even for the case of axisymmetrical model, the solution of the fill equations is numerically very intensive. As the target of the project is a 3-D model, the question of computing time economy becomes very important. Aiming at this target, POD coupled with radial basis function (RBF) was applied to reduce the cost of modeling the heat and mass transfer in the fill. Eigenvalues were derived from the covariance matrix. The ROM was developed as a linear combination of radial basis functions. In the original version of the POD technique, a snapshot is produced by exciting the object under consideration by changing a single parameter. The technique used in this article extends this approach to a case when the object is excited by an input vector k [113]. In this case – $k(T) = 1 + s\,T$, $s = 0.5$. In this study the problem was solved using the shooting method [113]. The authors developed the unsteady case (in theory) but only looked at two steady heat conduction cases using constant properties.

More recently, Galbally et al. [87] applied the techniques of gappy POD, EIM, and BPIM to develop an approach to uncertainty quantification in a nonlinear combustion problem governed by an advection-diffusion-reaction PDE. The nonlinear term involved an exponential nonlinearity of Arrhenius type. The authors give a detailed explanation here as to why POD-Galerkin does not reduce the complexity of evaluating the nonlinear term.

Biglari and Sutherland [114] developed a PCA/MARS (Principal Component Analysis/Multivariate Adaptive Regression Spline) technique to regress source terms and regenerate state-variables from the principal components to capture nonlinearity in a reduced basis. PCA (aka POD) has been shown as an effective methodology to identify manifolds in turbulent combustion [115-118]. Multivariate Adaptive Regression Spline (MARS) is used for regressing source terms and regenerating state-variables from the ROM to capture nonlinearity in the reduced basis [118, 119]. Prior to carrying out a PCA transformation, the authors centered and scaled the data appropriately [117, 118, 120]. This work results in an a posteriori study using PCA as a combustion model for evolving jet flame – extinction and re-ignition. Several aspects are neglected including radiation and source term heating due to the fact that the principal components for these terms are small compared to the transport terms. Scaling is done in the PCA method, and the model is reduced to a 2 parameter problem. Results showed that PCA-based models can match profiles well while retaining only 2 parameters, however estimates across other Re numbers require choosing a new training data set to accurately predict results in a new regime. The authors note that the ROMs can be 'tuned' to capture different state variables based on the choice of scaling parameters. When a simulation accesses regions outside where the model was trained, the model behavior is not guaranteed to be physically realistic. The authors propose to design the regression technique so that source terms should be either zeroed or designed to move the trajectory back toward the manifold to avoid divergence from the manifold in higher dimensions.

1.4 Research Objectives

Despite gains in creating POD-based ROMs for use in complex thermal model prediction, an approach for estimating results unknown *a priori* is still limited to low nonlinearity cases. Research has identified that the diffusion term is the driving force, however limited progress has been made to accurately assess nonlinear material properties across a wide range of temperatures. Additional nonlinearities such as radiation boundary conditions and source heating terms have either been treated separately from material properties (constants only) or neglected from the problem entirely. A ROM is sought to combine all these features for use in estimating results from inputs unknown *a priori.*

In this research, a transient heat transfer reduced order model is explored in order to

(1) Integrate nonlinear temperature dependent material properties
(2) Construct the ROM to include additional sources of nonlinearities such as radiation boundary conditions, temperature dependent source heating terms, and complex geometry
(3) Develop a single robust ROM for use in predicting over a wide domain

1.5 Paper Organization

In this work, a reduced order model was developed to account for various sources of nonlinearities. A 1D ROM was initially developed and progressively enhanced to address nonlinear material properties, radiation boundary conditions, and nonlinear source terms. A

variety of material types were investigated for optimal accuracy and computational speed. The same ROM framework was then extended to multiple dimensions to treat 3D/complex geometries.

This work is presented in the following chapters organized in the following manner:

- Chapter 2 – Detailed Reduced Order Model Development
- Chapter 3 – Results for nonlinear material property treatment
- Chapter 4 – Results for radiation boundary condition
- Chapter 5 – Results for nonlinear source terms
- Chapter 6 – Results for 3D/complex geometry
- Chapter 7 – Conclusions and Future Work

2 Reduced Order Model Development

A one-dimensional (1D) transient heat transfer model was developed that contains features to make the solution nonlinear including temperature dependent properties, radiation boundary conditions, and nonlinear source terms. A reduced order model (ROM) was developed based on POD and was specifically designed to account for the nonlinearities of this problem. The ROM can then be used to provide computationally efficient solutions with different applied boundary conditions that are similar to that used to construct the ROM.

An initial full sized Finite Difference model was developed to produce a solution set for use in the ROM as well as provide a comparison against the ROM results. Proper Orthogonal Decomposition was used on the full solution set to identify key characteristics within the data and generate a projection operator to approximate the system in a smaller subspace. The reduced order equation is then solved, projected back to the original space, and compared to the full scale solution in terms of accuracy and solution times. In order to treat complex geometry, a three dimensional Finite Element model is derived in order to produce a solution set for use in the ROM as well as provide a comparison against the ROM results. This is done by using a commercially available program. The same ROM developed for the 1D case is then applied to the 3D case.

The following chapter describes how the one-dimensional (1D) and three-dimensional (3D) reduced order models were developed. A detailed development is provided for the 1D case, outlining the methodology to account for nonlinear material properties, radiation boundary conditions, and nonlinear source heating terms. The extension of the model into three dimensions is then described.

2.1 One-Dimensional Heat Transfer Model

A 1D transient heat transfer model was developed that contains features to make the solution nonlinear including temperature dependent properties, radiation boundary conditions, and nonlinear source terms.

2.1.1 Governing Equations

The 1D transient energy equation is

$$\frac{\partial T}{\partial t} = \alpha \frac{\partial^2 T}{\partial x^2} \qquad \text{Equation 3}$$

At the boundaries, convection occurs along with a surface heat flux, u(t), applied at one face.

$$-k\frac{\partial T}{\partial x} = u(t) + h_0(t)\left(T_{\infty,0} - T_{x=0}\right) \ , \qquad x = 0 \qquad \text{Equation 4}$$

$$-k\frac{\partial T}{\partial x} = h_L(t)\left(T_{\infty,L} - T_{x=L}\right) \ , \qquad x = L \qquad \text{Equation 5}$$

The initial temperature distribution is specified as

$$T = T_0(x), \qquad t = 0 \qquad \text{Equation 6}$$

Notice material properties (α) have been written initially as constant.

2.1.2 Finite Difference Model

In order to effectively reduce the system of interest, a solution set as a series of data points is needed in order to capture the phenomenon of interest. For this research, the heat transfer system is initially treated in a 1D transient Finite Difference model. The physical and temporal domains are discretized into a series of grid points and used to evaluate a solution set $S \in \mathbb{R}^{Nxm}$ where m is the number of state variables (discretized points) and N is the number of time intervals. The model was developed based on an implicit finite differencing scheme using a central differencing approximation for the spatial derivative and a backwards differencing approximation for the transient term.

A typical interior node is discretized as –

$$\frac{T_i^{p+1} - T_i^p}{\Delta t} = \frac{\alpha\left(T_{i-1}^{p+1} - 2T_i^{p+1} + T_{i+1}^{p+1}\right)}{(\Delta x)^2} \qquad \text{Equation 7}$$

For the boundary at x = 0,

$$\frac{T_1^{p+1} - T_1^p}{\Delta t} = \frac{1}{\rho c_p}\frac{2}{\Delta x}\left(k\frac{\left(T_2^{p+1} - T_1^{p+1}\right)}{\Delta x} + u(t) + h_0\left(T_\infty - T_1^p\right)\right) \qquad \text{Equation 8}$$

For the boundary at x = L,

$$\frac{T_n^{p+1} - T_n^p}{\Delta t} = \frac{1}{\rho c_p}\frac{2}{\Delta x}\left(k\frac{\left(T_{n-1}^{p+1} - T_n^{p+1}\right)}{\Delta x} + h_0\left(T_\infty - T_n^p\right)\right) \qquad \text{Equation 9}$$

For the initial state at t = 0,

$$T = T_0(x) \qquad \text{Equation 10}$$

The result is a simultaneous set of equations for the temperatures at the grid points that can then be assembled into a state-space equation using matrices.

$$[E]\frac{d\mathbf{T}}{dt} = \alpha[A]\,\mathbf{T} + [B]u(t) + [C] \qquad \text{Equation 11}$$

$$y = [D]\,\mathbf{T} \qquad \text{Equation 12}$$

In the model, [E] is an identity matrix applied to the differential term. [A] is a tridiagonal matrix that contains the spatial derivatives as well as the temperature dependent terms of the convection boundary conditions. Matrix build is done using a built-in sparse matrix function. [B] is column matrix that assigns the applied heat flux at the node of interest. The matrix contains a definition for a single node. [C] is a column matrix that contains the remaining portion of the convection boundary conditions. The matrix only contains definitions for the two exterior nodes. Last, [D] is a column matrix that can be used to pull out the results for a specific node of interest. For the purposes of this research, the full solution set as well as the node at the unexposed face were both investigated.

2.2 Basic ROM Development

A reduced order model (ROM) was develop based on Proper Orthogonal Decomposition (POD) and was specifically designed to account for the nonlinearities of this problem. The ROM can then be used to provide computationally efficient solutions with different applied boundary conditions that are similar to that used to construct the ROM. An initial full sized Finite Difference model is developed to produce a solution set for use in the ROM as well as provide a comparison against the ROM results. Proper Orthogonal Decomposition is used on the full solution set to identify key characteristics within the data and generate a projection operator to approximate the system in a smaller subspace.

For any given function of interest, the function can be approximated as a function z(x, t) over the domain of interest as a finite sum in a variables-separated form

$$z(x,t) \approx \sum_{k=1}^{M} a_k(t)\phi_k(x) \qquad \text{Equation 13}$$

With the understanding that as M approaches infinity, the approximation becomes exact. It should be noted that there is no fundamental difference between x and t, however x is treated as a spatial coordinate and t as a temporal coordinate.

POD is developed based on choosing φ_k to be an orthonormal basis function

$$\int_x \phi_{k1}(x)\phi_{k2}(x)dx = \begin{cases} 1 \text{ if } k_1 = k_2 \\ 0 \text{ otherwise} \end{cases} \qquad \text{Equation 14}$$

Then it follows that

$$a_k(t) = \int_x z(x,t)\phi_k(x)dx \qquad \text{Equation 15}$$

Where $a_k(t)$ depends only on $\phi_k(x)$. For this case, ϕ_k is selected so that it is orthonormal and so that M is as good as possible in a least squares sense. These special ordered, orthonormal functions are called proper orthogonal nodes for the function z(x,t).

For a general system, consider that measurements of *m* state variables are taken at *N* instants of time. All the data points can be arranged in a matrix A such that it is *N* x *m*. The singular value decomposition of a matrix A is of the form:

$$A = U\Sigma V^T \qquad \text{Equation 16}$$

Where U is an N x N orthogonal matrix, V is an m x m orthogonal matrix, the T superscript indicates the matrix transpose, and Σ is an N x m matrix with all elements equal to zero except along the diagonal. The diagonal elements Σ_{ii} are made up of r = min (N, m) nonnegative numbers σ_i, which are arranged in descending order such that $\sigma_1 \geq \sigma_2 \geq \cdots \geq \sigma_r \geq 0$. The σ terms are called the singular values of A and are unique. The rank of A equals the number of nonzero singular values it has. Since the singular values are arranged in a specific order, the index k of the kth singular value is called the singular value number.

The discrete version of POD uses the SVD – singular value decomposition – to reduce a data set in matrix form. The discrete form of the POD Equation 13 is

$$A = QV^T = \sum_{k=1}^{m} q_v v_k^T \qquad \text{Equation 17}$$

Where the matrix A corresponds to the function z (x, t), column matrix q_v corresponds to the function $a_k(t)$, and v_k^T corresponds to the function $\phi_k(t)$. This form of the equation is now exact because the dimension is finite.

An optimal lower rank approximation of A can be obtained using a subset of the results obtained from the singular value decomposition. The Σ matrix is reduced to Σ_k by setting all σ values above rank k+1 equal to 0. The reduced matrix A_k is then determined by

$$A_k = U\Sigma_k V^T \qquad \text{Equation 18}$$

The overall goal of this research is to most effectively approximate a large scale system by a much smaller subspace using this approach. Now, a matrix of data points $A \in R^{Nxm}$ can be well approximated by the smaller size matrix $A_k \in R^{kxk}$. For computational purposes, a given matrix is decomposed using the singular value decomposition into U, Σ, and V matrices. Then, an optimal reduced rank matrix A_k can be generated from Equation 18 by using the leading k x k principal minor matrix of Σ and replacing U and V with the matrices of their first k columns.

For the case where m >> N, this would be a highly discretized system that has fewer evolutions per time, it is more efficient to first compute the matrix U as the matrix of eigenvectors AA^T. This is referred to as the method of snapshots.

In the model, a solution set was generated using Equation 11 and Equation 12 and the data set was then decomposed using the SVD such that S = UΣV using MATLAB's built-in SVD

function. It is then truncated to its first k columns to a reduced rank, now referred to as ϕ, and used as a projection matrix to reduce each of the matrices in the state space equation. Optimal rank selection is further discussed in Section 3.3.

It should be noted that it is common to subtract from each column of A the mean value of the column (Chatterjee [60]). This shift allows for the data point cloud to be centered around the origin. While this does not affect the calculations, it does affect the results interpretation. However, in recent research a case has been made for not subtracting the mean in. POD analysis on in-cylinder engine flows was done with and without subtracting the mean (Chen [121]). Results indicated that when not subtracted, the coefficients of mode 1 reveal the extent to which the mean flow is present and its cycle-to-cycle variability. This can be used to identify cycles with unusual conditions such as engine misfires. It was concluded that the POD of V was more useful than V–(V). In this research, the mean also was not subtracted from each column in the data set so that material properties could be evaluated directly in the ROM using temperature dependent functions.

Using the previously developed state-space equation (Equation 11 and Equation 12) and the projection matrix, ϕ, a reduced order model was then created. For constant material properties, the state space equation matrices do not update with the solution and the reduced order matrices are readily defined as

$$[E]_r = \phi^T [E] \phi \quad \text{Equation 19}$$

$$[A]_r = \phi^T [A] \phi \quad \text{Equation 20}$$

$$[B]_r = \phi^T [B] \quad \text{Equation 21}$$

$$[C]_r = \phi^T [C] \quad \text{Equation 22}$$

$$[D]_r = [D]^T \phi \quad \text{Equation 23}$$

$$\mathbf{T}_r = \phi^T \mathbf{T} \quad \text{Equation 24}$$

$$\mathbf{T}_{r,0} = \phi^T \mathbf{T}_0 \quad \text{Equation 25}$$

With an overall reduced order system equation of the form -

$$[E]_r \frac{d\mathbf{T}_r}{dt} = \alpha [A]_r \mathbf{T}_r + [B]_r u(t) + [C]_r \quad \text{Equation 26}$$

$$y = [D]_r \mathbf{T}_r \quad \text{Equation 27}$$

2.3 Temperature Dependent Properties Effects

The ROM approach is extended to treat temperature dependent nonlinear material properties. Temperature dependent material properties were initially treated in a 1D transient Finite Difference model. The same previously developed discretization model is updated for nonlinear material properties.

2.3.1 Finite Difference Model

A typical interior node is discretized as –

$$\frac{T_i^{p+1} - T_i^p}{\Delta t} = \frac{\alpha_{i-1} T_{i-1}^{p+1} - 2\alpha_i T_i^{p+1} + \alpha_{i+1} T_{i+1}^{p+1}}{\Delta x^2} \qquad \text{Equation 28}$$

For the boundary at x = 0,

$$\frac{T_1^{p+1} - T_1^p}{\Delta t} = \frac{2}{\Delta x}\left(\frac{\left(\alpha_2 T_2^{p+1} - \alpha_1 T_1^{p+1}\right)}{\Delta x} + \frac{u(t)}{\rho c} + \frac{h_0}{\rho c}(T_\infty - T_1)\right) \qquad \text{Equation 29}$$

For the boundary at x = L,

$$\frac{T_n^{p+1} - T_n^p}{\Delta t} = \frac{2}{\Delta x}\left(\frac{\left(\alpha_{n-1} T_{n-1}^{p+1} - \alpha_n T_n^{p+1}\right)}{\Delta x} + \frac{h_0}{\rho c}(T_\infty - T_n)\right) \qquad \text{Equation 30}$$

The result is a set of simultaneous equations for the temperatures at the grid points that can then be assembled into matrices.

$$[E]\frac{d\mathbf{T}}{dt} = [A(T)]\,\mathbf{T} + [B(T)]u(t) + [C(T)] \qquad \text{Equation 31}$$

$$y = [D]\,\mathbf{T} \qquad \text{Equation 32}$$

In the model, [A] is a tridiagonal matrix that contains the spatial derivatives as well as the temperature dependent terms of the convection boundary conditions. For the full solution, material properties are determined at each time step as a function of temperature. Temperature dependent functions for the specific heat and thermal conductivity are evaluated at a nodal basis and applied to the [A] matrix at each time step. Matrix build is done using a 'for loop'. [B] and [C] are column matrices.

2.3.2 Average Nodal Temperature ROM for Nonlinear Materials

For the case of temperature dependent material properties, additional steps must be taken to reduce the state space equation adequately while maintaining solution integrity. Two approaches are presented here for comparison. The first is to treat the material properties at the average temperature for each node. Average temperature values are determined based on the snapshots generated by the full solution set. The matrices are still constant however, a unique alpha value is now applied to each node. It does not update with each time step.

This approach is presented because taking the average temperature value at each node accounts for changing material properties. Matrices are constant and still easily reduced. However, the accuracy is lost over a large temperature range and results based on a single applied heat flux may not be able to represent other heat flux cases.

Average nodal temps are determined from the solution set. A single temperature vector is then used to create [A], [B], and [C] matrices, which are constant. The ROM is created by reducing each matrix term just as in the case for constant material properties.

2.3.3 Unique Nodal Temperature ROM for Nonlinear Materials

Another approach is to consider by pulling the material properties out of the matrices all together. The remaining content in the matrix is just the Taylor series approximation of the second order spatial derivative and is now constant and can be pre-computed. The material properties, which are approximated by polynomial functions, are distributed to the appropriate matrix so that the coefficients are now matrix pre-multiplier, and the temperature is treated as a column matrix whereby material properties are determined on a nodal basis.

The material properties are approximated by quadratic polynomial functions. For example, thermal diffusivity and the inverse volumetric heat capacity are approximated by

$$\alpha(\mathrm{T}) = \mathrm{c}_1 \cdot \mathrm{T}^2 + \mathrm{c}_2 \cdot \mathrm{T} + \mathrm{c}_3 \qquad \text{Equation 33}$$

$$\frac{1}{\rho c_p}(\mathrm{T}) = \mathrm{c}_4 \cdot \mathrm{T}^2 + \mathrm{c}_5 \cdot \mathrm{T} + \mathrm{c}_6 \qquad \text{Equation 34}$$

The material properties can also be treated on a unique nodal basis by creating vectors using the full temperature field vector and the polynomial coefficients. When applied to a matrix, terms can be rearranged so that the coefficients are constants in front of the matrix and the temperature vector now appears to the right hand side of the matrix. In the case of the first term in the state space equation, the [A] matrix contains the diffusion terms scaled by thermal diffusivity as well as the convection boundary condition terms scaled by the inverse volumetric heat capacity as shown in Equation 28, Equation 29, and Equation 30. The [A] matrix is split into two constant matrices to account for each of these constituents.

By pulling the temperature term out as a vector that is then multiplied with matrix [A] using standard matrix multiplication, the unique nodal material properties and the relationship between neighboring nodes due to the Taylor series approximations are preserved.

In addition, [A] is already being multiplied by vector **T** as a result of the model development, so the additional temperature terms from the material properties can be combined using an element wise power treatment.

For example, the first term in the state space Equation 31 is expanded and rewritten as

$$\begin{aligned}\alpha(\mathrm{T})[\mathrm{A}]\mathbf{T} = \; & c_1[\mathrm{A_{diff}}]\mathbf{T}^3 + c_2[\mathrm{A_{diff}}]\mathbf{T^2} + c_3[\mathrm{A_{diff}}]\mathbf{T} \\ & + \; c_4[\mathrm{A}_{BC}]\mathbf{T}^3 + c_5[\mathrm{A}_{BC}]\mathbf{T^2} + c_6[\mathrm{A}_{BC}]\mathbf{T}\end{aligned} \qquad \text{Equation 35}$$

All of the matrices in the state space Equation 31 are examined in turn and expanded in a similar manner. For the column matrices [B] and [C], element wise multiplication with the temperature vector is done to preserve unique nodal properties. The fully expanded equation is as follows -

$$\begin{aligned}[\mathrm{E}]\frac{\mathrm{d}\mathbf{T}}{\mathrm{dt}} = \; & c_1[\mathrm{A_{diff}}]\mathbf{T}^3 + c_2[\mathrm{A_{diff}}]\mathbf{T^2} + c_3[\mathrm{A_{diff}}]\mathbf{T} \\ & + \; c_4[\mathrm{A_{BC}}]\mathbf{T}^3 + c_5[\mathrm{A_{BC}}]\mathbf{T^2} + c_6[\mathrm{A_{BC}}]\mathbf{T} \\ & + c_4[\mathrm{B}]\mathrm{u(t)} \circ \mathbf{T}^2 + c_5[\mathrm{B}]\mathrm{u(t)} \circ \mathbf{T} + c_6[\mathrm{B}]\mathrm{u(t)} \\ & + c_4[\mathrm{C}] \circ \mathbf{T}^2 + c_5[\mathrm{C}] \circ \mathbf{T} + c_6[\mathrm{C}]\end{aligned} \qquad \text{Equation 36}$$

The ODE is now explicitly written as a function of temperature only, and all other terms are constant. Like terms, such as matrix terms $c_1[\mathrm{A_{diff}}]$ and $c_4[\mathrm{A}_{BC}]$, can now be combined and the overall equation reduced via Proper Orthogonal Decomposition. In order to reduce the model, a slightly different approach is needed to effectively handle each term. The POD projection matrix, φ, is generated the same way as previously stated in Section 2.2.3. It should be noted however, that since the material properties in the ROM are evaluated at actual temperatures, the mean values are not subtracted from the snapshots when producing the POD projection matrix and when executing the ROM. Each of the constant matrices ([E], [A_{diff}], [A_{BC}], [B], [C], and [D]) are created and reduced using the same approach outlined in Equation 19 through Equation 23. The reduced matrices are then scaled by the material coefficients as necessary and the like terms are then combined.

Now, the temperature vector also has to be reduced, and is treated the same as in Equation 23. However, for the temperature terms in the model raised to a power, they must be treated a bit differently as the exponents apply in a piece wise manner in order to reflect the unique nodal treatment.

The following is proposed for any exponent n greater than 1 -

$$\mathbf{T}_\mathrm{r}^\mathrm{n} = \; \phi^\mathrm{T}(\phi\mathbf{T}_\mathrm{r})^\mathrm{n} \qquad \text{Equation 37}$$

Where the reduced temperature vector is first projected back to the original space, then raised to a power in a piece wise manner, and the result is then projected to the subspace again.

The final reduced order model is now

$$\begin{aligned}[\mathrm{E}]_\mathrm{r}\frac{\mathrm{d}\mathbf{T}_\mathrm{r}}{\mathrm{dt}} = {} & (\mathrm{c}_1[\mathrm{A}_{\mathrm{diff}}]_\mathrm{r} + \mathrm{c}_4[\mathrm{A}_{\mathrm{BC}}]_\mathrm{r})\mathbf{T}_\mathrm{r}{}^3 \\ & + (\mathrm{c}_2[\mathrm{A}_{\mathrm{diff}}]_\mathrm{r} + \mathrm{c}_5[\mathrm{A}_{\mathrm{BC}}]_\mathrm{r})\mathbf{T}_\mathrm{r}{}^2 \\ & + (\mathrm{c}_3[\mathrm{A}_{\mathrm{diff}}]_\mathrm{r} + \mathrm{c}_6[\mathrm{A}_{\mathrm{BC}}]_\mathrm{r})\mathbf{T}_\mathrm{r} \\ & + \mathrm{c}_4([\mathrm{B}]_r\mathrm{u}(\mathrm{t}) + [\mathrm{C}]_r) \circ \mathbf{T}_\mathrm{r}{}^2 + \mathrm{c}_5([\mathrm{B}]_r\mathrm{u}(\mathrm{t}) + [\mathrm{C}]_r) \circ \mathbf{T}_\mathrm{r} \\ & + \mathrm{c}_6([\mathrm{B}]_r\mathrm{u}(\mathrm{t}) + [\mathrm{C}]_r)\end{aligned} \qquad \text{Equation 38}$$

Note all of these terms except the temperature vector are constant and can be pre-computed.

2.4 Boundary Condition Effects

The ROM approach is extended to treat radiation boundary conditions.

2.4.1 Governing Equations

The 1D transient energy equation and boundary conditions are updated to include radiation.

$$-\mathrm{k}(\mathrm{T})\frac{\partial \mathrm{T}}{\partial \mathrm{x}} = \mathrm{u}(\mathrm{t}) + \mathrm{h}_0\left(\mathrm{T}_{\infty,0} - \mathrm{T}\right) + \epsilon\sigma\left(T_{x=0}^4 - T_{\infty,0}^4\right) \quad , \ \mathrm{x} = 0 \qquad \text{Equation 39}$$

$$-\mathrm{k}(\mathrm{T})\frac{\partial \mathrm{T}}{\partial \mathrm{x}} = \mathrm{h}_\mathrm{L}\left(\mathrm{T}_{\infty,\mathrm{L}} - \mathrm{T}\right) + \epsilon\sigma\left(T_{x=L}^4 - T_{\infty,\mathrm{L}}^4\right) \quad , \quad \mathrm{x} = \mathrm{L} \qquad \text{Equation 40}$$

The fourth order polynomial terms for radiation require excessive computational effort. To minimize that while maintaining a close approximation, the equations are linearized such that a new heat transfer coefficient, h, is defined based on a combination of the convection and radiation terms in Equation 41.

$$\mathrm{h} = \mathrm{h}_{\mathrm{conv}} + \mathrm{h}_{\mathrm{rad}} \qquad \text{Equation 41}$$

$$\mathrm{h}_{\mathrm{rad}} = \epsilon\sigma\left(\mathrm{T}_\mathrm{x} + \mathrm{T}_\infty\right) \cdot \left(\mathrm{T}_\mathrm{x}^2 + \mathrm{T}_\infty^2\right) \qquad \text{Equation 42}$$

$$-\mathrm{k}(\mathrm{T})\frac{\partial \mathrm{T}}{\partial \mathrm{x}} = \mathrm{h} \cdot \left(\mathrm{T}_\mathrm{x} - \mathrm{T}_\infty\right) \qquad \text{Equation 43}$$

The heat transfer coefficient term is generalized here. However, the heat flux given by Equation 43 is determined uniquely at each face for either the heated (x = 0) or unheated (x = L) surface.

2.4.2 Finite Difference Model – Snapshot Generation

The previously developed discretization model is updated for radiation boundary conditions at the surfaces by incorporating the updated heat transfer coefficient term from Equation 41. This results in a slightly modified version of Equation 31.

In the updated model, [A] is a tridiagonal matrix that additionally contains the temperature dependent terms of the linearized radiation boundary conditions. Also, the column matrix [C] is updated to reflect the ambient temperature terms of the linearized radiation boundary conditions.

2.4.3 Radiation Boundary Condition ROM

The radiation term is included in the ROM by amending the boundary treatments in the $[A_{BC}]_r$ and $[C]_r$ matrices from Equation 38. First, constant matrices $[A_{BC}]$ and [C] are generated by evaluating the radiation term (Equation 42) using the average boundary temperatures at each face from the snapshots. These constant matrices are then reduced and solved by using the same approach previously outlined.

2.5 Source Term Effects

The ROM approach is extended to treat temperature dependent nonlinear source terms.

2.5.1 Governing Equations

The 1D transient energy equation is updated to include a generalized source heating.

$$\frac{\partial T}{\partial t} = \alpha(T)\frac{\partial^2 T}{\partial x^2} + \frac{1}{\rho c_p(T)}\big(S(T)\big) \qquad \text{Equation 44}$$

2.5.2 Finite Difference Model – Snapshot Generation

Similar to the radiation term, if the source heating term is a nonlinear function of temperature, an iteration procedure can be employed by linearizing the source term as a first order Taylor series approximation.

$$S^{p+1} = S^p + \left(\frac{dS}{dT}\right)^p (T^{p+1} - T^p) \qquad \text{Equation 45}$$

The source term can now be expressed with two coefficients as shown in Equation 46.

$$S(x) = S_c(x) - S_p(x)T \qquad \text{Equation 46}$$

This is a convenient form of the source term as it allows for usual internal heat generation, fin like terms, other linear approximations of nonlinear physics, and is in general a useful mechanism to iterate nonlinear problems. In this case, the [A] matrix is updated to include the S_p terms and the [C] matrix is updated to include the S_c terms in Equation 31. For source heating in a different form that may not be well approximated by a linear term, such as an exponential term, direct computation can be made within the [A] matrix. The POD projection matrix is created the same way as previously presented

2.5.3 Nonlinear Source Term ROM

In this research, the focus is on creating a ROM from a state-space equation that has polynomial form dependent variables. For constant coefficient values, the $[A_{source}]$ matrix is created to contain the S_p terms and the [C] matrix is updated to include the S_c terms. The $[A_{source}]$ matrix is a square matrix with source heating terms contained only on the diagonal.

$$\begin{aligned}[E]\frac{d\mathbf{T}}{dt} &= c_1[A_{diff}]\mathbf{T}^3 + c_2[A_{diff}]\mathbf{T^2} + c_3[A_{diff}] \\ &+ c_4[A_{BC}]\mathbf{T}^3 + c_5[A_{BC}]\mathbf{T^2} + c_6[A_{BC}]\mathbf{T} \\ &+ c_4[A_{source}]\mathbf{T}^3 + c_5[A_{source}]\mathbf{T^2} + c_6[A_{source}]\mathbf{T} \\ &+ c_4[B]u(t) \circ \mathbf{T}^2 + c_5[B]u(t) \circ \mathbf{T} + c_6[B]u(t) \\ &+ c_4[C] \circ \mathbf{T}^2 + c_5[C] \circ \mathbf{T} + c_6[C]\end{aligned} \qquad \text{Equation 47}$$

This is a linearized treatment of the source term, which represents a "fin-like" term, but can easily be extended to higher order polynomials, etc. Any additional polynomial temperature dependencies can be treated similar to the material properties where the coefficients are combined with the material property coefficients and the temperature terms are combined with the temperature vectors. The matrices are then reduced using the POD projection matrix using the same procedure previously presented.

2.5.4 DEIM Algorithm

For other types of nonlinear source terms that cannot be well represented by a polynomial function, such as exponential sources, an alternate secondary computational treatment is required. The Discrete Empirical Interpolation Method (DEIM) technique can be used with POD to effectively create a reduced order representation for the nonlinear terms. This previously developed method is used to select a set of interpolation indices used to approximate the nonlinear term.

DEIM is used on the general equation of the form in order to reduce the F(y(t)) term so it is mathematically compatible with the other terms

$$\frac{\partial}{\partial t}\mathbf{y}(t) = \mathbf{A}\mathbf{y}(t) + \mathbf{F}(\mathbf{y}(t)) \qquad \text{Equation 48}$$

The computational complexity of the nonlinear term F still depends on the size of the initial fully discretized system. In order to achieve a reduced basis specifically for this term, a projection term is determined based on a series of interpolation indices which are selected by minimizing error.

Consider setting up the state space equation so that the source terms are separated from the diffusion terms as in Equation 49.

$$[E]\frac{d\mathbf{T}}{dt} = [A(T)]\,\mathbf{T} + [B(T)]u(t) + [C(T)] + [D_{source}] \qquad \text{Equation 49}$$

In the form provided by Equation 49, a solution set of temperature snapshots due to just the $[D_{source}]$ matrix can be isolated and used to create a separate projection matrix. Using the data set associated with just the source term, the DEIM algorithm is then used to determine a set of interpolation indices using the previously developed algorithm shown in Figure 3.

ALGORITHM 1. DEIM

INPUT: $\{\mathbf{u}_\ell\}_{\ell=1}^m \subset \mathbb{R}^n$ linearly independent
OUTPUT: $\vec{\wp} = [\wp_1, \ldots, \wp_m]^T \in \mathbb{R}^m$

1: $[|\rho|, \ \wp_1] = \texttt{max}\{|\mathbf{u}_1|\}$
2: $\mathbf{U} = [\mathbf{u}_1]$, $\mathbf{P} = [\mathbf{e}_{\wp_1}]$, $\vec{\wp} = [\wp_1]$
3: **for** $\ell = 2$ to m **do**
4: Solve $(\mathbf{P}^T\mathbf{U})\mathbf{c} = \mathbf{P}^T\mathbf{u}_\ell$ for $\mathbf{c}$
5: $\mathbf{r} = \mathbf{u}_\ell - \mathbf{U}\mathbf{c}$
6: $[|\rho|, \ \wp_\ell] = \texttt{max}\{|\mathbf{r}|\}$
7: $\mathbf{U} \leftarrow [\mathbf{U} \ \ \mathbf{u}_\ell]$, $\mathbf{P} \leftarrow [\mathbf{P} \ \ \mathbf{e}_{\wp_\ell}]$, $\vec{\wp} \leftarrow \begin{bmatrix} \vec{\wp} \\ \wp_\ell \end{bmatrix}$
8: **end for**

Figure 3. Discrete Empirical Interpolation Method (DEIM) algorithm for nonlinear model reduction (Chaturantabut [108])

The $[D_{source}]$ matrix is then reduced using the DEIM generated projection matrix and is now the same dimension as the other reduced matrices. All other terms are reduced using previously developed methodology with POD, including nonlinear material property treatment.

2.6 Steps for ROM Generation and Testing

Snapshots were generated by using the 1D finite difference model. The results were decomposed using the Singular Value Decomposition Technique and used to create a projection matrix in order to reduce the full scale problem. The ROMs presented above are solved by MATLAB R2016 using a built-in ODE solver. The reduced space solution sets are then re-projected back to the original space using the POD projection matrix and compared to the full solution.

Comparison is made by looking at both run times and accuracy. Computational run times are captured when the full solution is generated, when the POD projection matrix is created, and when the ROM is solved. Accuracy was assessed in multiple ways. One approach was by looking at the absolute error between the full solution and re-expanded solution at all discretization points. The result was a surface of errors that can be used to visually assess where in the solution set the ROM may be less effective (boundaries, steady state, etc.). Additionally,

the relative POD error was determined by looking at the norm of the difference between the two surfaces over the norm of the full solution set.

$$\text{Relative Error} = \frac{\text{norm}\left(T_{full} - T_{expanded}\right)}{\text{norm}\left(T_{full}\right)} \qquad \text{Equation 50}$$

This provides a single error value that can be used to assess the overall fit of a single solution and is used to compare across multiple ROM solutions. Optimal rank was determined for each material and discretization effects were studied. The ROMs were then used to estimate material response for applied heat fluxes unknown a priori.

2.6 Three-Dimensional Transient Heat Transfer

The ROM approach is extended to treat the domain of interest in three dimensions.

2.6.1 Governing Equations

The 3D transient energy equation is

$$\frac{\partial T}{\partial t} = \alpha(T)\left(\frac{\partial^2 T}{\partial x^2} + \frac{\partial^2 T}{\partial y^2} + \frac{\partial^2 T}{\partial z^2}\right) + \frac{1}{\rho c_p(T)}\left(S(T)\right) \qquad \text{Equation 51}$$

$$-k(T)\frac{\partial T}{\partial x} = u(t) + h_0\left(T_{\infty,0} - T_{x=0}\right), \quad x = 0 \qquad \text{Equation 52}$$

$$-k(T)\frac{\partial T}{\partial x} = h_L\left(T_{\infty,L} - T_{x=Lx}\right), \quad x = Lx \qquad \text{Equation 53}$$

$$-k(T)\frac{\partial T}{\partial y} = h_0\left(T_{\infty,0} - T_{y=0}\right), \quad y = 0 \qquad \text{Equation 54}$$

$$-k(T)\frac{\partial T}{\partial y} = h_L\left(T_{\infty,L} - T_{y=Ly}\right), \quad y = Ly \qquad \text{Equation 55}$$

$$-k(T)\frac{\partial T}{\partial z} = h_0\left(T_{\infty,0} - T_{z=0}\right), \quad z = 0 \qquad \text{Equation 56}$$

$$-k(T)\frac{\partial T}{\partial z} = h_L\left(T_{\infty,L} - T_{z=Lz}\right), \quad z = Lz \qquad \text{Equation 57}$$

Boundary conditions are needed for every direction. A heat flux is applied at x = 0 as an example, but can be applied to any face. Temperature dependent material properties are retained and for this research are isotropic.

2.6.2 Commercial Code – Snapshot Generation

Snapshots can be generated by developing a unique FEM code to process a specific problem or by using the results from a 3rd party commercial software. Commercial software can be used to

effectively reproduce the geometry, apply boundary conditions and source terms, generate a suitable mesh, and provide unique nodal temperatures for a range of times.

In this case, a simple 3D cube model was generated in Abaqus version 6.13-3. A uniform mesh was created using an 8 node linear brick element type (DC3D8) typical for multidimensional heat transfer. Initial temperature and boundary conditions were applied as described above including convection at all the boundaries and an applied heat flux at one surface. The model was then executed for an extended time length, and both the mesh definition and thermal data points were exported for additional processing.

2.6.3 3D ROM Development

For this research, all nonlinearities previously treated in a 1D transient Finite Difference model are extended to a general 3D transient Finite Element model.

A POD projection matrix is created similar to the previous 1D method. The snapshot data were arranged into a matrix so that *m* state variables (nodes) were taken at *N* instants of time. Again, all the data points can be arranged in a matrix A such that it is *N* x *m.* Nodes can be arranged in any order. In this case, nodes were organized by increasing node number. The POD projection matrix is then created the same manner as presented.

In order to create a reduced order model, a function is required. The previously developed state-space equation (Equation 31 and Equation 32) can be utilized, however the associated matrices are reconstructed using an FEM multi-dimensional approach.

Using an 8 node brick element type, a typical interior element is discretized in all three dimensions as –

$$\frac{T_i^{p+1} - T_i^p}{\Delta t} = \frac{\alpha_{i-1,j,k} T_{i-1,j,k}^{p+1} - 2\alpha_{i,j,k} T_{i,j,k}^{p+1} + \alpha_{i+1,j,k} T_{i+1,j,k}^{p+1}}{\Delta x^2} + \frac{\alpha_{i,j-1,k} T_{i,j-1,k}^{p+1} - 2\alpha_{i,j,k} T_{i,j,k}^{p+1} + \alpha_{i,j+1,k} T_{i,j+1,k}^{p+1}}{\Delta y^2} + \frac{\alpha_{i,j,k-1} T_{i,j,k-1}^{p+1} - 2\alpha_{i,j,k} T_{i,j,k}^{p+1} + \alpha_{i,j,k+1} T_{i,j,k+1}^{p+1}}{\Delta z^2} \quad \text{Equation 58}$$

For a uniform mesh, this function can be easily reduced down. The boundary conditions are updated similarly to reflect multiple dimensions. The result is a set of simultaneous equations for the temperatures at the grid points that can then be assembled into matrices identical to the form provided in Equation 31 and Equation 32.

For the multi-dimensional ROM, the matrices used in the state space equation require a bit more effort to generate. The most critical element is assembling the square [A] matrix correctly as this captures the spatial relationship between the nodes. In order to assemble this matrix, a mesh map was created in order to identify neighboring nodes and correctly assemble the spatial matrix [A]. The mesh definition, which includes node number and three dimensional coordinates, was

imported into MATLAB. The spatial coordinates were then converted to integer nodal coordinates by using the nodal spacing. The neighbors of each node can then be quickly identified by incrementing nodal coordinates in each direction. This allows the matrix to be quickly and easily built in MATLAB for use in the ROM. The result is a sparsely banded m x m matrix.

The mesh map is also used to identify nodes that lie on all the surfaces. The boundary conditions are applied to select nodes in the [A] matrix and [D] column vector as well as identify the nodes with the incident heat flux used in the [B] column vector. The [C] column vector can then be adjusted to pull out any nodes of interest e.g. – points, edges, surfaces, etc. The matrices are then reduced using the POD projection matrix using the same procedure previously presented. Material properties, boundary conditions, and source terms are also treated the same way as previously presented. The ROM is then solved by MATLAB using a built-in ODE solver. The reduced space solution sets are then re-projected back to the original space using the POD projection matrix and compared to the full solution. If desired, the results can be displayed in a 3D format by using the mesh map.

3 Nonlinear Material Property Results

Few materials have properties that are constant, independent of temperature. Most materials have properties such as specific heat and thermal conductivity that are uniquely tabulated as a function of temperature as linear or quadratic functions. For nonlinear properties, basic problems that can be solved by hand usually use an estimated set of properties evaluated at an average temperature. However, there is a loss of result accuracy over large temperature ranges when this strategy is employed. The proposed model presented previously provides an approach to apply nonlinear material properties in heat transfer models while maintaining solution accuracy and decreasing the computational costs.

3.1 Nonlinear Material Property Introduction

Several materials with a wide range of material properties were investigated in the model. An initial study was done comparing two reduced order models in order to assess ROM solution accuracy. An Average Nodal Temperature ROM was created by applying constant and nodal-specific material properties based on the average temperature for each node within the spatial-temporal domain of based on the full solution set. A Unique Nodal Temperature ROM was created by re-arranging the material property functions so that they are evaluated with temperature. Thermal response of materials that have nonlinear material properties are rapidly and more accurately predicted using the Unique Nodal Temperature ROM compared to the Average Nodal Temperature ROM.

Through analysis of the POD projection matrix, a method for assessing the optimum reduced order rank was determined, and mode energies were investigated as a function of material property. The model was then used to estimate material thermal response for applied heat flux values unknown a priori using a single POD projection matrix.

3.2 Full Order Model Verification

The two ROMs are created based on results from the same 1D transient heat transfer model. The overall length for model domain was restricted to 0.0254 m. The initial temperature was set to 20 °C (298 K). Convection boundary conditions at both faces were defined by a heat transfer coefficient of 15 $W/m^2 \cdot K$ and an ambient temperature of 20 °C (298 K) was used. Model solutions were generated for times up to 1000 seconds. Initially, snapshots were generated for an applied heat flux of 25 kW/m^2, and the results were used to create a POD projection matrix for use in the two ROMs.

A range of materials properties were investigated using both the Average Nodal Temperature and Unique Nodal Temperature ROMs. Temperature dependence for each of the properties varied amongst the materials and is categorized as temperature independent (constant), linear, or quadratic temperature dependence. A summary of how each parameter was modeled is given below in Table 1.

Table 1. Materials and properties for use in model

Material	Thermal conductivity, k(T)	Specific heat capacity, $c_p(T)$	Density, ρ	Thermal diffusivity, α(T)	1/Volumetric heat capacity, $\frac{1}{\rho c_p}$(T)
AA 5083-H116	Constant	Constant	Constant	Constant	Constant
AA 6082-T651	Linear	Linear	Constant	Quadratic	Quadratic
Stainless Steel 302	Quadratic	Quadratic	Constant	Quadratic	Quadratic
Macor	Quadratic	Quadratic	Constant	Quadratic	Quadratic
Marinite	Constant	Linear	Constant	Quadratic	Quadratic
Unifrax	Quadratic	Linear	Constant	Quadratic	Quadratic

Materials are generally arranged based on decreasing thermal conductivity in Table 1. The AA5083-H116 material with constant properties was used as a baseline as its material response is easy to predict, having constant material properties along with a fairly high thermal conductivity. AA6082-T651 also has a higher thermal conductivity but has properties that change linearly with temperature for both the thermal conductivity and specific heats. Stainless Steel 302 and Macor machinable ceramic have mid-range values for thermal conductivity. Two materials with a low thermal conductivity, Marinite and UNIFRAX Ceramic Board, were also investigated.

Functions for all the material properties were developed based on published values and are shown in Appendix A. Values of thermal conductivity and specific heat capacity were either given as functions of temperature or tabulated at various temperatures. The thermal diffusivity and the inverse volumetric specific heat terms were then determined at discrete temperature values and plotted as a function of temperature. The resulting property distributions were analyzed using a polynomial fitting technique to create continuous functions for use in the ROM. Example material properties for AA6082-T651 are plotted as a function of temperature in Figure 4.

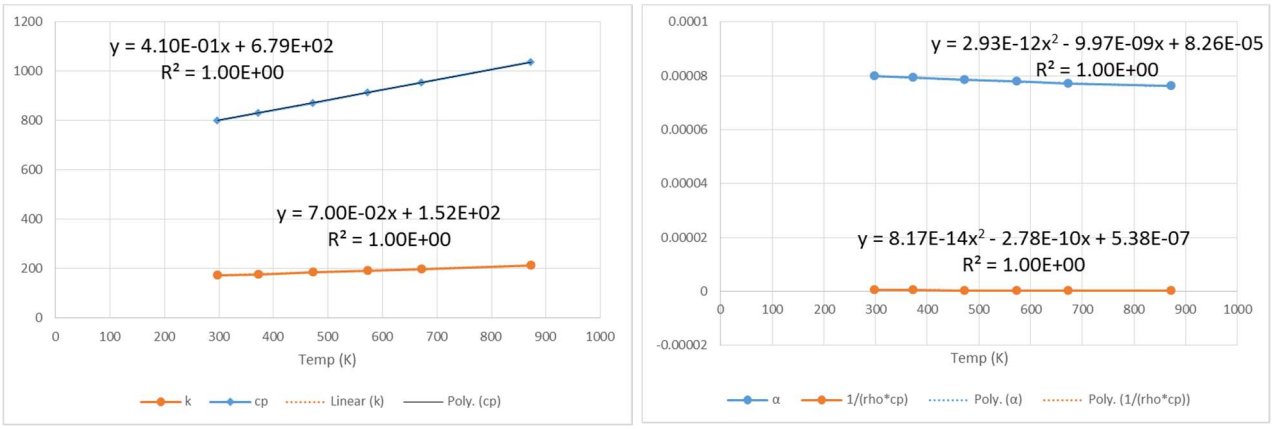

Figure 4. Example material property functions as determined for AA6082-T651 – thermal conductivities and specific heats were given (left), and thermal diffusivity and the inverse volumetric heat capacity were determined (right)

3.3 ROM Rank selection

Reduced order modeling using POD depends on creating a projection matrix that was reduced, as developed by Equation 18. This reduced rank matrix was used to capture the phenomenon of interest while using a limited amount of information in order to maintain accuracy but decrease computational time. The question becomes how to determine the minimum rank necessary to achieve an optimal solution. Proper orthogonal decomposition of a discretized system provides additional insight into the data set, namely energy modes and energy content. Previous research using POD on discretized systems suggests investigating the energy content with rank in order to determine an optimal value. This was done by looking at the eigenvalues, which are the squares of the singular values, determined by singular value decomposition. Eigenvalues are produced for every rank as shown in Figure 5.

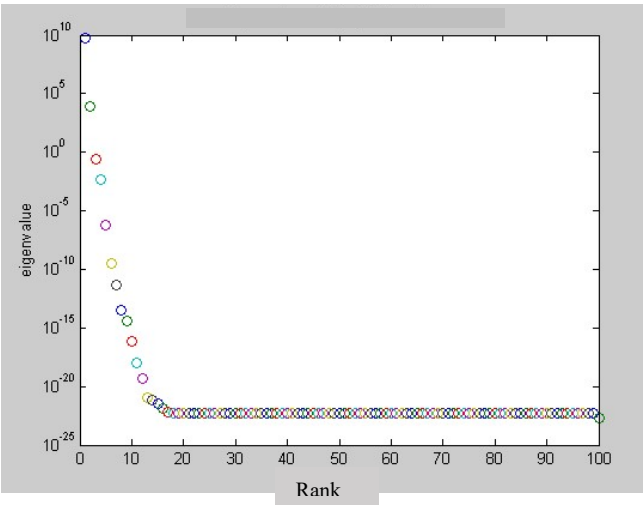

Figure 5. Example output of eigenvalues from Singular Value Decomposition as a function of rank number

Previously, a rule of thumb was presented so that minimum rank was chosen based on the energy content from the SVD that captured 0.999 of the energy as shown in Figure 6 (Chatterjee [60]). However, from a computational standpoint, that criterion was not always sufficient to generate representative solutions for the 1D heat transfer problem with nonlinear material properties. A better approach was to look at the ROM solution accuracy as a function of rank and determine the rank at which the error stabilizes. For this material, the rank associated with the 0.999 energy content was used as a lower bound for the range.

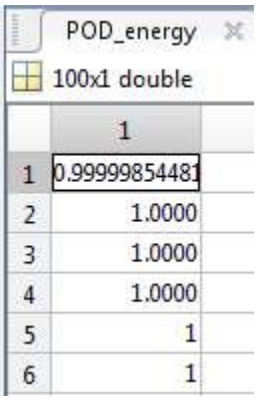

Figure 6. Example output of energy content from Singular Value Decomposition as a function of rank number

Above a certain rank, the reported eigenvalues are smaller than the floating point accuracy of the program used. For MATLAB, the floating point double precision accuracy as determined from the program itself is on the order of 10^{-16}. Therefore, the lowest rank associated with energy content of at least 10^{-16} is considered the upper bound for rank selection for any material.

For each material, relative errors were plotted as a function of rank to determine at what rank the error stabilizes. The average value ROM for nonlinear materials was used for this determination. From the example plot shown in Figure 7, for this particular material the error appears to stabilize at rank 3, therefore this rank was used on subsequent model/material investigations.

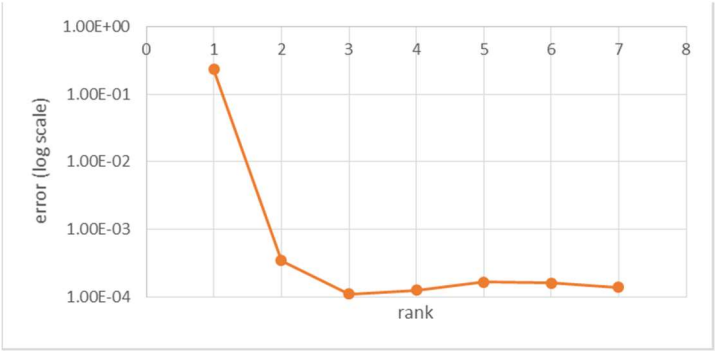

Figure 7. Example plot of relative error as a function of rank

3.4 Average Nodal and Unique Nodal ROMs

The Average Nodal Temperature ROM was developed as an initial attempt to capture material property changes with temperature and to validate the use of POD to predict material response and to establish the approach for investigating the models. Material properties are determined at the average temperature for each node as a function of time. Therefore, material properties are set once and not updated at time increments. This is used as a comparison to the Unique Nodal Temperature ROM. The Unique Nodal Temperature ROM is a refined approach to handle any set of material properties across a wide range of temperatures. In this model, material properties are updated at every node at each time increment as a function of temperature. Both models are initially verified using a material with constant properties so that the use of POD can be validated and to check the implementation of both models. The models are then extended to more complex material properties and compared to each other for differences in accuracy.

3.4.1 AA 5083-H116

The AA 5083-H116 material properties were used as a baseline for ROM development verification and validation, and to establish the approach for investigating the two models. Snapshots were initially generated for this material using a spatial discretization of 1000 nodes and a temporal increment of 1 second for a full time domain of 1000 seconds. By looking at the POD energy content from the SVD for various ranks and numerical accuracy, rank range was determined to be between $r = 3$ and $r = 7$ based on the error stability criteria.

Using the Average Nodal Temperature ROM approach, ROMs were then generated for each rank and compared to the snapshots in terms of solution time and accuracy in order to determine the minimum optimal rank. Time ratios were determined by dividing the Full Order Model (FOM) solution time by the ROM solution time. Results are plotted as a function of rank in Figure 8. From the plot on the left, it is shown that the time ratios decrease with increasing rank. Since the snapshot generation times are the same in each case, the ratio changes are due to the ROM solution times slightly increase with increasing rank. As to be expected, the increase in rank equates to adding columns to POD projection matrix thus an increase in computational time. The plot on the right indicates that the error stabilizes at rank $r = 3$.

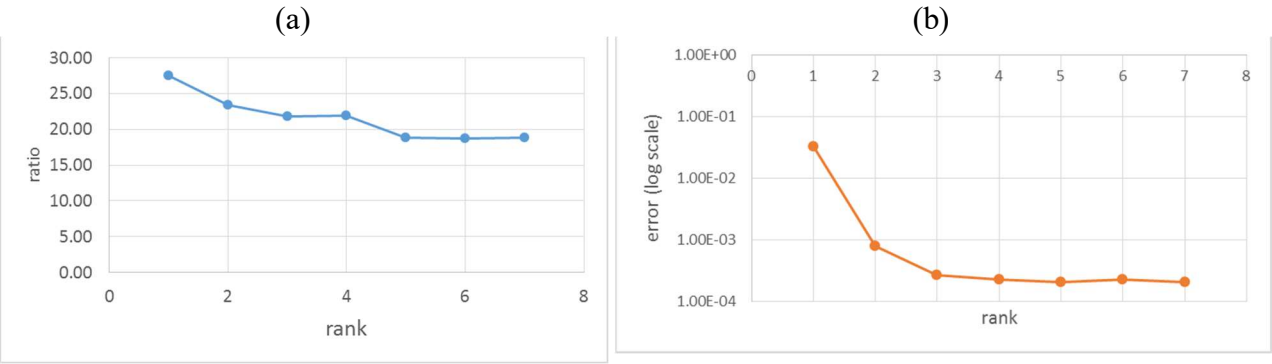

Figure 8. Plots of AA 5083-H113 using the Average ROM (a) Ratio of FOM vs. ROM solution times and (b) Relative Error using the average nodal ROM model

The effects of discretization were also investigated using the optimal rank. Results are presented in Figure 9. From the results shown in Figure 9 (a), as to be expected, ROM efficiency increases with an increase in discretization nodes. This is due to the increase in time to generate the snapshots while the ROM solution time remains constant. However, from Figure 9 (b), with the increase in nodes comes an increase in the time to generate the POD projection matrix since the snapshot data set that is being decomposed is increasing in size. Last, Figure 9 (c) indicates the error is slightly decreasing with an increase in nodes. However, the actual errors are on the order of 10^{-3} and remain within a fairly narrow range for this material. A discretization scheme of 1000 nodes was used for the remainder of the investigation.

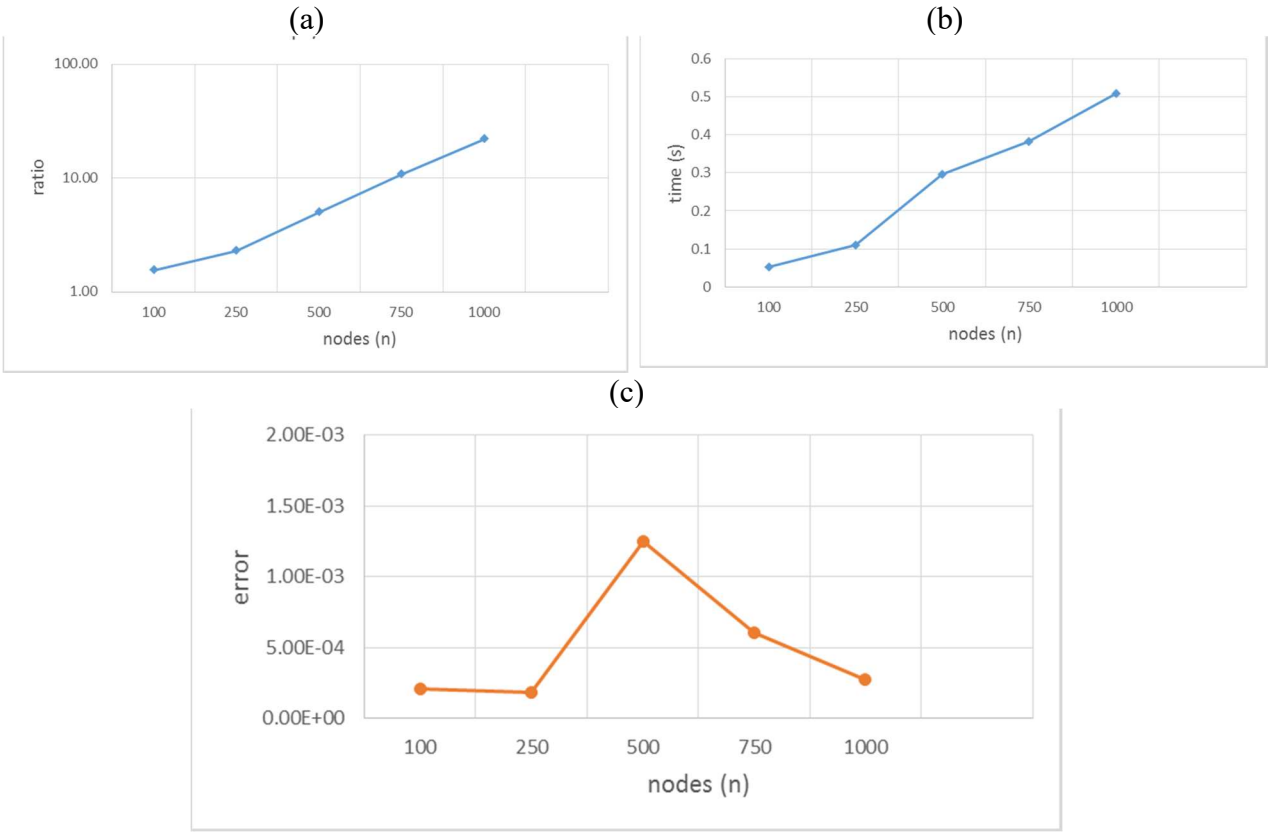

Figure 9. Average Nodal Temperature ROM results for the discretization study on AA 5083-H116 (a) solution time ratio, (b) POD generation time, and (c) Relative Error plotted as a function of increasing discretization using

The Unique Nodal Temperature ROM was investigated similarly. Using the Unique Nodal ROM approach, ROMs were also generated for each rank and compared to the snapshots in terms of solution time and accuracy in order to determine the minimum optimal rank. Results are plotted as a function of rank in Figure 10. Looking at the rank analysis, Figure 10 (a) shows similar time scale results for this model. From the plot of error with rank, Figure 10 (b) indicates that the Unique Nodal ROM also is best suited at rank r = 3. As expected, the error results from both the Average Nodal and Unique Nodal ROMs were the same given the constant material properties.

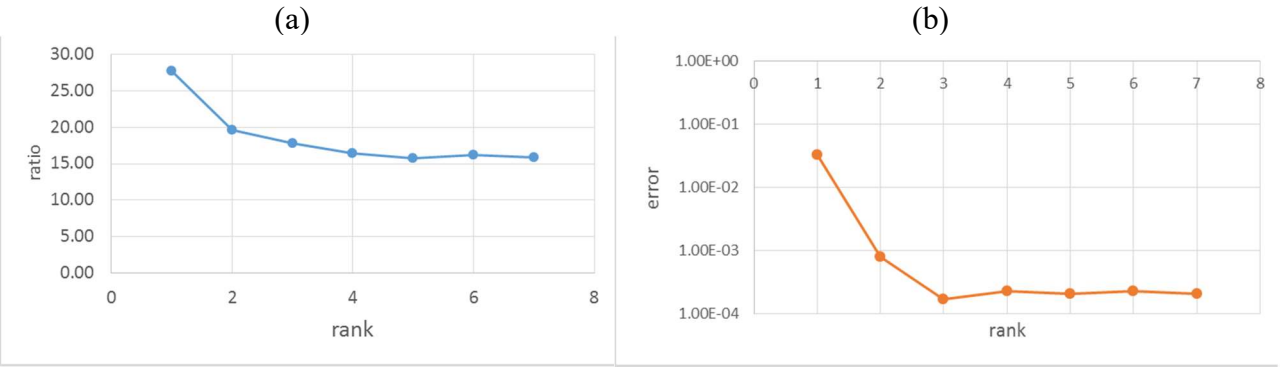

Figure 10. Plots of AA 5083-H113 from Unique Nodal Temperature ROM (a) ratio of snapshot solution times vs. ROM solution times and (b) Relative Error using the Unique Nodal ROM model

Results were then generated using the two ROM approaches with 1000 spatial nodes. Comparisons were made against the full snapshot solution set, generated using the 1D Finite Difference code as shown in Figure 11. From the full solution set, the temperature profile across the sample is flat at every time step as expected due to the material's higher thermal conductivity. Run times and accuracy were generated for each ROM and are summarized in Table 2. As to be expected, the snapshot, POD generation, and ROM solution times are very similar for the two approaches due to the constant thermal properties. It is important to note that since the ROM is an approximation method, it is possible to observe a "ringing" in the solution if insufficient rank is chosen. As seen in Figure 11, there is no "ringing" or oscillations in the solution and it is smooth.

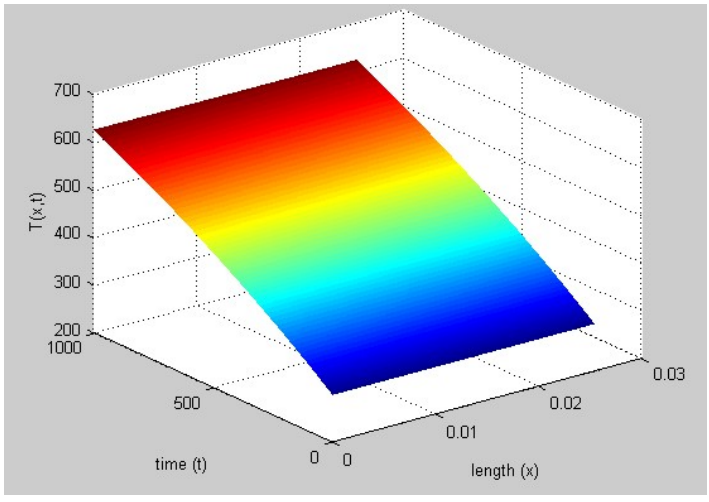

Figure 11. Full solution snapshots for AA 5083-H116

Table 2. Comparison between the two ROMs for AA 5083-H116

Metrics	Average Nodal ROM	Unique Nodal ROM

Snapshot Solution time (s)	5.95	4.32
POD generation time (s)	0.51	0.41
ROM Solution Time (s)	0.27	0.24
t FOM/t ROM	21.85	17.85
Relative Error = norm (Y-yp)/norm(Y)	1.73E-4	1.72E-04

A summary of the models' results are shown in Figure 12, the Average Nodal ROM solution is in the left column, while the Unique Nodal ROM solutions are in the right column. Overall, both ROMs predict the material response well for this particular material with constant properties, and as expected the ROMs produce results that are identical. A method is established for determining optimal rank for use in the ROMs, and the effects of discretization initially show how run times are affected by mesh density.

Average Nodal ROM

(a)

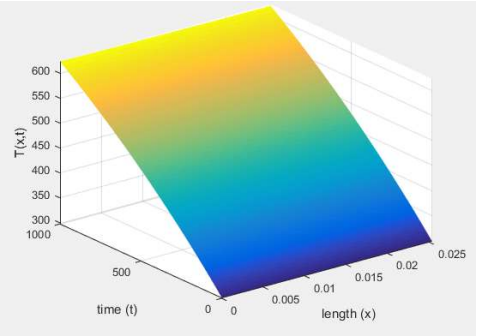

Unique Nodal ROM

(b)

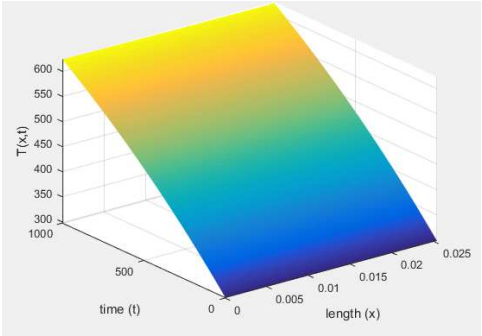

(c)

(d)

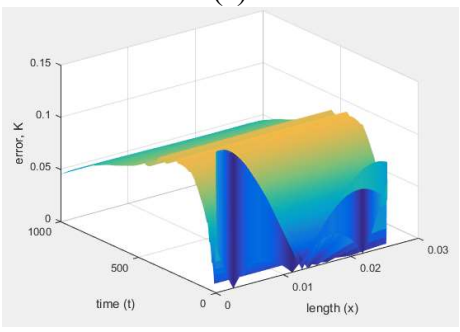

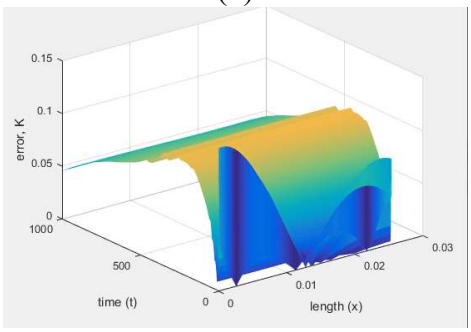

(e)

(f)

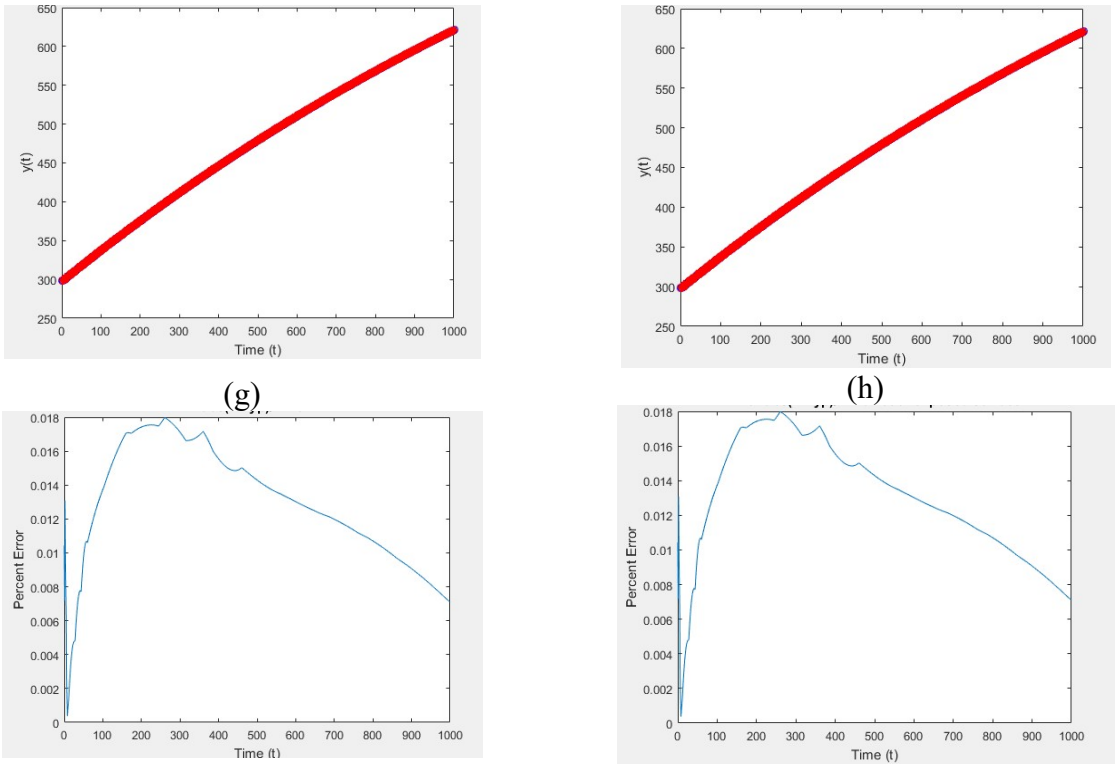

Figure 12. Plots of re-expanded ROM solutions (a) Average and (b) Unique Nodal, errors for ROM solution surfaces (c) Average and (d) Unique Nodal, unexposed surface ROM (red) vs snapshot (blue) solutions for (e) Average and (f) Unique Nodal, and unexposed surface ROM solutions errors for (g) Average and (h) Unique Nodal.

3.4.2 Unifrax Ceramic Board

The two models were then used to investigate a variety of materials including Unifrax ceramic board. This material is particularly challenging to predict as its thermal conductivity is very low and also changes dramatically with temperature. Lower conductivity values drive significant spatial variations in the temperature field. The model properties were updated and the same initial and boundary conditions were applied. The full order model solution from the 1D transient heat transfer model using Unifrax is shown below using a spatial discretization of 1000 nodes and a time increment of 1 second.

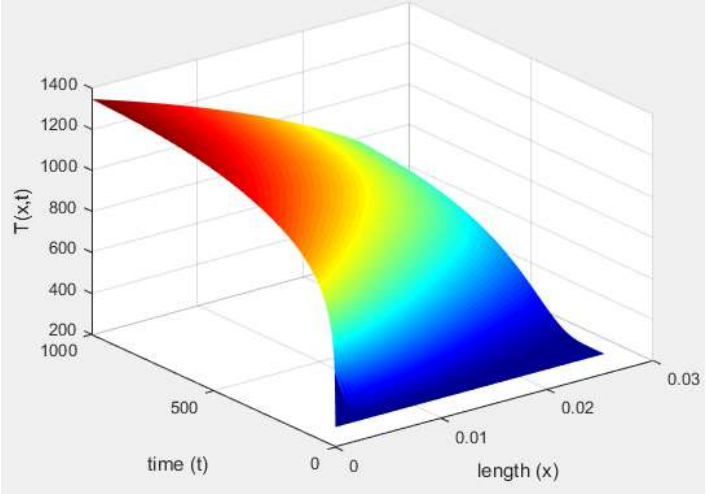

Figure 13. Full solution snapshots for Unifrax

The exposed heat flux face (x = 0) changes temperature rapidly and then levels off, while the unexposed face (x = 0.0254) is slow to experience a temperature increase. The result is a complex solution surface that curves dramatically in both the spatial and temporal domains.

Using the approach outlined above, errors determined at increasing rank using the Average Nodal Temperature ROM in order to determine an optimal rank are provided in Figure 14. For this material, ROM solution effectivity decreases slightly with increasing rank as shown in Figure 14(a). Looking at the change in error with rank Figure 14(b), there is an initial drop in error and then some oscillations are present. Due to the complex nature of this material, rank r = 5 was chosen beyond these fluctuations in order to ensure more accurate results from the model. It should be noted that using the energy content approach for rank selection, shown in Figure 15, would have resulted in using rank r = 2 which would not have sufficiently captured the material behavior across the entire spatial-temporal domain. Again, since the ROM is an approximation method, it is possible to observe a "ringing" in the solution if insufficient rank is chosen. As seen in Figure 14, there is no "ringing" or oscillations in the solution and it is smooth.

(a)

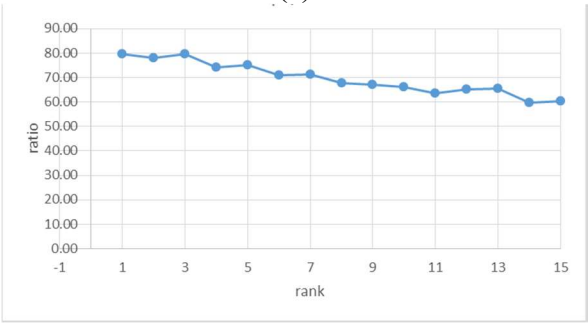

(b)

Figure 14. Plots of Unifrax rank results from the Average Nodal Temperature ROM (a) ratio of snapshot solution times vs. ROM solution times and (b) Relative Error using the Unique Nodal ROM model

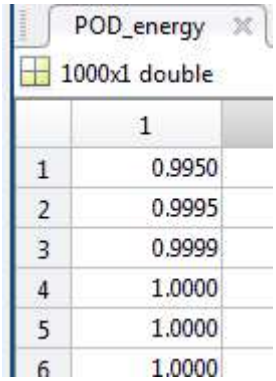

Figure 15. Output of energy content from Singular Value Decomposition as a function of rank number for Unifrax.

Run times and accuracy were generated for each ROM and are summarized in Table 3. As to be expected, the snapshot, POD generation times are very similar. The ROM solution time are almost twice as long for the Unique Nodal ROM which is likely due to the increased effort needed by the solver to handle the higher order material properties. The result is a speed up that is still significant (50 times), but not as high as with the Average Nodal ROM (92 times). There is significant difference also in the relative error. The relative error produced by the Unique Nodal ROM solution is smaller than the Average Nodal ROM error.

Table 3. Comparison between the two ROMs for Unifrax

Metrics	Average Nodal ROM	Unique Nodal ROM
Snapshot Solution time (s)	18.44	18.39
POD generation time (s)	0.37	0.35
ROM Solution Time (s)	0.20	0.36
t FOM/t ROM	92.11	50.64
Relative Error = norm (Y-yp)/norm(Y)	8.06E-02	1.75E-03

A summary of the models' results are shown in Figure 16, the Average Nodal ROM solution is in the left column, while the Unique Nodal ROM solutions are in the right column. Overall, the Unique Nodal ROM predicts the Unifrax material response better than the Average Nodal ROM. Looking specifically at the re-expanded solutions, Figure 16 (a) and (b), the Uniquely Nodal ROM captures the solution better across the entire node set at the largest time increment. Additionally, the steep change in temperature for the node at the exposed heat flux face is better represented in the Unique Nodal model. Looking at the overall errors, Figure 16 (c) and (d) as well as Figure 17(a) and (b), shows that the scale of errors across the entire domain is decreased by a full order of magnitude. Last, Figure 16 (e) and (f), which show the actual results at the

unexposed surface, further show that the Unique Nodal ROM more fully captures the material response.

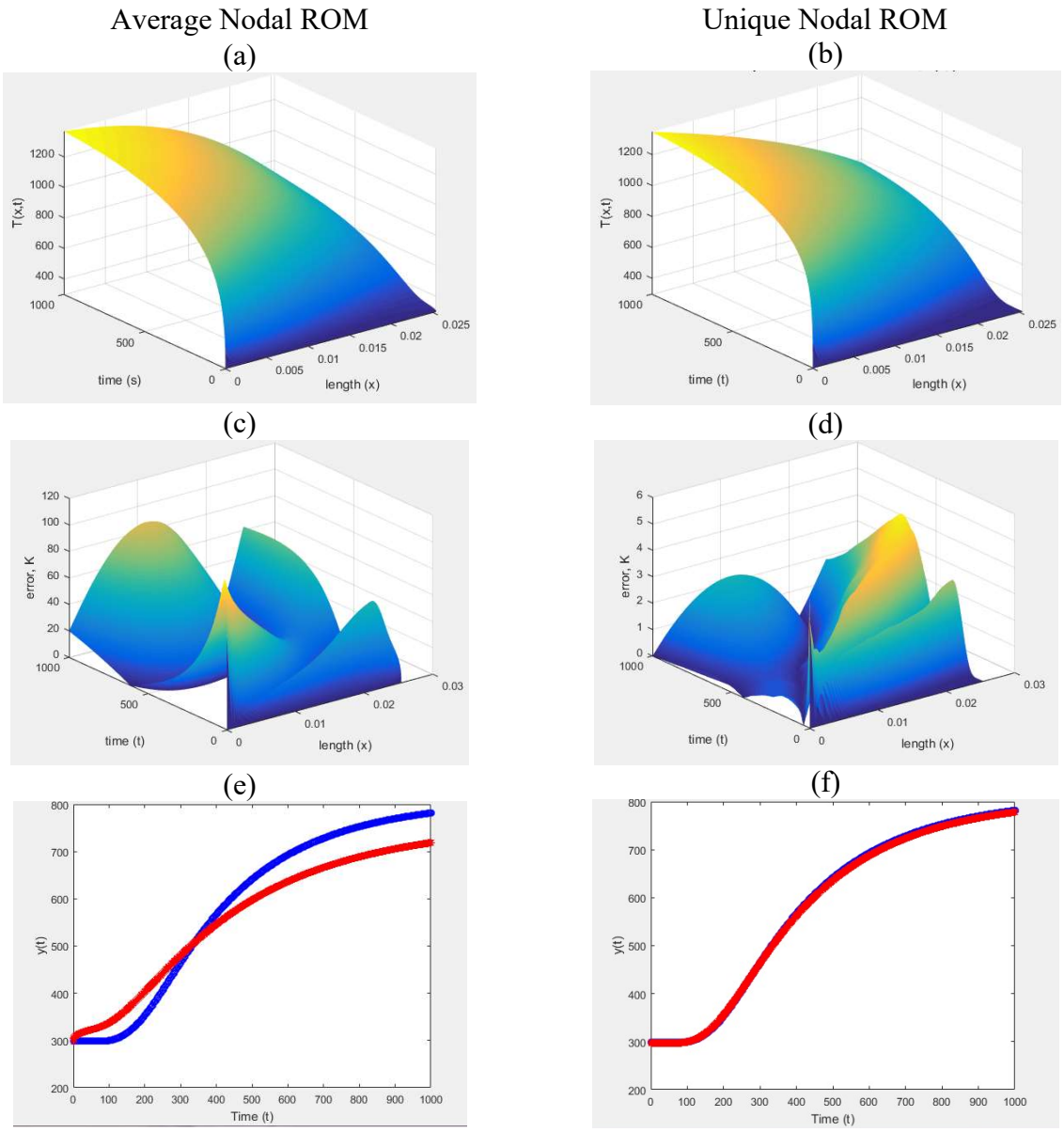

Figure 16. Plots of re-expanded ROM solutions for Unifrax material (a) Average and (b) Unique Nodal, errors for ROM solution surfaces (c) Average and (d) Unique Nodal, unexposed surface ROM (red) vs snapshot (blue) solutions for (e) Average and (f) Unique Nodal.

Average Nodal ROM
(a)

Unique Nodal ROM
(b)

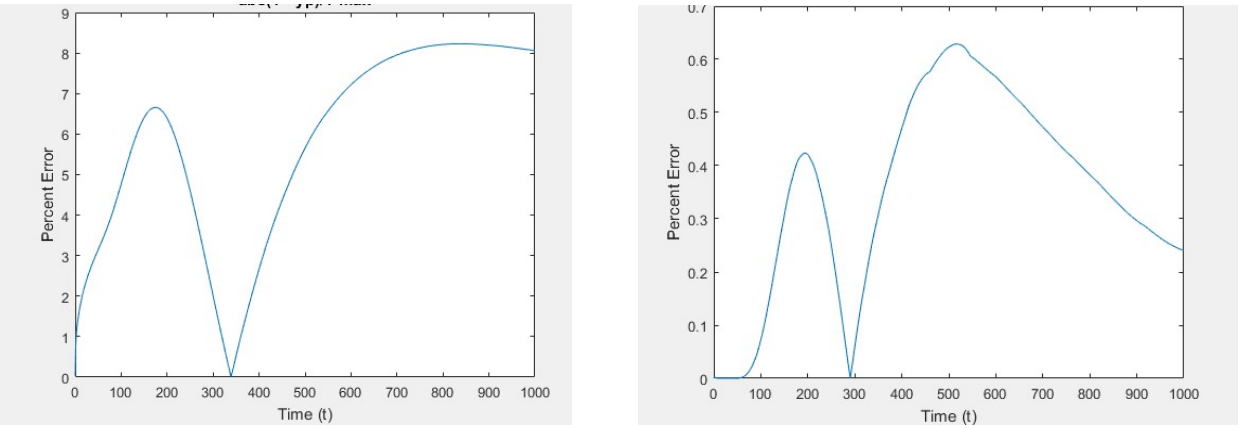

Figure 17. Plots of re-expanded ROM solutions for Unifrax material unexposed surface ROM solutions errors for (a) Average and (b) Unique Nodal.

The method for determining optimal rank in the ROMs appeared to work well, and is an improvement from previous work. In particular, the Unique Nodal ROM evaluates the temperature dependent properties within the ROM and results in a solution that is better approximated in both space and time. Previous research has also shown that re-projecting a ROM solution back to the original space may result in a loss of accuracy (Antoulas [1]). That does not appear to be the case for either ROM.

3.5 Increased Spatial Discretization

A study was performed to evaluate the impact of increasing spatial discretization for two materials (AA 5083 and Unifrax). After establishing the optimal rank for each material, discretization effects were investigated by holding all parameters constant except for the spatial increment. Spatial increments of 100, 250, 750, 1000, 5000 evenly spaced nodes were investigated while the temporal increment was held constant at 1 second. Full solution snapshot times, POD generation times, ROM solution times, and POD relative error was captured for each increment. Results were plotted as a function of discretized nodes. The ratio of time to produce a full solution versus the time to execute the ROM was plotted against node count. This investigation was done using the Unique Nodal Temperature ROM. The results provide a sense of scale on how effective a ROM approach might be for other discretized systems with a larger mesh size.

Results for the AA 5083 material are presented in Figure 18. The results in the Figure 18(a) demonstrate that the efficiency of the ROM run time increases dramatically with mesh density while POD generation times (see Figure 18(b)) and ROM errors remain relatively flat (see Figure 18(c)). Errors across the solution surfaces are shown for 50 nodes and 5000 nodes (see Figure 18(d) and (e)), and show a similar range of errors across the solution domain.

(a) (b)

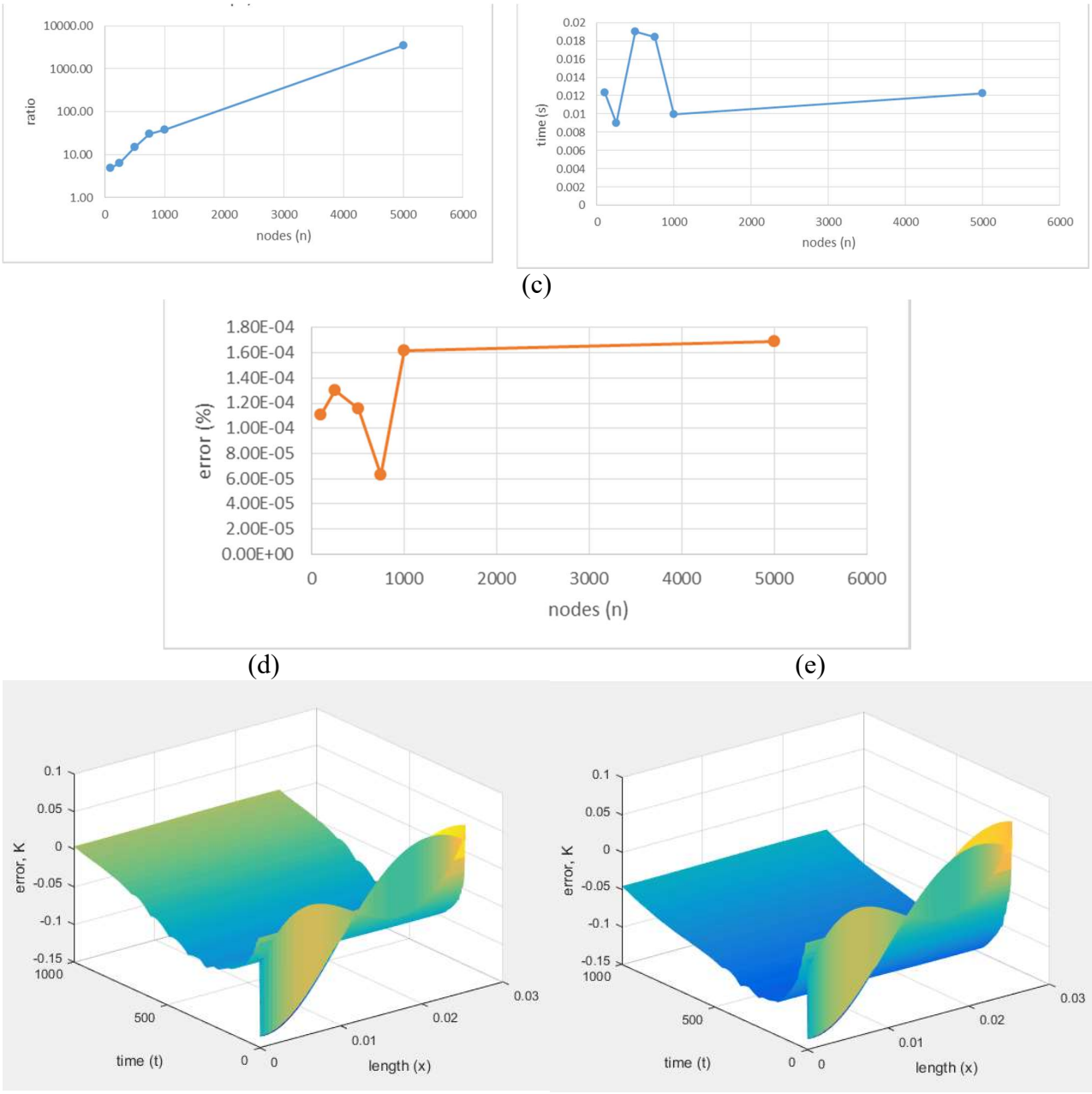

Figure 18. Plots of advanced discretization results for AA 5083 material using Unique Nodal Temperature ROMs (a) ratio of snapshot solution times vs. ROM solution times, (b) POD generation times, (c) Relative Error, (d) surface errors for 50 nodes, and (e) surface errors for 5000 nodes.

Results for the Unifrax material are presented in Figure 19. Similar to the AA 5083 results, the Unifrax simulation results in Figure 19(a) show that the efficiency of the ROM run time increases dramatically with mesh density while ROM errors remain relatively flat and POD generation time starts to increase significantly with larger mesh size up to 1000 nodes (see Figure 19(b)). Errors across the solution surfaces are shown for 50 nodes and 10 000 nodes (see Figure 19 (d) and (e)), and show a similar range of errors across the solution domain.

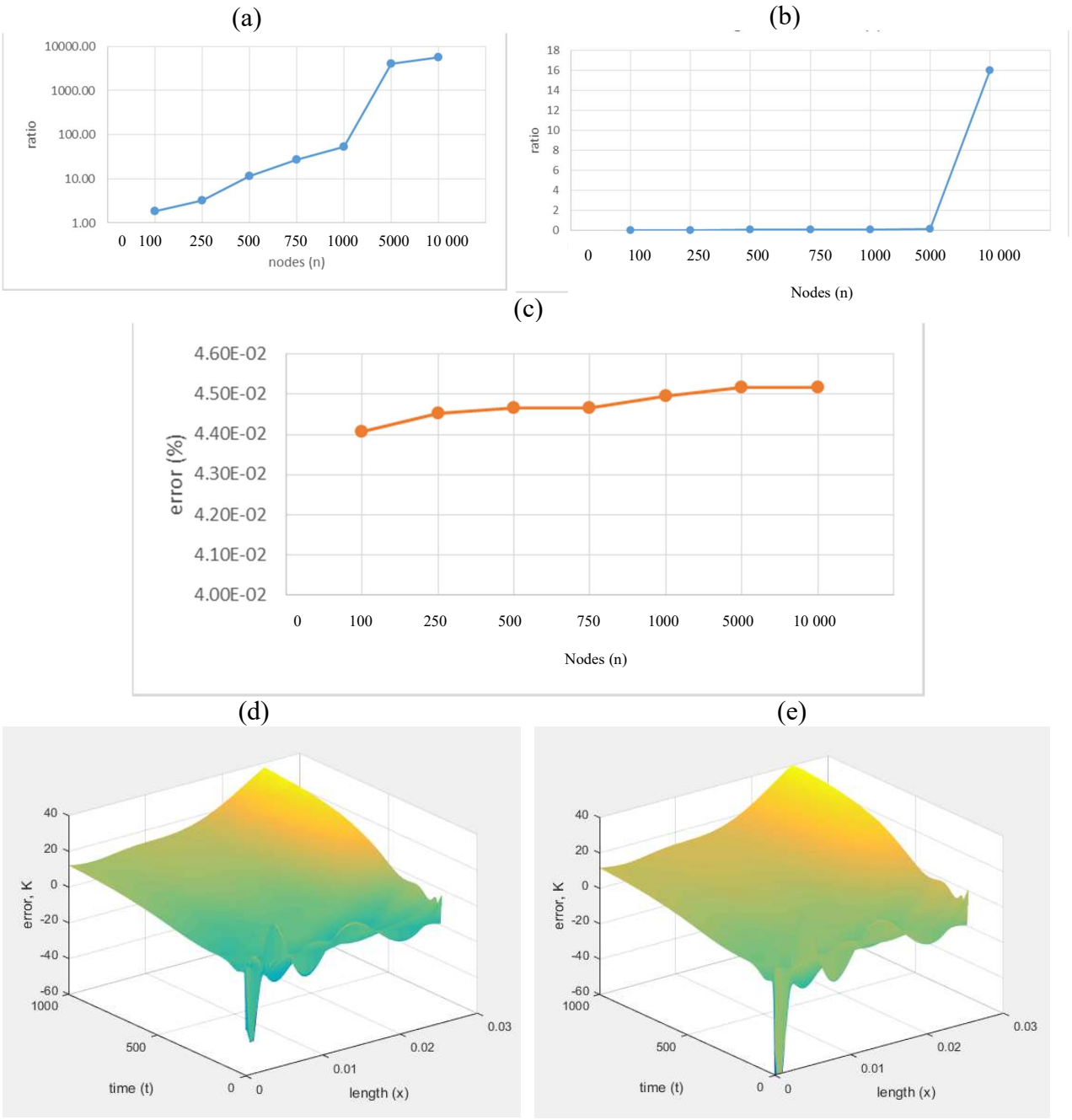

Figure 19. Plots of advanced discretization results for Unifrax material using Unique Nodal Temperature ROMs (a) ratio of snapshot solution times vs. ROM solution times, (b) POD generation times and (c) Relative Error, (d) surface errors for 50 nodes, and (e) surface errors for 5000 nodes.

3.6 Estimated Heat Flux Results

Ultimately, one would want to use the ROM to predict the material response when exposed to boundary conditions different than those used to construct the ROM. The ROM was then investigated as a method to predict material responses for other applied heat flux values using a single POD projection matrix as an additional way to save computational time. This investigation was done using the Unifrax material. Several different PODs were created using a variety of initial inputs to generate snapshots and determine an optimal projection matrix as shown in Table 4. This included lower and higher constant heat flux values as well as a step function and a ramp function. The step function is defined with 5 step intervals from 0 to 200 (kW/m^2) evenly spaced within the time domain. The ramp function is a linear ramp from 0 to 200 (kW/m^2) within the time domain. POD projection matrices were determined for each of the input functions (known heat fluxes). They were then applied to the ROM and used to estimate material responses for unknown applied heat flux values. The results from the ROM were compared back to separately determined full order model results using the unknown applied heat flux.

Table 4. Table of Initial Heat Flux values used to create a ROM and the associated heat flux values that are investigated by the ROM

Known Heat Flux (kW/m^2)	Estimated Heat Flux Values (kW/m^2)						
5	-	10	25	50	100	150	200
25	5	10	-	50	100	150	200
50	5	10	25	-	100	150	200
Step Function	5	10	25	50	100	150	200
Ramp Function	5	10	25	50	100	150	200

The error results for all of the ROMs are presented in Figure 20. From the plot, the ROM created from the lowest heat flux, u(t) = 5 kW/m^2, predicts material response fairly well up to 50 kW/m^2. Beyond that, the model is no longer effective. Increasing the initial heat flux term leads to better material prediction at both higher and lower estimated heat flux values. This is likely because these PODs contain information about the system response for a larger temperature range. The PODs based on a higher maximum input heat flux predict other heat flux results that are equivalent or lower.

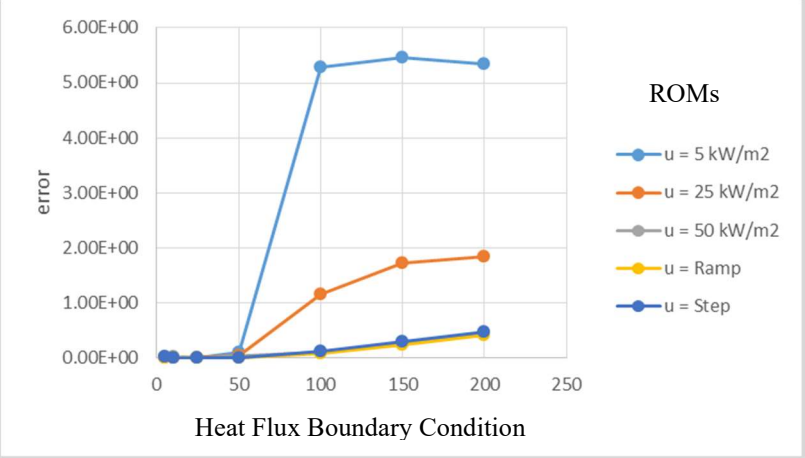

Figure 20. Relative errors for each ROM shown for estimated heat flux values.

The results presented in Figure 21 show the ROM computational times for re-use after the initial set of snapshots are generated, the POD is determined, and the ROM is created. From the plot, the ROMs all performed at generally the same speeds, however the ROM from the step function was on average 7% faster across the full range of estimated heat flux values. Based on both speed and accuracy, the step function is the optimal choice for generating an initial ROM to estimate these additional unknown heat flux values.

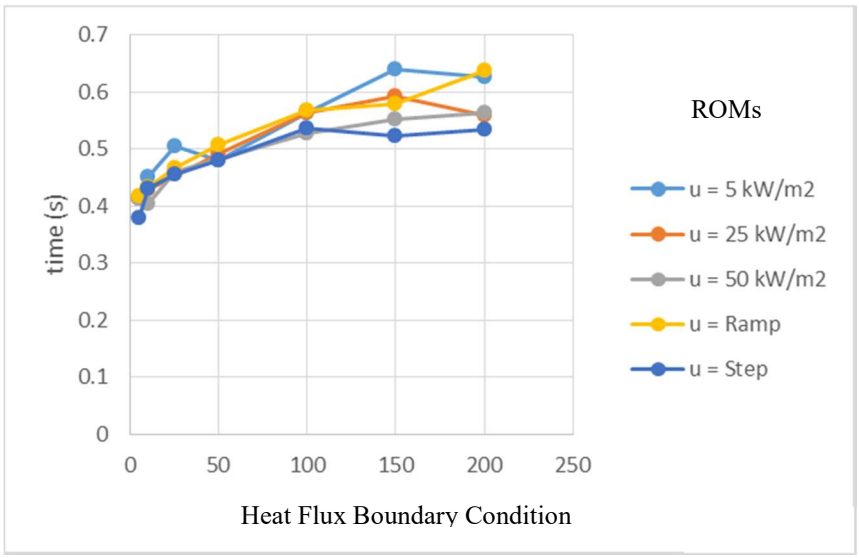

Figure 21. Computational re-use times for ROMs developed from various input conditions used to estimate unknown Heat Flux Boundary Conditions.

3.7 Summary

Nonlinear temperature dependent material properties were treated in the full order model and in two ROMs. Optimal rank was determined by looking at errors as a function of rank, and

identifying the lowest rank where errors stabilized. An Average Nodal Temperature ROM was developed using constant temperature properties determined at time-averaged temperatures. A Unique Nodal Temperature ROM was then developed to determine material properties uniquely at each time step as a function of temperature. The Unique Nodal Temperature ROM reduced errors by an order of magnitude and still achieved a computational efficiency of over 50 times the full scale model for Unifrax properties in a lower mesh density (n = 1000). Mesh density was further investigated up to 5000 nodes using the Unique Nodal Temperature ROM and AA 5083 and Unifrax material properties. Scaling up in mesh density resulted in a computational efficiencies of around 10 000 over the full scale model while errors remained flat.

4 Nonlinear Boundary Conditions Results

Radiation plays a large role in affecting material response at high temperatures. While other boundary conditions such as convection are easily modeled, the nonlinear nature of the radiation term makes it computationally expensive. A method of linearizing the radiation term allows it to be integrated into a full scale model while still providing accurate results. The proposed model presented here provides an approach to incorporate the radiation boundary condition terms within the reduced order model while maintaining accuracy and decreasing the computational costs.

The previously developed Unique Nodal Temperature ROM developed in Section 2.3.3 was advanced to include radiation terms at the boundaries. Several materials with different emissivity values were investigated in this research. Optimal rank was determined by the previously presented error-based method, and results showed that the additional nonlinearity at the boundaries required a higher rank. The results were then further investigated by use of POD Modal Energy Analysis in order to confirm that additional rank was needed to resolve fitness at the boundaries.

4.1 Full Order Model Verification

The 1D transient model in MATLAB was updated to include radiation effects at the boundaries. This model development is detailed in developed in Section 2.4.3. The model was verified using a 3D Abaqus model modified to restrict heat transfer to one dimension. As shown in Figure 22, a 3D rectangular prism was constructed with one dimension much larger than the other two, and one dimensional heat transfer configuration was imposed by insulating the faces parallel to the length. The overall length for the validation model domain was 1 m. The initial temperature was set to 0 °C (273 K). Convection boundary conditions at the small faces were defined by a heat transfer coefficient of 1 $W/m^2 \cdot K$ and an ambient temperature of 0 °C (273 K) was used. Radiation boundary conditions were also defined at these faces using the same ambient temperature and an emissivity of 0.5. Constant material properties were used, and the surface heat flux applied at one face was 1 W/m^2. The model was run to steady state.

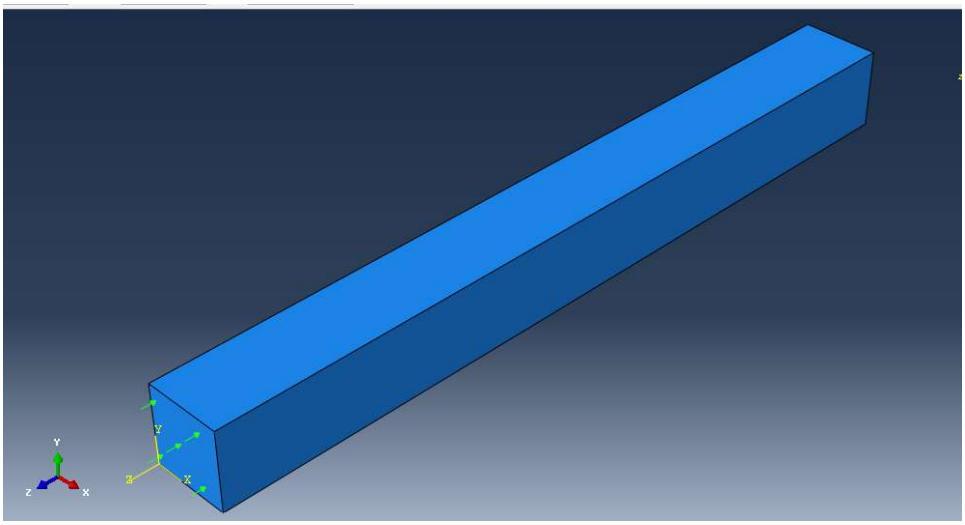

Figure 22. Abaqus 3D model used for verification on 1D finite difference model.

The results from the 1D finite different model in MATLAB and Abaqus are provided in Figure 23. From the plot, the full order model predicts radiation boundary conditions as well as the known commercially available software. Comparing 5 equally spaced nodes with the sample, at the worst case the 1D finite difference code was able to predict within 0.1% of the Abaqus model.

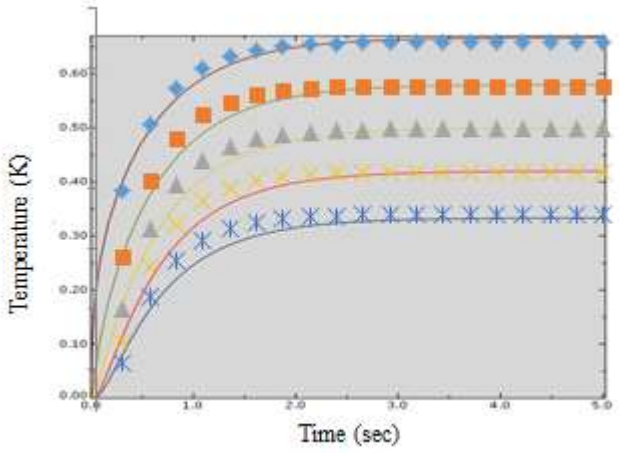

Figure 23. Results from full order finite difference model (symbols) and Abaqus model (lines) using radiation boundary conditions.

The finite difference model was then updated to assess radiation boundary conditions in conjunction with real material properties, with and without nonlinear temperature dependence. The problem was also updated to reflect realistic physical conditions. The overall length for model domain was 0.0254 m. The initial temperature was set to 20 °C (298 K). Convection boundary conditions at both faces were defined by a heat transfer coefficient of 15 $W/m^2 \cdot K$ and an ambient temperature of 20 °C (298 K) was used. Radiation boundary conditions were also added at both faces and were defined with a settable emissivity value and the same ambient

temperatures used in convection conditions. Model solutions were generated for times up to 1000 seconds. Initially, snapshots were generated for an applied heat flux of 25 kW/m^2, and the results were used to create a POD projection matrix for use in the ROM. AA 5083 and Unifrax material properties were then used to investigate radiation effects at the boundaries. Worst case emissivity values of 0.9 were used in both cases.

Full order 1D model solutions are shown in Figure 24 for constant property AA 5083 material with convection only boundary conditions as well as convection and radiation boundary conditions. From the results, the AA 5083's constant material properties are such that there is a very weak thermal gradient within the sample. The addition of the radiation boundary condition decreases the temperatures experienced by the material by approximately 100 K at maximum time compared to the case with convection only.

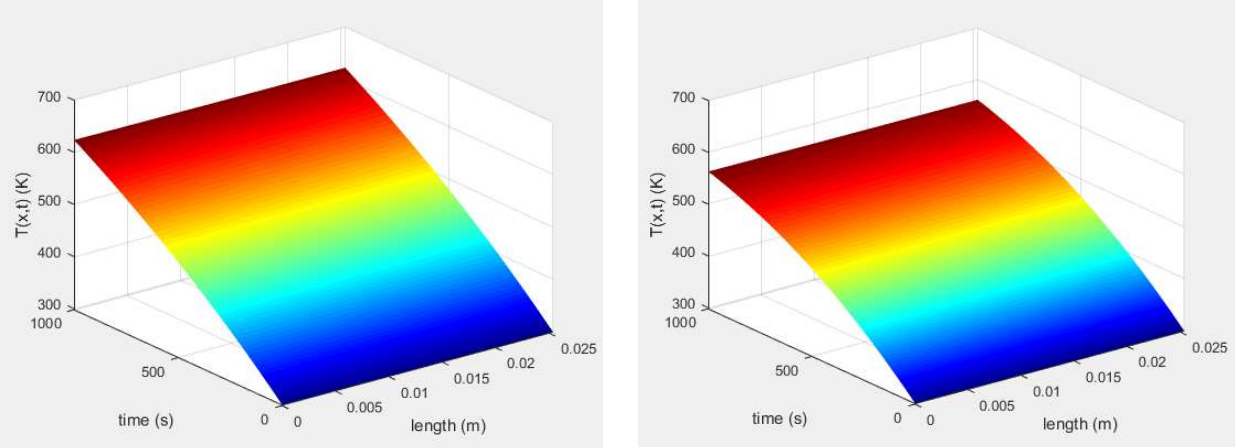

Figure 24. Full order model solutions for AA 5083 with convection boundary conditions only (left) and with convection and radiation boundary conditions (right).

Full order 1D model solutions are shown in Figure 25 for highly nonlinear temperature dependent Unifrax material with convection only boundary conditions as well as convection and radiation boundary conditions. From the plot, Unifrax has a significant thermal gradient within the sample, and the additional radiation boundary condition drives the response temperatures down by around 700 K through the sample. This demonstrates that radiation boundary effects can significantly affect material response and need to be accounted for in a reduced order model.

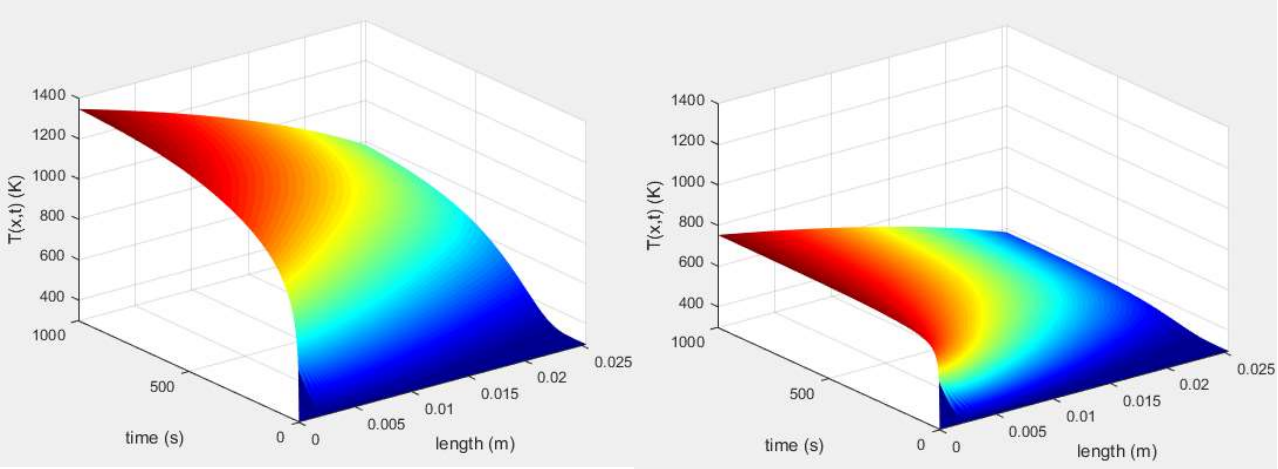

Figure 25. Full order model solutions for Unifrax with convection boundary conditions only (left) and with convection and radiation boundary conditions (right).

4.2 POD Rank selection

Rank was investigated to determine if the radiation nonlinearity drives changes to the POD projection matrix rank for an associated material. The previously developed method of assessing error stability with increasing rank was used to determine optimal rank. The addition of the radiation term affects the optimal rank for each material. Plots of eigenvalues as a function of rank are shown for AA 5083 material for a case with convection only and a case with convection and radiation are shown in Figure 26. The plot is restricted to the first 20 eigenvalue ranks for clarity. The eigenvalue sets are very similar, however there is a slight difference starting at Rank 4 and then there is a noticeable separation between the eigenvalue sets at Rank 7. Individual energy modes (solution sets corresponding to individual ranks) are further explored in Section 4.4.

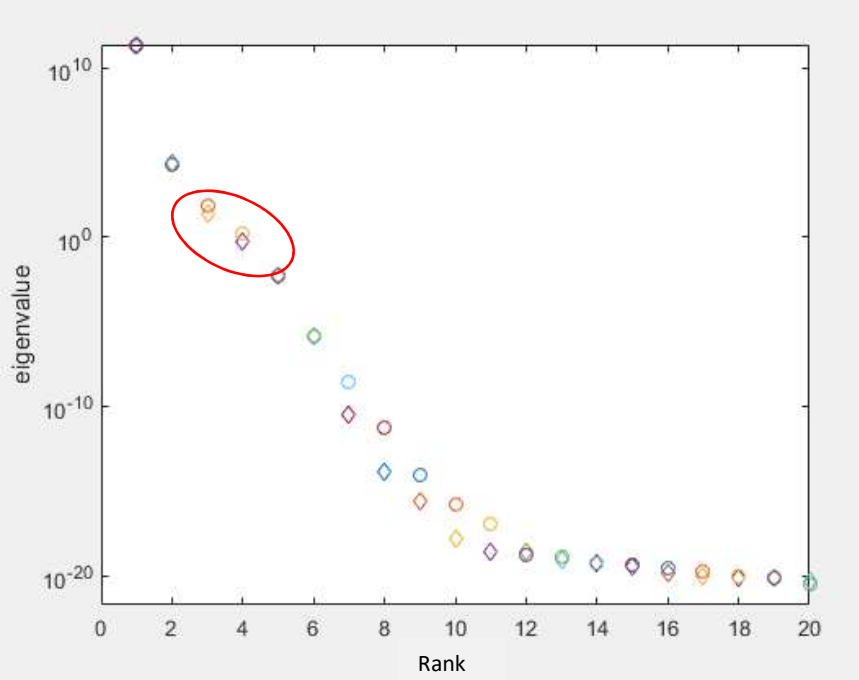

Figure 26. Eigenvalues for AA 5083 POD with convection only (diamond) and with convection and radiation boundary conditions (circle)

POD analysis may be used to determine how impactful the nonlinearities will be to the solution set. From the 5083 simulation, there are several important implications. The first is that with the addition of the radiation term nonlinearity shows up in the energy content, and therefore POD analysis can be used to identify the addition of nonlinearities. The second is that the energy content decreases at rank 3 for this material. Since the eigenvalues are arranged in descending order, this indicates the additional nonlinearity due to radiation contributes to the shape of the solution surface, but is not the most significant element. Also, the solution set has a decreased thermal response in the case where radiation is added, and that is seen in the decrease in eigenvalues.

Similarly, eigenvalues for the Unifrax material shown in Figure 27 show that the convection plus radiation results (circle) drive lower overall values compared to convection only. This is likely due to the decreased temperatures observed in the solution set. A more detailed look at error will be necessary to determine an optimal rank. Compared to the AA 5083 data, the two sets of eigenvalues are very different. The addition of nonlinearity due to radiation is not as clearly evident in the upper ranks, and it may be that the radiation nonlinearity shows up in rank r = 1.

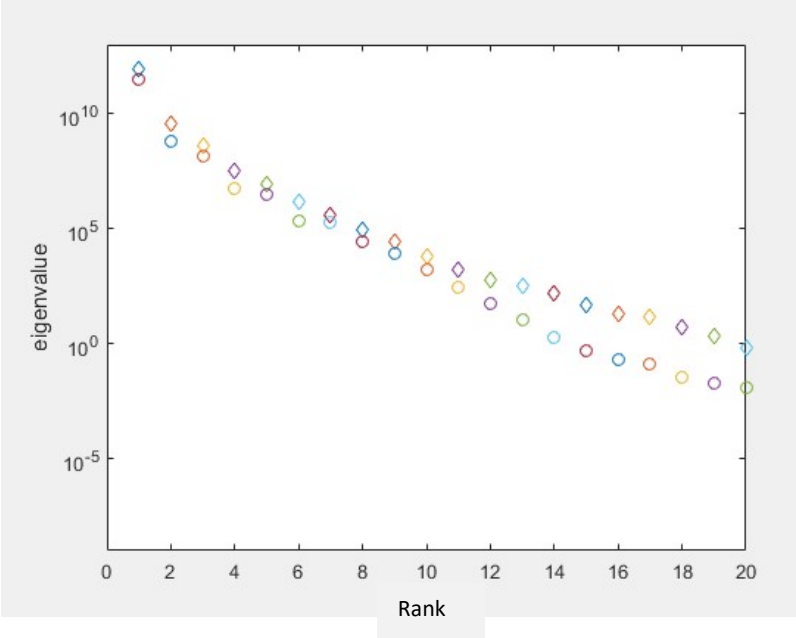

Figure 27. Eigenvalues for Unifrax POD with convection only (diamond) and with convection and radiation boundary conditions (circle)

4.3 ROM with Radiation

Boundary conditions were updated in the Unique Nodal Temperature ROM to reflect the radiation condition. The linearized radiation term was included as part of the modified heat transfer coefficient similar to the full order model. However, in order to keep the ROM boundary condition matrix constant, a time-average temperature value at each surface node is used in the radiation portion of the combined heat transfer coefficient value. For the overall convection treatment, surface nodal temperature is still treated as a unique nodal temperature.

4.3.1 AA 5083 Results

The AA 5083 material properties were used as a baseline for radiation ROM development verification and validation in order to remove the effects of temperature dependent material properties. The radiation term was linearized in the full order model to allow for easier and faster computation. Snapshots were initially generated for this material using a time increment of 1000 seconds. By looking at the POD energy content from the SVD for various ranks and numerical accuracy, rank range was determined to be between r = 4 and r = 9 based on energy content and digital accuracy. ROMs were generated for each rank and compared to the snapshots in terms of solution time and accuracy in order to determine the minimum optimal rank. Results for both are plotted in Figure 28. Compared to the case without radiation, optimal rank increased for this material from r = 3 to r = 4. In addition, ratios of computational run times were determined at each rank as full order model run time over reduced order run time. Computational efficiency of the ROM against the full order model show that it is about 15 times faster than the full order.

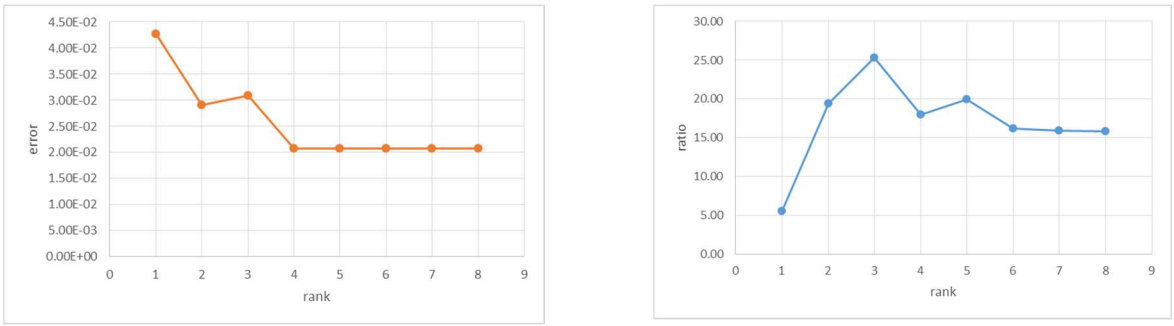

Figure 28. Solution error as a function of rank for AA 5083 material with radiation at boundaries *(left) and r*atio of solution times *(right)*.

The errors across the entire solution set as well as a closer look at the exposed face, center, and exposed face are presented in Figure 29. From the plots, the AA 5083 material with radiation at the boundaries is fairly well predicted by the ROM. The ROM had some difficulty resolving the problem at around 800 seconds across the entire node range. This may be a result of using a constant temperature value in the linearized radiation term for this material. Despite that, looking at the error across the full solution set, using rank r = 4 allows for a maximum error of about 2.5%.

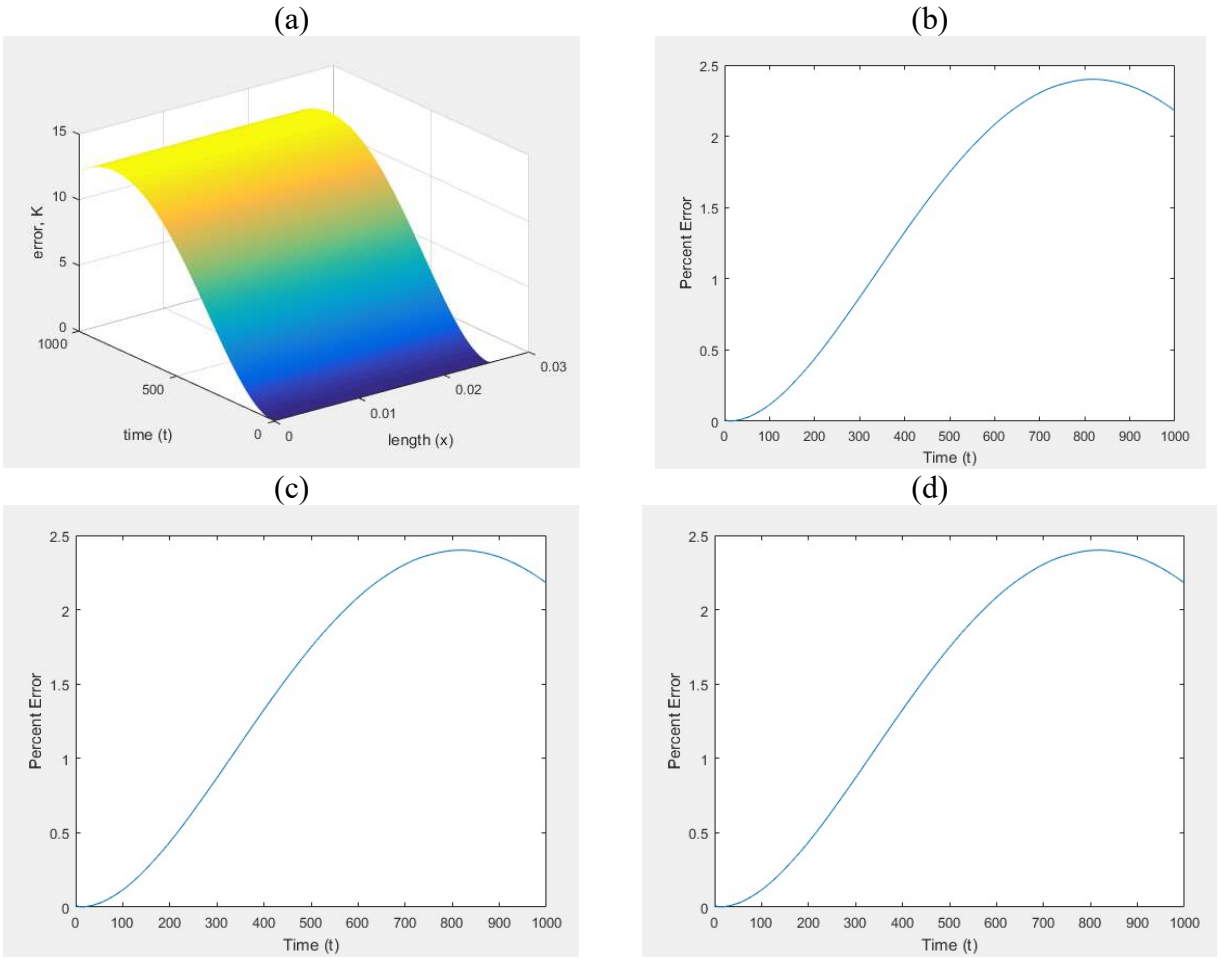

Figure 29. ROM with AA 5083 material properties and radiation boundary conditions (a) absolute error, (b) maximum relative error at x = 0, (c) maximum relative error at x = L/2, and (d) maximum relative error at x = L.

4.3.2 Unifrax Ceramic Board Results

The effect of radiation boundary conditions on a low thermal conductivity material was also investigated to see how well the ROM works with multiple sources of nonlinearities. Snapshots were initially generated for this material using a time increment of 1000 seconds. By looking at the POD energy content from the SVD for various ranks and numerical accuracy, rank range was determined to be between r = 3 and r = 50 based on energy content and digital accuracy. ROMs were generated for each rank and compared to the snapshots in terms of solution time and accuracy in order to determine the minimum optimal rank. Results for both are plotted in Figure 30. Compared to the case without radiation, optimal rank increased for this material from r = 6 to r = 12. Computational efficiency of the ROM against the full order model show that it is about 40 times faster than the full order.

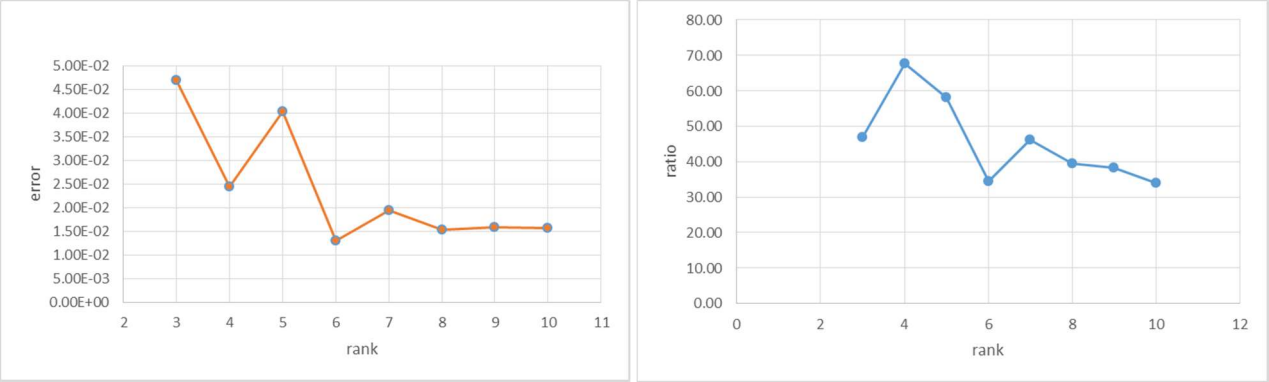

Figure 30. Solution error as a function of rank for Unifrax material with radiation at boundaries (left) and ratio of solution times (right).

The errors across the entire solution set as well as a closer look at the exposed face, center, and exposed face are presented in Figure 31. The Unifrax material with radiation at the boundaries is also fairly well predicted by the ROM. The ROM had the most difficulty resolving the problem during the transient range at the face where the heat flux was applied (x = 0). At the worst case, the ROM has a maximum 5.5% relative error.

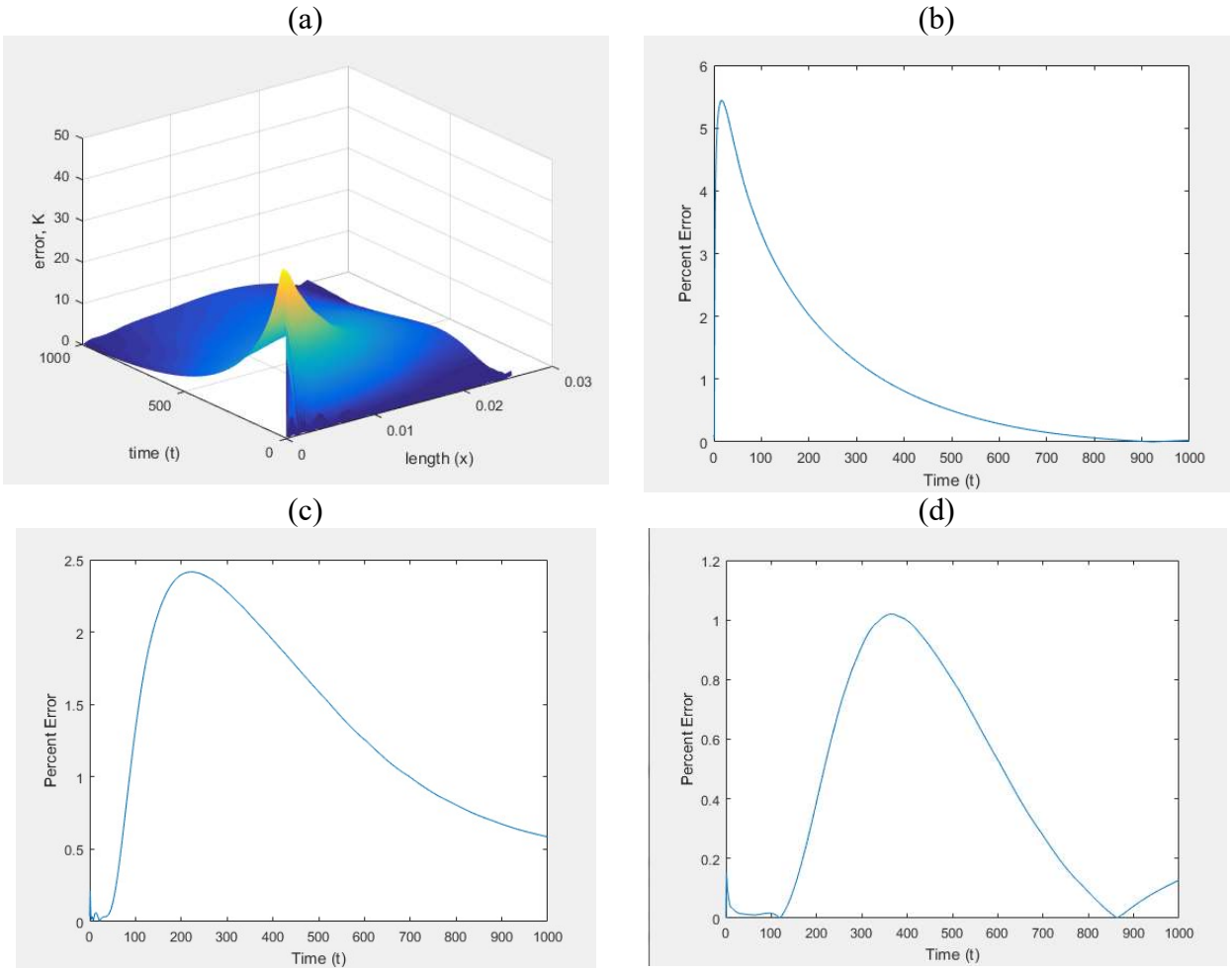

Figure 31. ROM with Unifrax material properties and radiation boundary conditions (a) absolute error, (b) maximum relative error at x = 0, (c) maximum relative error at x = L/2, and (d) maximum relative error at x = L.

4.4 Modal Energy Analysis

The two materials are additionally explored using Modal Energy Analysis. Aside from using the eigenvalues to determine the optimal rank, successive solutions surface are generated to see where within the solution set information or energy is being added when a rank is increased. Solution sets are generated using the Full Order Model and decomposed using SVD. Energy modes are determined by subtracting the approximations from the previous rank's solution and are shown as $\theta = T\text{-}T_{init}$. Solutions are plotted as a surface and examined to see where information is being added at each mode. Modal results are shown for each material with and without radiation.

4.4.1 AA 5083 Modal Energy Analysis

As previously determined, the optimal rank for AA 5083 material properties with convection only was r = 3 and with convection and radiation was r = 4. The contributing energy modes for the first 5 ranks of each case are shown in Figure 32. Looking at the results for the case with convection only, mode 1 (Figure 32 (a)) contains most of the information for the solution set. Mode 2 (Figure 32 (b)) contains updates at the boundaries that adjust across the entire surface, and Mode 3 through 5 (Figure 32 (c)(d) and (e)) contain small adjustments at the initial state. For the case with radiation, Mode 1 (Figure 32 (f)) also contains most of the information for the solution set. The solution surface exhibits more curvature in the time direction compared to the convection only case. The remaining modes for the radiation case compare similarly to the corresponding modes for the convection only case. Modes 2 through 5 (Figure 32 (g)-(j)) all have similar shapes and are on a similar scale when compared to the convection only counterparts. In these cases, at Rank 5 temperature adjustments of ~10^{-3} K are being made at the boundaries.

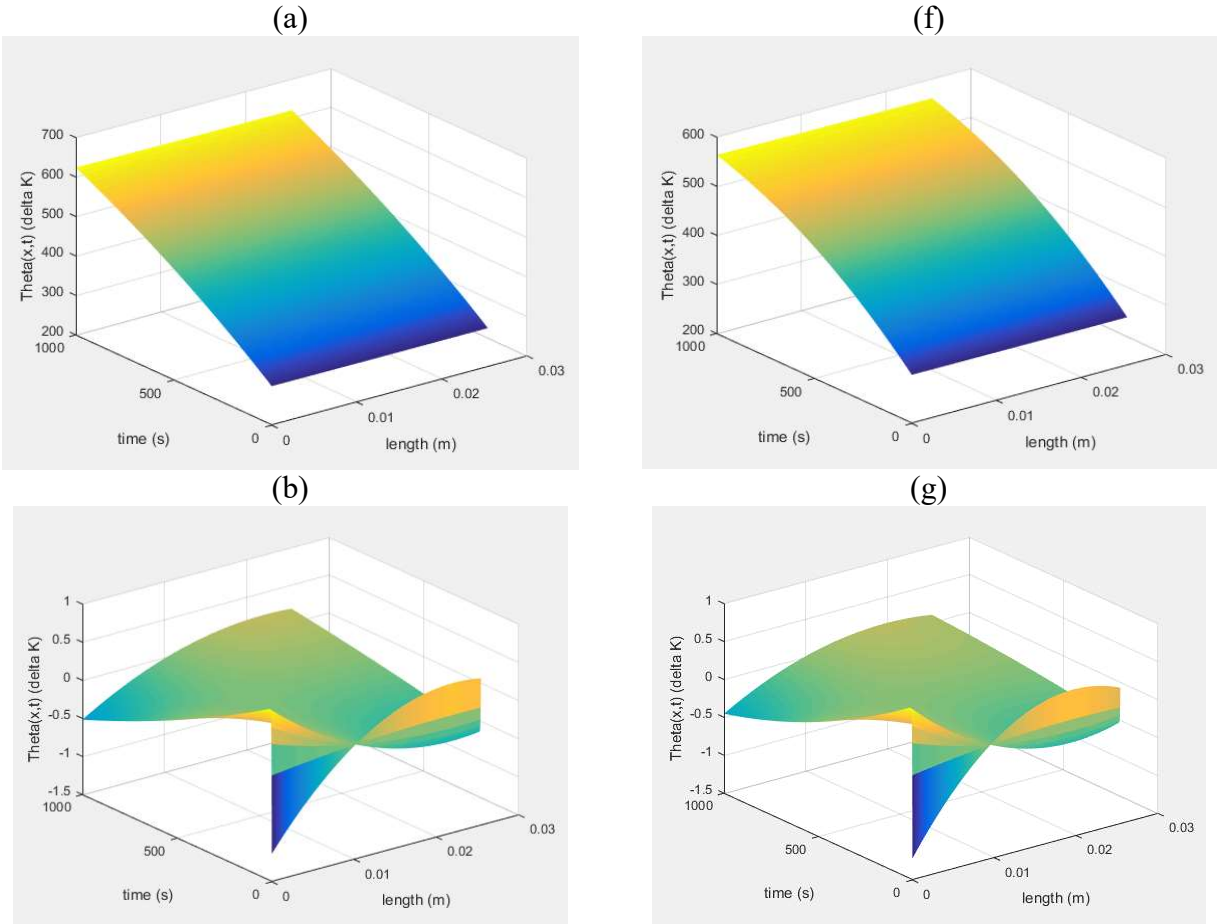

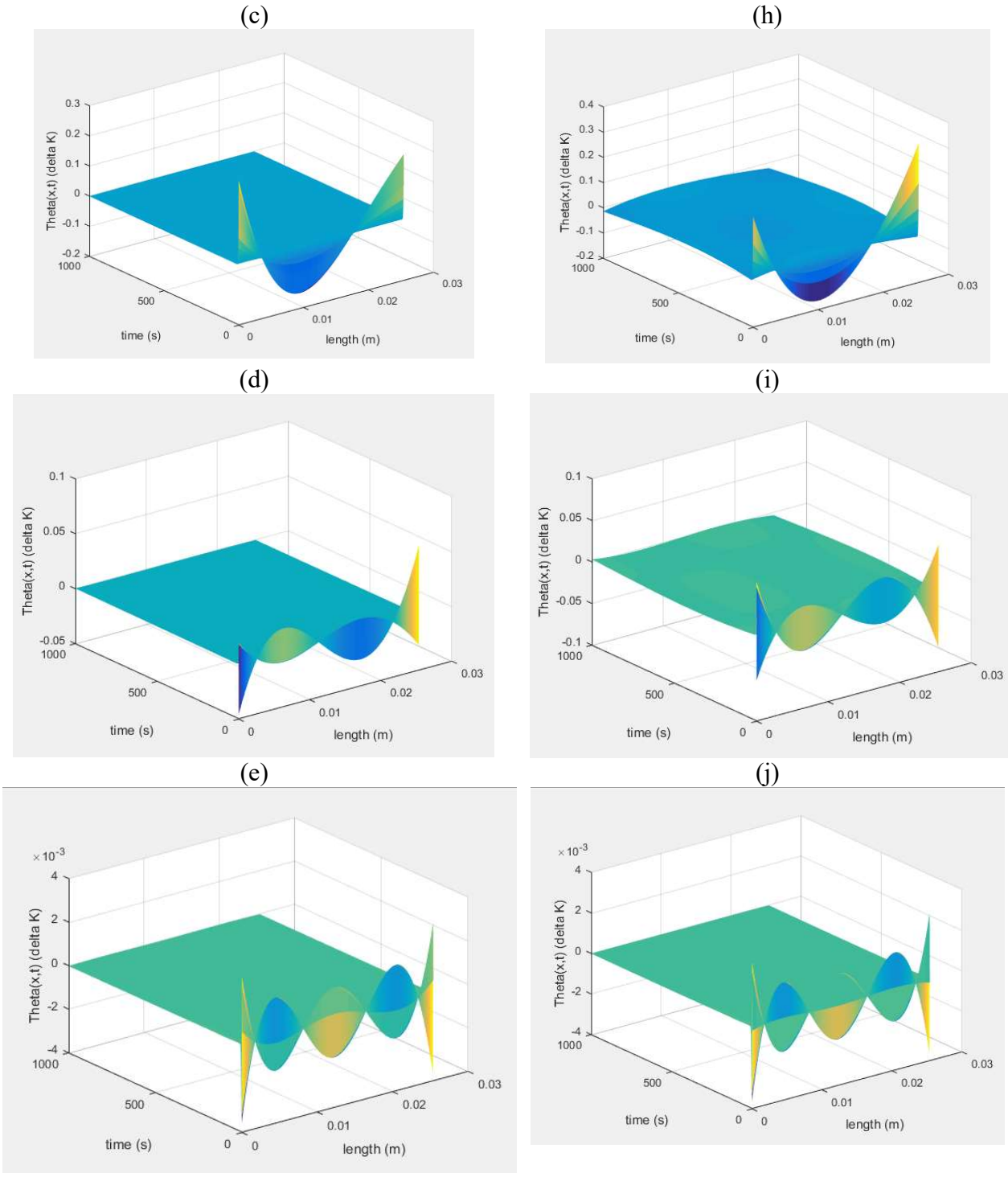

Figure 32. First 5 contributing energy modes for AA 5083 with convection only (a) – (e) and with radiation applied (f) – (j).

4.4.2 Unifrax Modal Energy Analysis

As previously determined, the optimal rank for Unifrax material properties with convection only was r = 6 and with convection and radiation was r = 12. The top 5 contributing energy modes for

these are shown in Figure 33. Looking at the results for the case with convection only, mode 1 (Figure 33 (a)) contains most of the information for the solution set. Mode 2 (Figure 33 (b)) contains updates at the boundaries that adjust across the entire surface, and in particular the first 100 seconds for the node at the applied heat flux face (x =0). Mode 3 through 5 (Figure 33 (c)(d) and (e)) primarily contain adjustments at the initial state, but the modes also contain small adjustments through the rest of the solution domain especially near the face where the heat flux is applied (x =0). For the case with radiation, Mode 1 (Figure 12 (f)) also contains most of the information for the solution set. The solution is much flatter in the time direction compared to the convection only case. The remaining modes for the radiation case compare similarly to the corresponding modes for the convection only case. Modes 2 through 5 (Figure 32 (g)-(j)) all have similar shapes and are on a similar scale when compared to the convection only counterparts. Notice, even at Rank 5 temperature adjustments of ~40 K are being made at the boundaries.

(a)

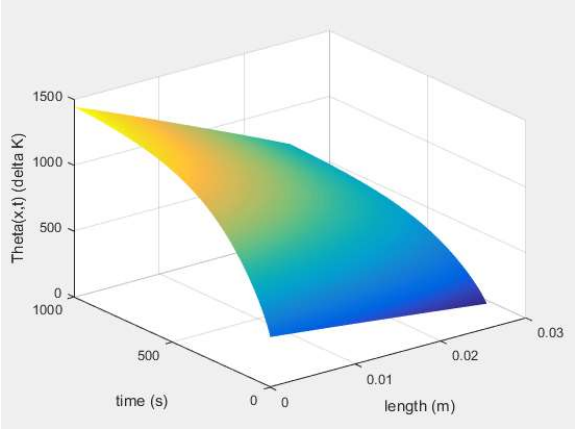

(b)

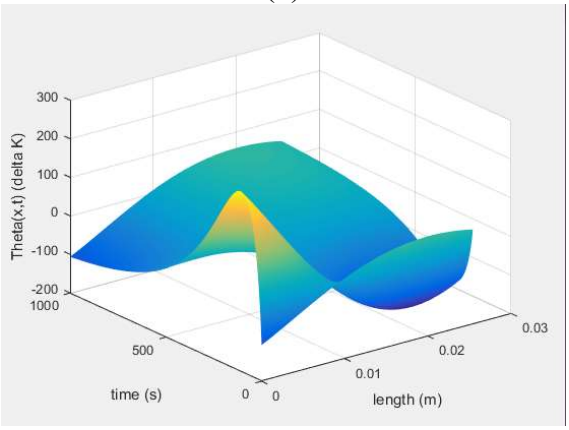

(c)

(f)

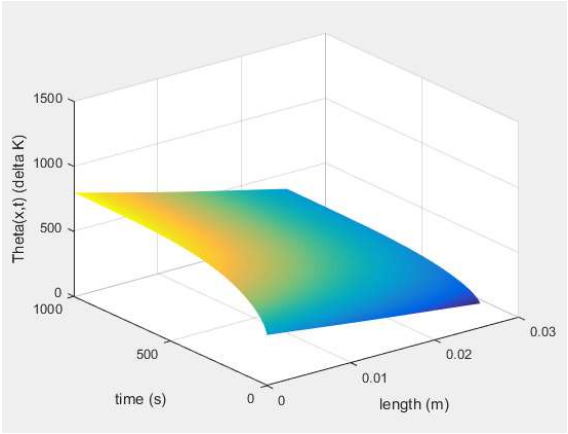

(g)

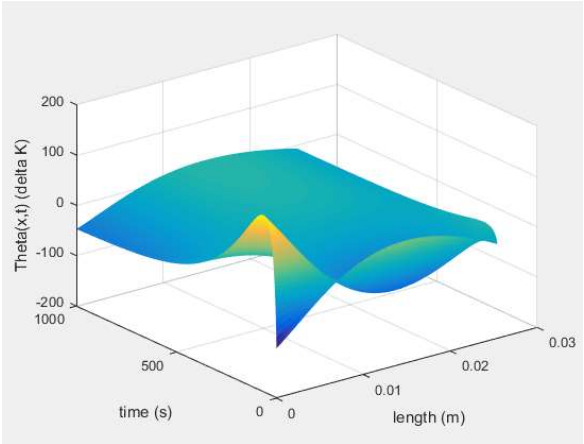

(h)

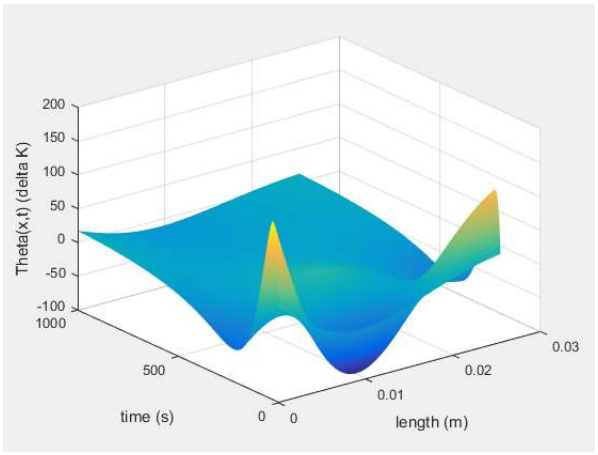

(d)

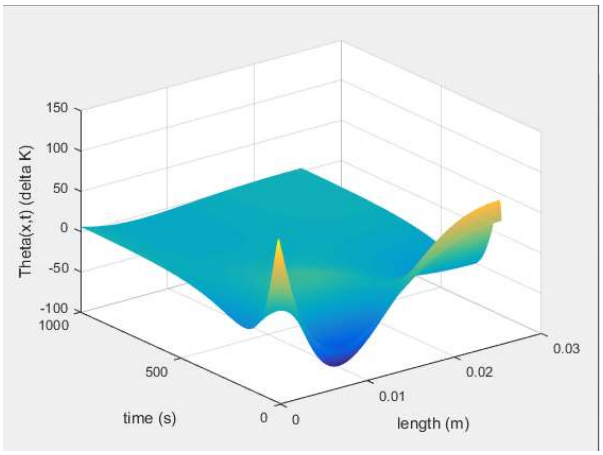

(i)

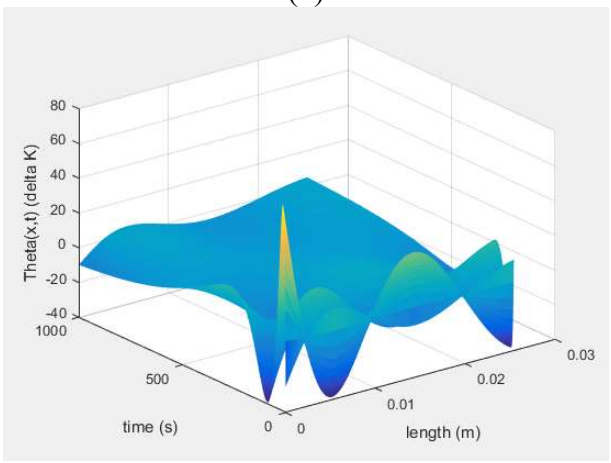

(e)

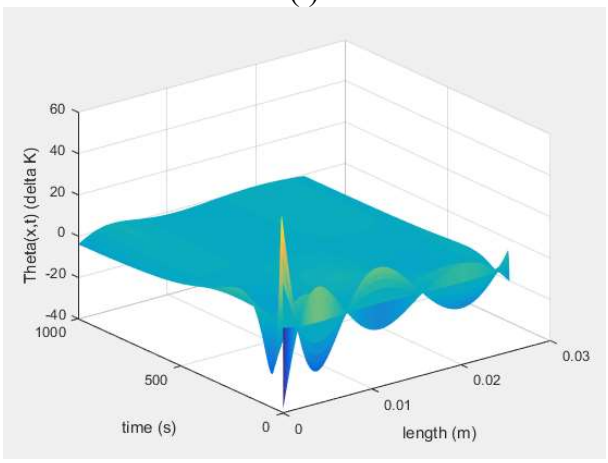

(j)

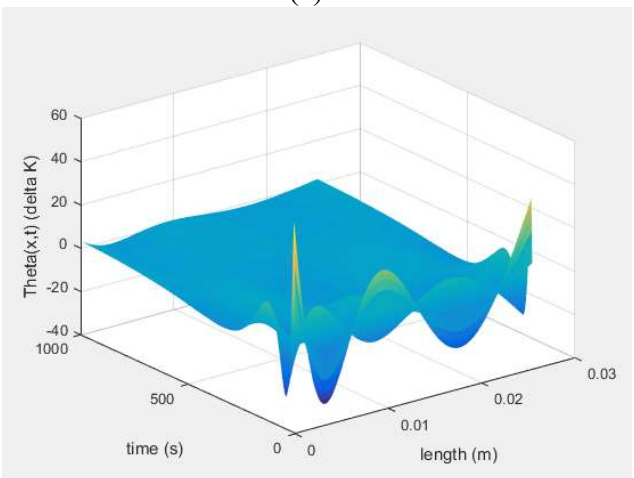

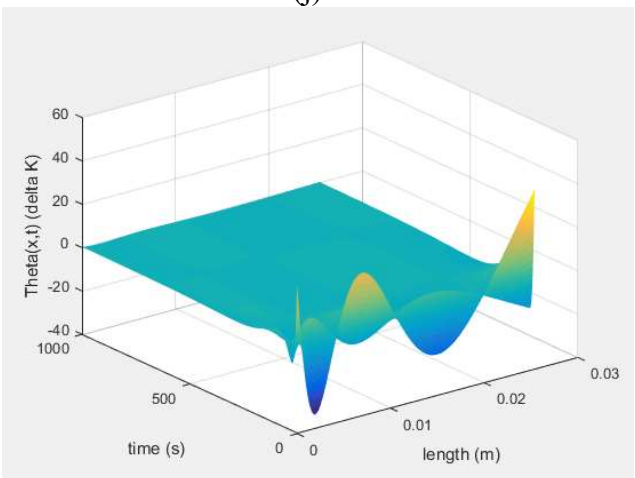

Figure 33 – First 5 contributing energy modes for Unifrax with convection only (a) – (e) and with radiation applied (f) – (j).

4.5 Summary

Radiation terms were added to full order model and the ROM. The additional radiation was observed in the eigenvalue energy content and increased the optimal rank selection for the ROM.

ROMs were able to predict results within 5.5% and with speed ups between 15 to 40 times faster than the full order models. Through Modal Energy Analysis, it was shown that radiation effects show up at different ranks depending on the material.

5 Nonlinear Source Heating Results

A heat transfer source term is a parameter that may include a wide range of phenomena. Some example source terms are energy for complex kinetically driven behaviors such as phase changes and chemical reactions as well as time, spatial, and temperature dependent electrical heating sources. However, adding nonlinear source heating increases the complexity of the solution. A previously determined method of assessing nonlinear sources for use with a POD technique was incorporated into the ROM. The proposed model presented here provides an approach to incorporate the DEIM algorithm for source terms within the reduced order model while maintaining accuracy and decreasing the computational costs.

5.1 Nonlinear Source Heating Introduction

The previously developed Unique Nodal Temperature ROM was advanced to include nonlinear source terms within the domain. Several materials were investigated in this research. Optimal rank was determined by the previously presented error-based method. Results showed that the additional nonlinearity from the internal heat generation source did not drive a rank change in the case with constant material properties, but it did drive an increase rank in the case with highly nonlinear material properties. As part of the treatment using the DEIM algorithm, the nonlinear terms were then further investigated using singular value decomposition to confirm any rank changes needed to resolve fitness across the domain.

5.2 Full Order Model Verification

The 1D transient finite difference model included source heating terms that are spatial and temperature dependent. As previously presented, source heating was modeled as a first order linearized term, however a nonlinear source term can also be directly calculated within the model. Model verification of a temperature dependent source term was done by comparing the full order model to the known existing steady state solution for an infinitely long 3D fin that behaves like a 1D heat transfer problem.

$$\frac{\partial T}{\partial x} - \frac{hP}{kA_c}(T - T_\infty) = 0 \qquad \text{Equation 59}$$

$$\frac{\theta}{\theta_b} = e^{-mx} \text{ where } \theta = T - T_\infty, m^2 = hP/kA_c \qquad \text{Equation 60}$$

The temperature-dependent convection boundary conditions perpendicular to the direction of heat transfer behave like a temperature dependent heat source/sink. The 3D cylinder domain in the validation modal had an overall length of 0.3 m and a radius of 0.005 m. Constant copper material properties were used and are defined in Appendix A. A rod base temperature of 100 °C (373 K) was used. Convection boundary conditions were defined by a heat transfer coefficient of 100 W/m^2·K and an ambient temperature of 25 °C (298 K). There was no radiation applied at

the boundaries. In the full order model, solutions were generated for 1000 seconds using 1 second increments. The source (sink) term is a function of heat transfer coefficient, perimeter, cross-sectional area, ambient temperature and local temperature. Results were compared at steady state and are shown in Figure 34. Results show that the full order model can predict source heating conditions within 1.5% of the known solution.

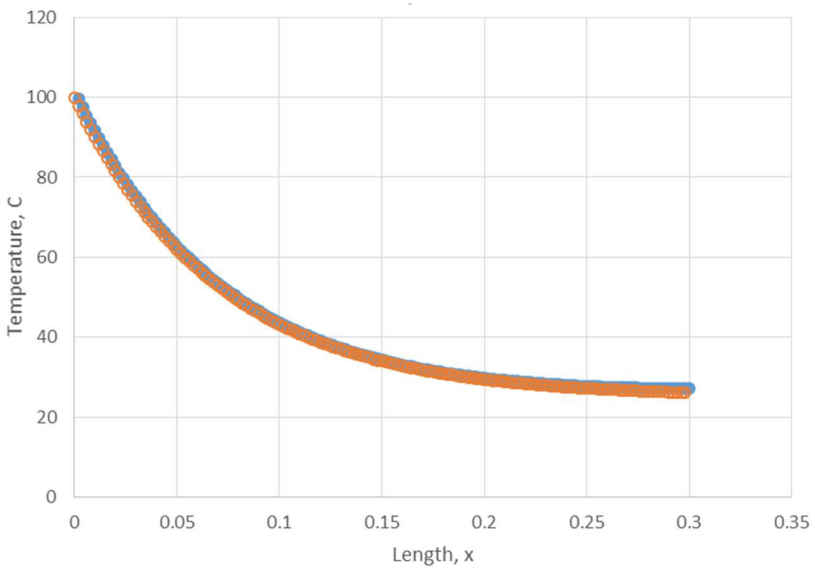

Figure 34. Steady state results for temperature-dependent source term Full Order Model (blue) against known solution (orange).

5.3 Simulation Case and Full Order Model Solutions

The finite difference model was then updated to assess nonlinear source heating in conjunction with real material properties, with and without nonlinearities. The overall length for model domain was updated to 0.0254 m. The initial temperature was set to 20 °C (298 K). Convection boundary conditions at both faces were defined by a heat transfer coefficient of 15 W/m^2·K and an ambient temperature of 25 °C (298 K) was used. A nonlinear, temperature dependent source heating term was added to the overall equation.

$$Sc = \alpha T^{3/2} \qquad \text{Equation 61}$$

Where 'α' values were used to scale the input and provide meaningful results. While source heating can be localized and/or time dependent as well, in this case the source heating term was applied at all nodes at all times and was nonlinear with temperature. Model solutions were generated for times up to 1000 seconds. Initially, snapshots were generated for an applied heat flux of 25 kW/m^2, and the results were used to create a POD projection matrix for use in the ROM. AA 5083 and Unifrax material properties were separately used to investigate nonlinear internal heat generation.

Full order solutions using AA 5083 material constant material properties with and without a nonlinear source heating term are presented in Figure 35. The AA 5083's constant material properties are such that there is a small temperature gradient within the sample (~5°C). Using $\alpha = 20$, the source term increases the temperatures across the domain by approximately 100 K at the final state compared to the case with convection only. The same 5°C thermal gradient is observed in this solution.

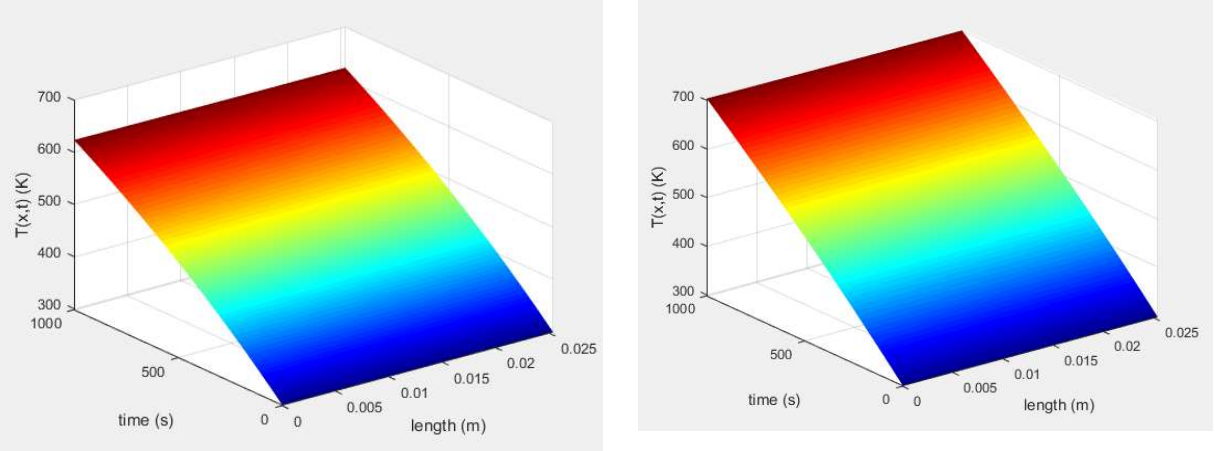

Figure 35. Full order model solutions for AA 5083 without source heating term (left) and with nonlinear source heating term (right).

Full order solutions shown in Figure 36 are for the Unifrax highly nonlinear material properties with and without a nonlinear source term. A much larger thermal gradient (~400°C) is seen within the sample both with and without the source heating. Using $\alpha = 10$, the additional source term drives the temperatures up across the domain by approximately 200 K at the final state compared to the case with convection only.

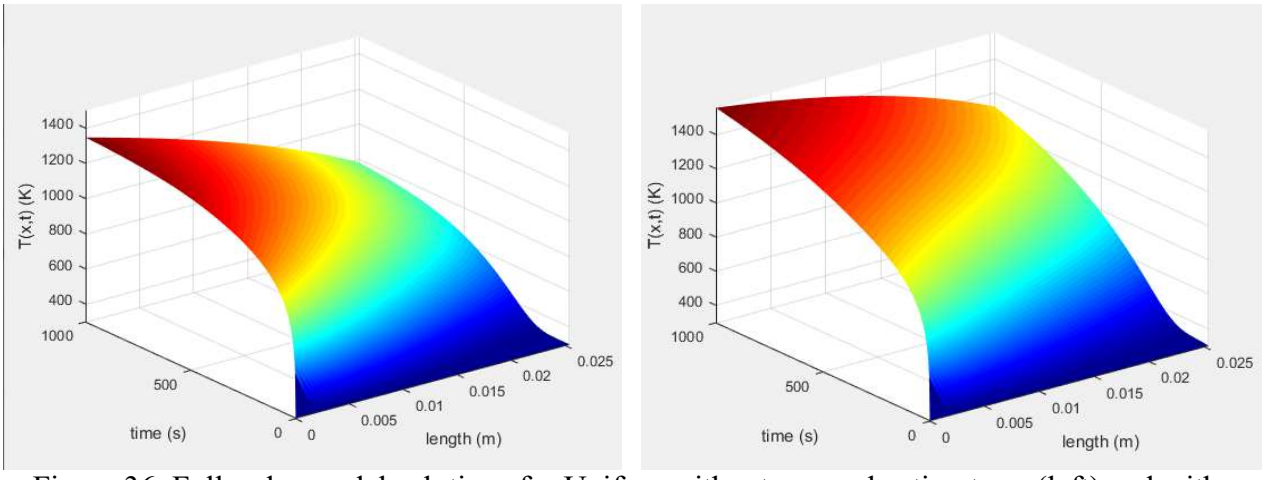

Figure 36. Full order model solutions for Unifrax without source heating term (left) and with nonlinear source heating term (right).

5.4 ROM Rank Selection

Rank was investigated to determine if the additional source term nonlinearity resulted in changes to the optimal POD projection matrix rank for an associated material. The previously developed method of assessing error stability with increasing rank was used to determine optimal rank. The addition of the source term affects the optimal rank for each material. Plots of eigenvalues as a function of rank for AA 5083 and Unifrax materials for a case without source heating and a case with source heating are shown in Figure 6. The plot is restricted to the first 20 eigenvalues for clarity. Looking at the AA 5083 plot, the eigenvalues are very similar at the lower ranks 1 and 3, however the nonlinear source rank 2 appears to be slightly higher than it's no source counterpart. The ranks are then similar again until the noticeable difference between the two sets above rank 7. The slight increase at rank 2 may indicate that more information is being captured at that rank. As previously discussed, eigenvalues are arranged in descending order. Since the differences in eigenvalues are predominantly at higher ranks (lower energy content), this indicates that this nonlinear source heating is not the most significant factor in determining the overall shape of the solution set. This agrees with what was observed in the full order solution set. For the Unifrax material, the eigenvalues are nearly identical for ranks 1 through 11, and differences emerge at rank 12 and onward. This indicates that the source heating term is not the significant driver for the shape of the solution set. It also indicates that additional ranks may be needed to capture the solution behavior. It should be noted that in this case, the nonlinear source term is only a function of temperature. If the source term were spatially or temporally dependent, eigenvalue rank changes may be observed based on the magnitude and duration of the source term. Note, the Singular Value Decomposition does not distinguish between space and time (Chatterjee [60]).

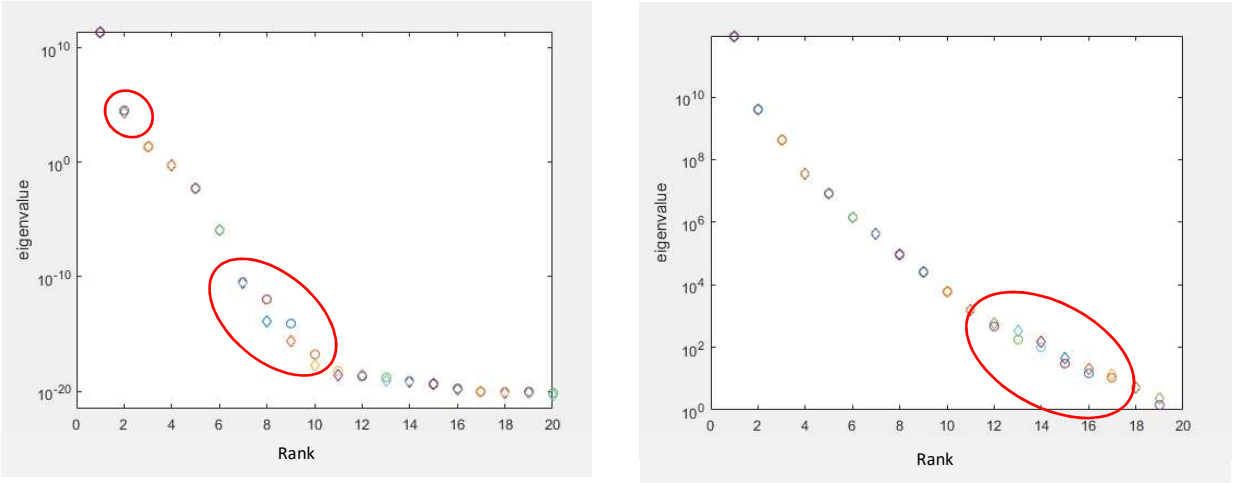

Figure 37. Eigenvalues for AA 5083 POD (left) and Unifrax POD (right) without source heating (diamond) and with nonlinear source heating (circle).

5.4 DEIM Algorithm

The DEIM algorithm provides specific insight into the nonlinear terms. Similar to the overall POD application, Singular Value Decomposition is done on the results from the nonlinear terms

exclusively as part of the DEIM algorithm. Details on the algorithm were presented in Section 2.5.4 DEIM Algorithm. Full order model results were generated, and the values specific to the nonlinear term were captured separately at each time step. In this model, it would be the results from the [D] matrix only. The results were then arranged in matrix form and Singular Value Decomposition was performed on this new matrix composed of snapshots from the nonlinear term only. Eigenvalues as a function of rank for these terms are shown in Figure 38. Note there are only 3 eigenvalues identified for the source term using AA 5083 material properties and 2 for the source term using Unifrax material properties. For each case, all of the nonlinear term eigenvalues were used in the DEIM algorithm to produce results from the ROM. Also, the first rank for each set is on the order of approximately 10^8 while the Rank 1 eigenvalues are greater than 10^{10}. This indicates that while the nonlinear heating term does contribute some energy content to the overall solution shape and will need to be accounted for in the ROM to achieve accurate results, in either of the two cases it is not the primary basis for the shape of the solution surface.

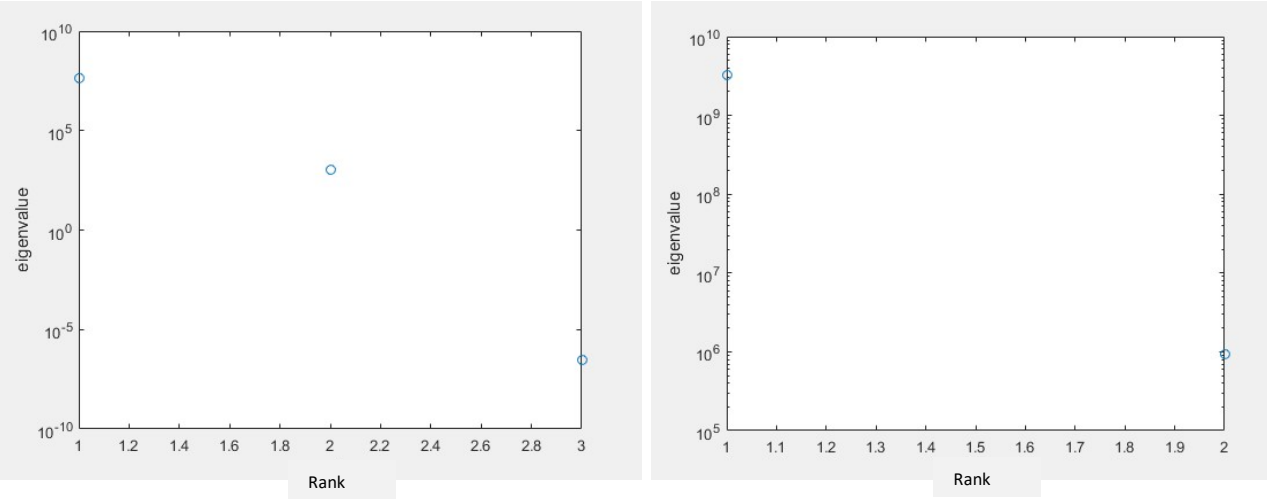

Figure 38. Eigenvalues for AA 5083 nonlinear source POD-DEIM term (left) and for Unifrax nonlinear source POD-DEIM term (right).

5.5 Nonlinear Source ROM

The ROM uses the DEIM algorithm to reduce the full order model nonlinear source heating term. The DEIM algorithm determines interpolation indices based on a POD of the data due solely to the nonlinear term. When the full order model snapshots are generated, results were segregated for the nonlinear term. These separated results were then assembled into a matrix and decomposed using Singular Value Decomposition. The previously presented DEIM algorithm (Section 2.5.4 DEIM Algorithm) was used to determine a reduced source matrix for use in the ROM based on interpolation indices unique to the nonlinearity.

5.5.1 AA 5083 Results

The AA 5083-H116 material properties were used as a baseline for source heating ROM development verification and validation in order to remove the effects of temperature dependent material properties. The nonlinear source heating term was not linearized, but determined directly within the full order model equation. Snapshots were initially generated for this material using a time 1000 seconds at increments of 1 second, and were explored using Singular Value Decomposition. Rank range was determined to be between r = 3 and r = 9 based on energy content and computational accuracy. ROMs were generated for each rank and compared to the snapshots in terms of solution time and accuracy in order to determine the minimum optimal rank. By looking at the POD energy content from the SVD for various ranks and numerical accuracy (Figure 39), optimal rank for this material remained at r = 3 compared to the case without nonlinear source heating terms. Computational efficiency of the ROM against the full order model show that it is about 18 times faster than the full order.

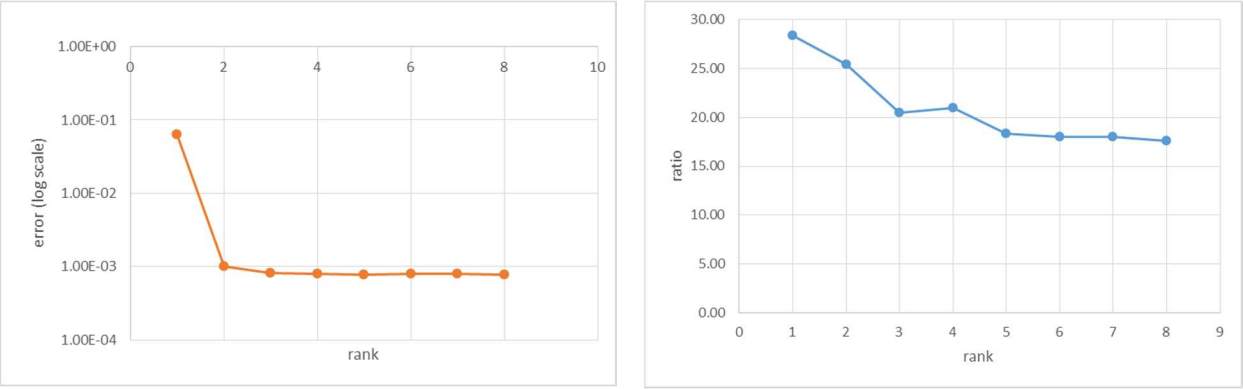

Figure 39. Solution error as a function of rank (left) and ratio of solution times for the ROM (right) for AA 5083 material with nonlinear source heating

Errors across the solution set and at the unexposed face are shown in Figure 29. The AA 5083 material with nonlinear source heating is very well predicted by the ROM. The solution from the ROM appears to be diverging from the full order solution with time; however, using rank r = 3 result in a maximum error of less than 0.1%.

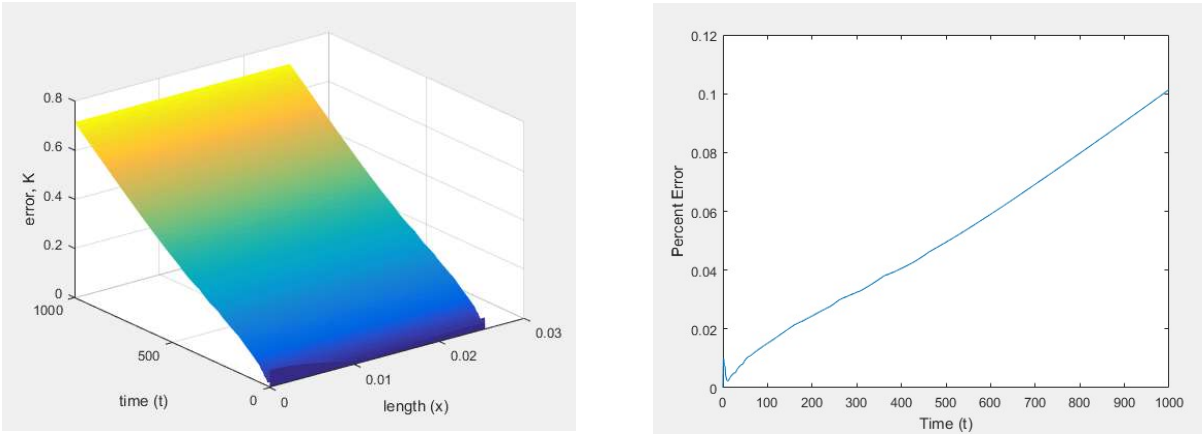

Figure 40. Absolute error (left) and maximum relative error at boundary each node (right) from ROM using AA 5083 and nonlinear source heating

5.5.2 Unifrax Ceramic Board Results

Unifrax material properties were used to further investigate the nonlinear source term ROM. The nonlinear source heating term was determined directly within the full order model equation. Snapshots were initially generated for this material using a time 1000 seconds and increments of 1 second, and were explored using Singular Value Decomposition. Rank range was determined to be between r = 3 and r = 10 based on energy content and digital accuracy. ROMs were generated for each rank and compared to the snapshots in terms of solution time and accuracy in order to determine the minimum optimal rank. By looking at the POD energy content from the SVD for various ranks and numerical accuracy (Figure 41), optimal rank for this material increased from r = 5 to r = 7 compared to the case without radiation. Computational efficiency of the ROM against the full order model show that it is about 17 times faster than the full order.

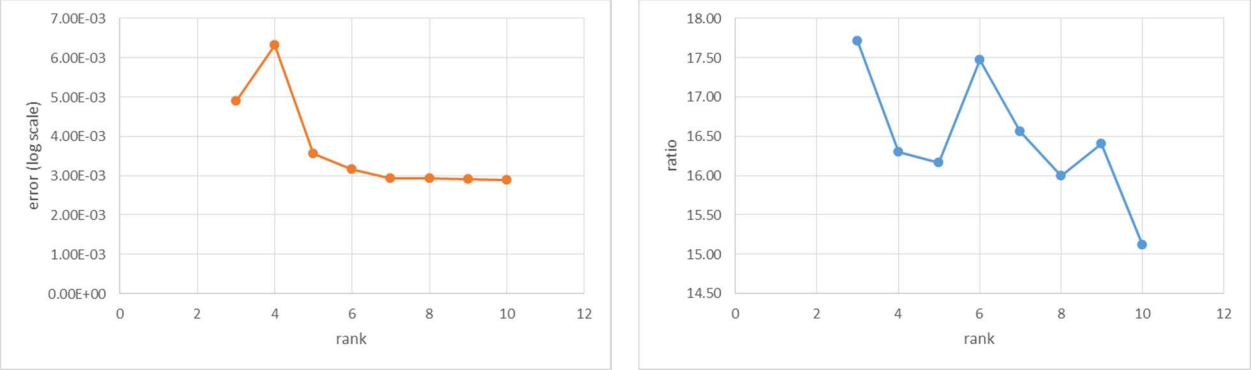

Figure 41 - Solution error as a function of rank (left) and ratio of solution times for the ROM (right) for Unifrax material with nonlinear source heating

Errors across the solution set and at the unexposed face are shown in Figure 42. The Unifrax material with nonlinear source heating is very well predicted by the ROM. The solution from the ROM appears to be diverging from the full order solution with time; however, using rank r = 7 result in a maximum error of less than 0.1%.

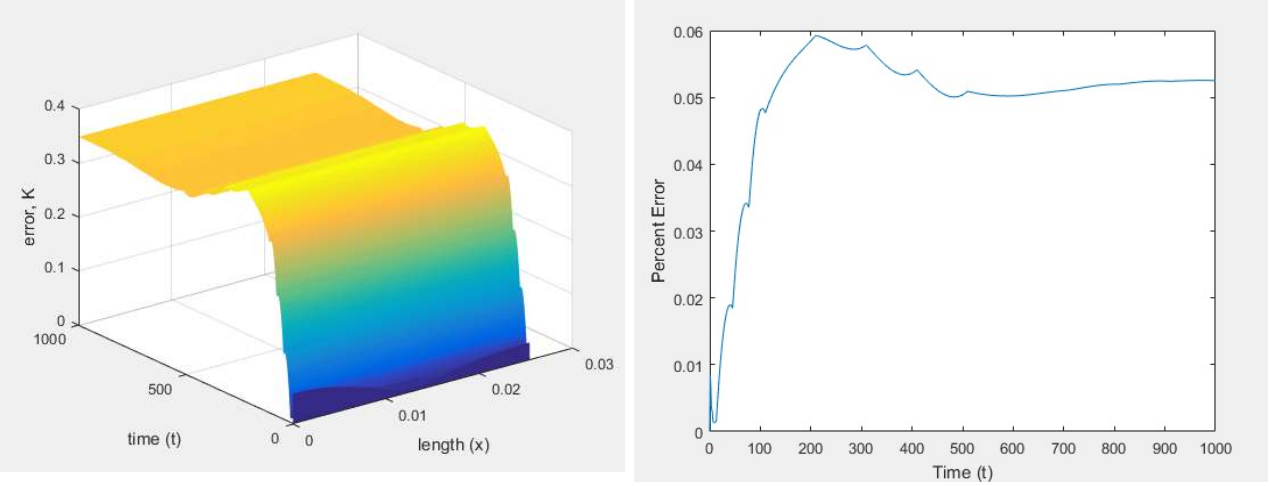

Figure 42 - Absolute error (left) and maximum relative error at boundary each node (right) from ROM using Unifrax and nonlinear source heating

5.6 Summary

Nonlinear source heating terms were added to the full order model, reduced using the DEIM algorithm and incorporated into the ROM. The additional nonlinearity was not observed in the constant material case in terms of the eigenvalue energy content and therefore did not increased the optimal rank selection for the ROM. However, the eigenvalue energy content of the nonlinear material case did show the need to increase the optimal rank selection for the ROM. The DEIM algorithm is executed on the results due solely to the nonlinear source terms. The additional POD analysis identified eigenvalues unique to the source term, and showed where they fall in the eigenvalues for the full order solution. ROMs were able to predict results within 0.1% and with speed ups between 17 to 18 times faster than the full order models.

6 Complex Geometry Results

Geometry plays a significant role in understanding thermal response. Real problems can be estimated by using lumped capacitance techniques or 1D approximations with limiting assumptions. However, in some cases meaningful results may only be achieved by accurately representing the physical domain. Three dimensional models need to account for complex spaces and meshes, multiple boundary conditions, and be able to manage heat transfer in multiple dimensions. The result is a large increase in computational costs. The proposed model presented here provides an approach to extend the previously developed 1D nonlinear model to a 3D ROM.

6.1 Complex Geometry Introduction

The previously developed 1D ROM was extended to multiple dimensions. Several materials with different nonlinear properties were investigated in this research. Full order model mesh definitions and results were imported from a commercial code. Optimal rank was determined by the previously presented error-based method, and results showed that the rank did not significantly increase with dimension. The results were then further investigated by use of POD Modal Energy Analysis in order to confirm the effect of geometry on the rank selection.

6.2 Full Order Model Verification

The previously developed 1D transient finite difference model was expanded for use in a 3D ROM. Full order model verification of multiple dimensions was done using a 3D Abaqus model. A 3D cubic shape was constructed with side dimensions of 0.01 m as shown in Figure 43, and the boundary conditions were applied so that heat transfer was allowed to occur in multiple directions. Convection boundary conditions at all six faces were defined by a heat transfer coefficient of 15 $W/m^2 \cdot K$, and an ambient temperature of 25 °C (298 K) was used. An applied heat flux of 25 kW/m^2 was applied at the face x = 0. The initial temperature was set to 25 °C (298 K), and the model was run to 1000 seconds. AA 5083 constant material properties were used in the model verification. Results at 1000 seconds are shown in Figure 43. The solution has very uniform surface temperatures at the applied heat flux face, ranging between 568.1 K and 567.9K. From the scale of the figure, the temperature difference between the applied heat flux face (x = 0) and the unexposed face (x = L) was a very low thermal gradient across (~1.4 °C).

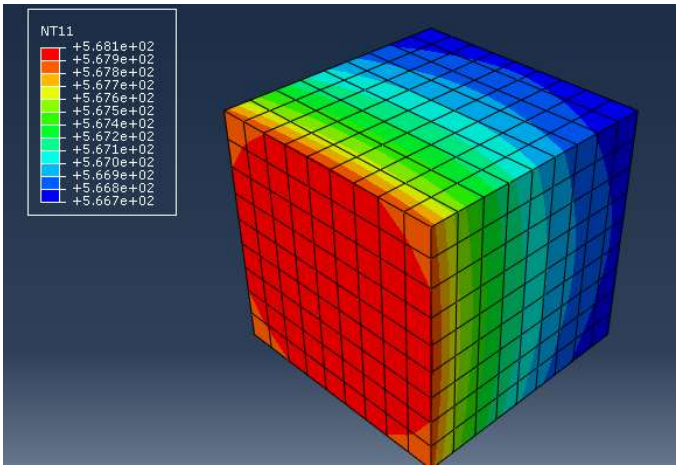

Figure 43. Abaqus 3D model and results used for model validation and snapshot generation in the 3D ROM.

As previously presented, creating a ROM requires a known function, therefore a 3D full order model was assembled in MATLAB. The build of the full order modal was aided by using a mesh map. The mesh definition was imported from Abaqus that included node number and associated 3D geometric coordinates. The geometric coordinates were transformed into nodal coordinates as a map to identify neighboring nodes, surface, edge, and corner nodes. Each of the matrices in the full order model (spatial term and boundary conditions) were then assembled by utilizing the definition contained in the nodal coordinate-based mesh map. The 3D transient results from Abaqus were then imported for comparison against the full order model developed in MATLAB as shown in Figure 44. The 3D results are re-arranged in this plot by node number. The MATLAB model predicted the results within 0.4%. Error peaks correspond to the back face, parallel to the face of the applied heat flux.

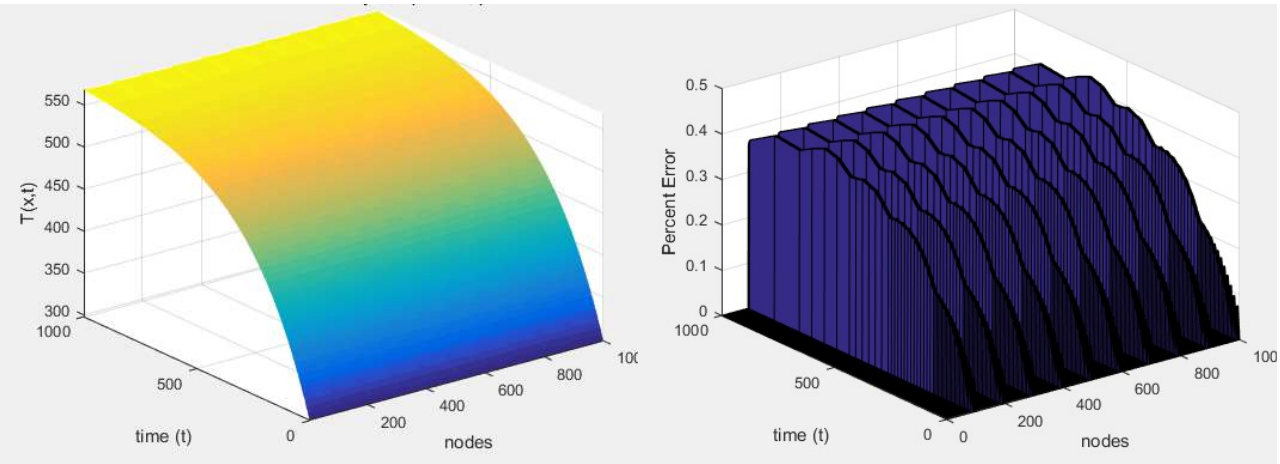

Figure 44. Full order model MATLAB solution (left) and errors across the sample domain (right) arranged by node number.

The finite difference model was then used in three dimensional domains in conjunction with real material properties, with and without nonlinearities. Aside from additional investigation using AA 5083 constant material properties, cases with low nonlinear Stainless Steel 302 material

properties as well as highly nonlinear Unifrax material properties were also explored. The full order models utilized the same boundary conditions and initial conditions with one exception. The Stainless Steel 302 material properties were used in a slightly larger cubic domain, with sides of 0.1 m in order to showcase a more complex thermal gradient within the sample. The sample with Unifrax was executed with a 0.01 m cubic domain. Steady state solutions from Abaqus are shown for both samples in Figure 45. Compared to the AA 5083 results, the thermal gradient of the Stainless Steel 302 solution is much greater in the direction of the applied heat flux (z direction). However, within the x-y planes, the isotherms are rather flat. For example, the surface temperature at the applied heat flux face is fairly uniform at 400 °C and the unexposed face temperature is approximately 330 °C. The result is a 3D domain that looks more like a 1D approximation. As for the Unifrax material sample, the result is a much more complex thermal response. Thermal gradients are more pronounced in the z direction. Temperatures at the applied heat flux face range between 800 and 1000 °C, while at the unexposed face are between 350 and 400 °C. Also, in the x-y planes, isotherms are more parabolic in shape.

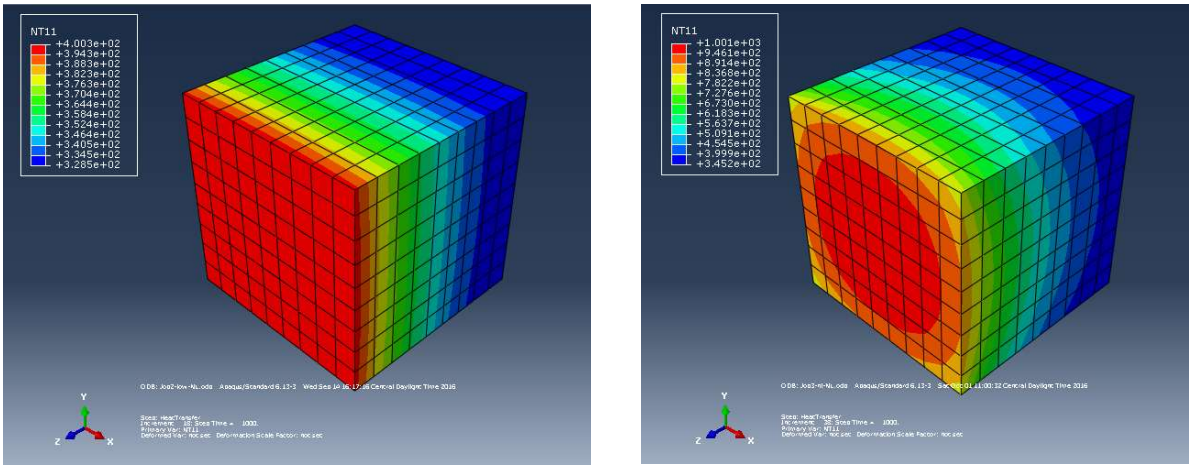

Figure 45. Steady state Abaqus 3D model solutions for Stainless Steel 302 (left) and Unifrax (right) used for snapshot generation in the 3D ROM.

6.3 ROM Rank Selection

Rank was investigated to determine if multiple dimensions drive changes to the POD projection matrix rank for an associated material. The previously developed method of assessing error stability with increasing rank was used to determine optimal rank. The expansion to multiple dimensions affects the optimal rank for each material case. Plot of eigenvalues as a function of rank are shown for AA 5083 material in Figure 46. Eigenvalues for the 3D case (circles) are overlaid with the results from the 1D case (diamonds). The plot is restricted to the first 20 ranks for clarity. The eigenvalues for the two sets coincide at low rank numbers and then separate at about rank r = 6. The eigenvalues for the 3D model in general have much higher values, with the exception of the first two eigenvalues in the 1D case. The change in slope at rank 6 indicates that no additional information about the solution set is gained after that, therefore fewer ranks may be needed to capture the material response in three dimensions. Since this case has isotherms that are approximately parallel to the x-y plane, a 1D approximation would suffice to

capture the material response. That is reflected in the coincidence of eigenvalues at the lower ranks.

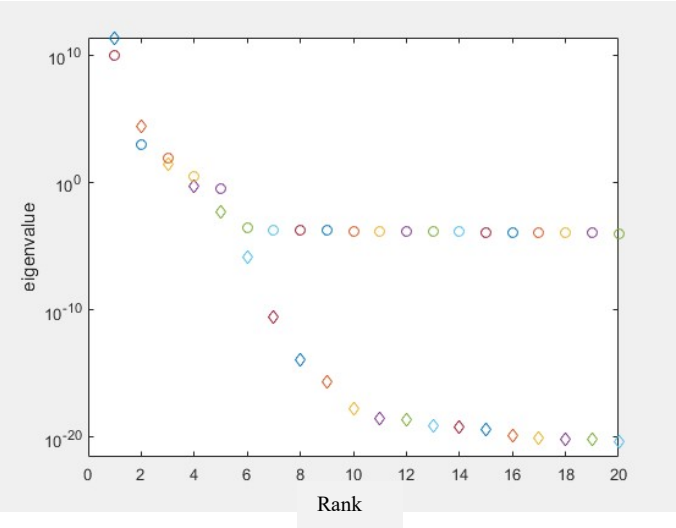

Figure 46. Eigenvalues for AA 5083 POD with convection only 1D model (diamond) and 3D model (circle).

Plot of eigenvalues as a function of rank are shown for Stainless Steel 302 material in Figure 47. Eigenvalues for the 3D case (circles) are overlaid with the results from the 1D case (diamonds). The plot is restricted to the first 20 ranks for clarity. The eigenvalues for the two sets coincide at low rank numbers and then separate at about rank r = 5. Again, the eigenvalues for the 3D model in general have much higher values, with the exception of the first eigenvalue in the 1D case. The 1D model eigenvalues slope linearly until rank 20, then it flattens out (not shown), while the 3D model eigenvalues decay very gradually with rank until approximately rank r = 14. This indicates that additional ranks may not be needed to capture material response in three dimensions. Since this case also has isotherms that are approximately parallel to the x-y plane, a 1D approximation would suffice to capture the material response. That is reflected in the high coincidence of eigenvalues at the lower ranks.

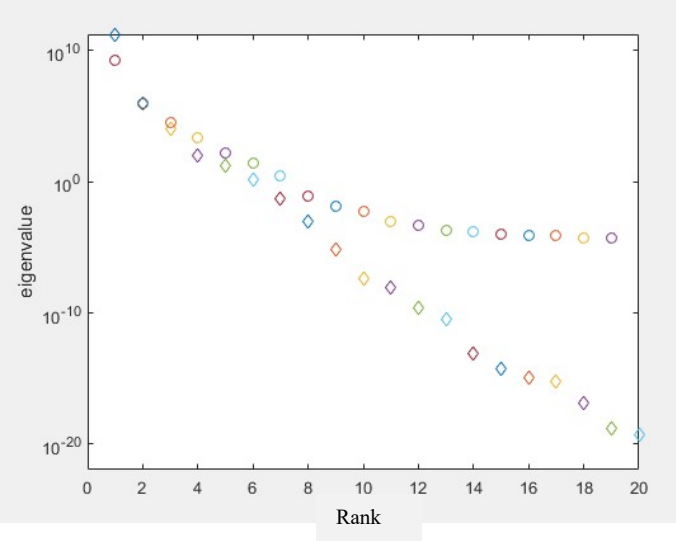

Figure 47. Eigenvalues for Stainless Steel 302 POD with convection only 1D model (diamond) and 3D model (circle)

Plot of eigenvalues as a function of rank are shown for Unifrax material in Figure 48. Eigenvalues for the 3D case (circles) are overlaid with the results from the 1D case (diamonds). The plot is restricted to the first 20 ranks for clarity. In the case of Unifrax, the eigenvalues for the 3D model are all less than the eigenvalues for the 1D case. For the Unifrax material, the solution isotherms are not parallel to the x-y plane, but have very complex shapes. A 1D approximation would not sufficiently capture the material response for this case. That is reflected in the two orders of magnitude difference in eigenvalues at all ranks. In the 3D model, there is a noticeable slope change at rank r = 8, while the 1D case does not have a noticeable slope change in this rank subset. This indicates that most of the information is stored in the lower initial ranks. Fewer eigenvalues may be needed to capture material response for this case.

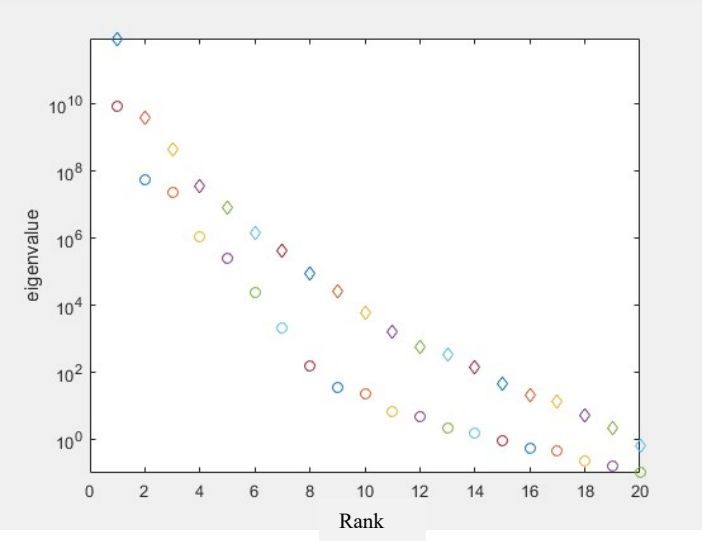

Figure 48. Eigenvalues for Unifrax POD with convection only 1D model (diamond) and 3D model (circle)

6.4 3D Transient ROM

The 3D reduced order model was generated from the full order model. The same initial condition and boundary conditions were applied. Geometries were updated as previously stated. Three material types investigated in this research were AA 5083 constant material properties, Stainless Steel 302 linear temperature dependent properties, and Unifrax highly nonlinear temperature dependent material properties.

6.4.1 AA 5083 Results

The AA 5083 material properties were used as a baseline for 3D ROM development verification and validation. Snapshots were initially generated using Abaqus commercially available software for a 0.01 m cubic domain. Results and the mesh definition were imported into MATLAB for additional processing. The full order model was expanded to 3D transient heat transfer using the mesh map. In order to create the ROM, the optimal rank was first determined. By looking at the POD energy content from the SVD for various ranks and numerical accuracy, rank range was determined to be between r = 3 and r = 9 based on energy content and computational accuracy. ROMs were generated for each rank and compared to the snapshots in terms of solution time and accuracy in order to determine the minimum optimal rank as shown in Figure 49. Compared to the 1D case, optimal rank increased for this material from r = 3 to r = 4. Computational efficiency of the ROM against the full order model show that it is about the same speed as the full order for this simple constant property case.

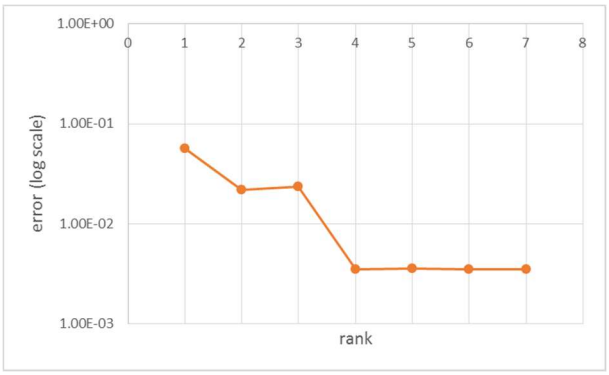

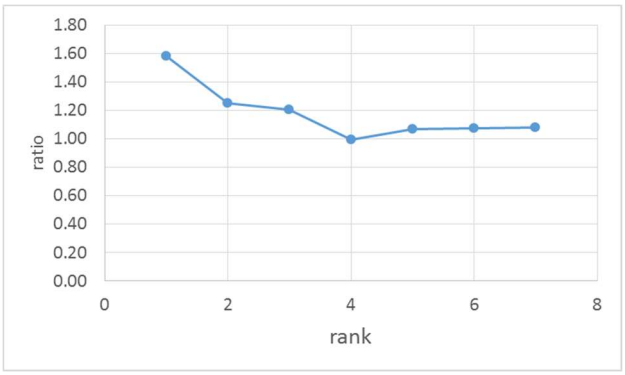

Figure 49. Solution error as a function of rank for AA 5083 material (left) and ratio of solution times for the ROM using AA 5083 material properties (right)

Using rank r = 4, errors and percent error between the Abaqus results and the ROM were plotted across the solution space, arranged by node number (Figure 50). Peak errors correspond to the face opposite of the incident heat flux, with a maximum delta of 2 K corresponding to less than 0.4% error. Notice the errors peak at 500 seconds and then decline. The AA 5083 material is very well predicted by this ROM, however the computational speed ups at this mesh density are not realized.

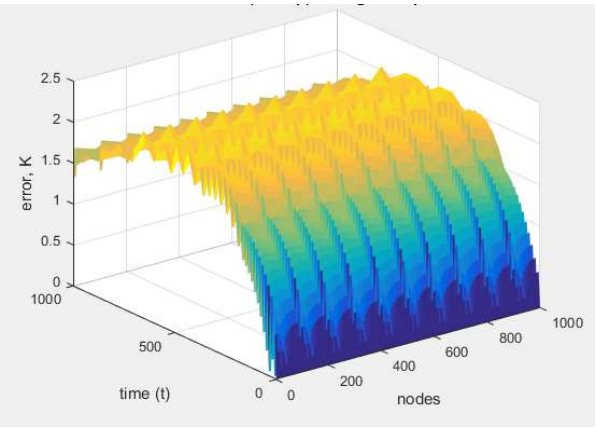

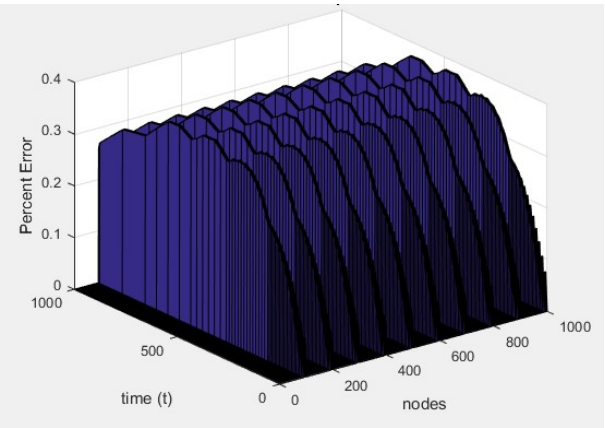

Figure 50. Absolute error (left) and maximum relative error at boundary each node (right) from 3D ROM using AA 5083 material properties.

6.4.2 Stainless Steel 302

The Stainless Steel 302 material properties were investigated in order to see how well the ROMs worked with a low nonlinear material case. Snapshots were initially generated using Abaqus commercially available software for a 0.1 m cubic domain. Results and the mesh definition were imported into MATLAB for additional processing. The full order model was expanded to 3D transient heat transfer using the mesh map. In order to create the ROM, the optimal rank was first determined. By looking at the POD energy content from the SVD for various ranks and numerical accuracy, rank range was determined to be between r = 3 and r = 9 based on energy content and computational accuracy. ROMs were generated for each rank and compared to the snapshots in terms of solution time and accuracy in order to determine the minimum optimal rank as shown in Figure 51. Compared to the 1D case, optimal rank decreased for this material

from r = 7 to r = 4. Computational efficiency of the ROM against the full order model show that it is about half the speed as the full order for this low nonlinear property case.

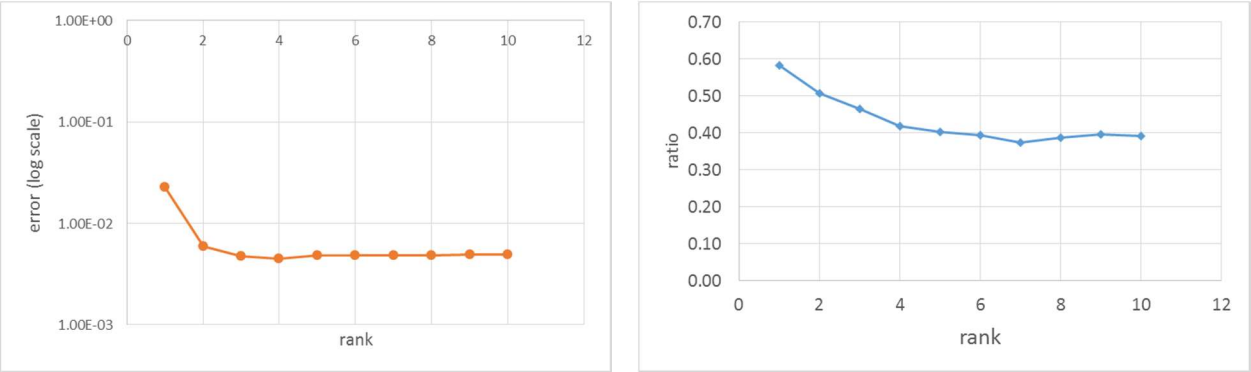

Figure 51. Solution error as a function of rank for Stainless Steel 302 material (left) and ratio of solution times for the ROM using Stainless Steel 302 material properties (right).

Using rank r = 4, errors and percent error between the Abaqus results and the ROM were plotted across the solution space, arranged by node number as shown in Figure 52. Peak errors correspond to the face opposite of the incident heat flux, with a maximum temperature delta of 5 K corresponding to less than 1.0% error. Note, the errors continue to increase with time. Appendix A shows the material properties for Stainless Steel 302. Properties were obtained from published values (Incropera [123]). The results show that the thermal conductivity and specific heats are not well predicted by a polynomial fitted function. As a result, the thermal diffusivity and volumetric heat capacity are in turn also not well predicted by functions. It should be noted that the exact values were used in Abaqus where linear interpolation is done between values as a function of temperature. The ROM depends on using a polynomial fitted function to describe the material properties. That may be why discrepancies are seen between the two. Despite that, the Stainless Steel 302 material in 3D is fairly well predicted by this ROM, however the computational speed ups at this mesh density are not realized.

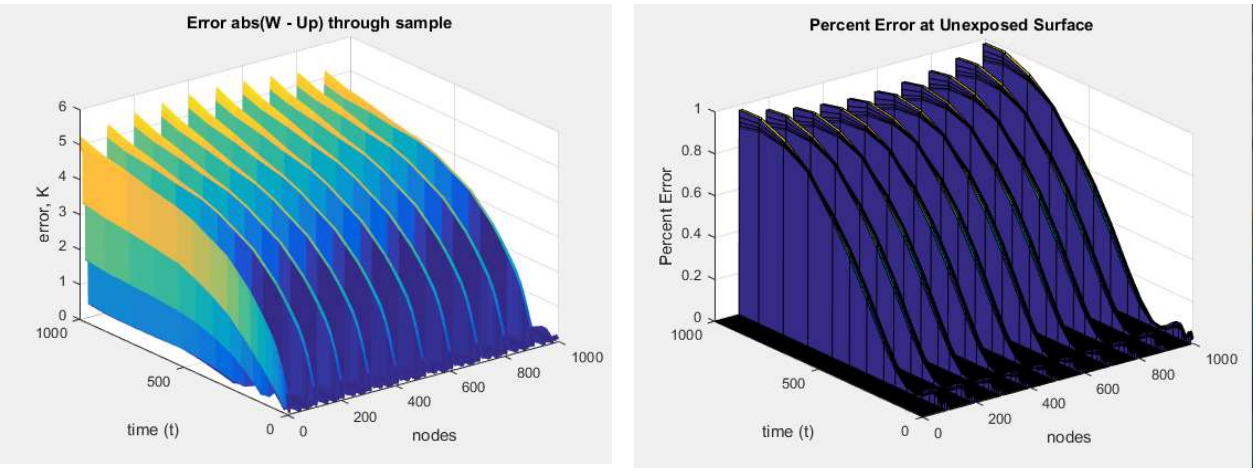

Figure 52. Absolute error (left) and maximum relative error at boundary each node (right) from 3D ROM using Stainless Steel 302 material properties.

6.4.3 Unifrax Results

The Unifrax highly nonlinear properties were also investigated for use in the 3D ROM. Snapshots were initially generated using Abaqus commercially available software for a 0.01 m cubic domain. Results and the mesh definition were imported into MATLAB for additional processing. The full order model was expanded to 3D transient heat transfer using the mesh map. In order to create the ROM, the optimal rank was first determined. By looking at the POD energy content from the SVD for various ranks and numerical accuracy, rank range was determined to be between r = 3 and r = 9 based on energy content and digital accuracy. ROMs were generated for each rank and compared to the snapshots in terms of solution time and accuracy in order to determine the minimum optimal rank as shown in Figure 53. Compared to the 1D case, optimal rank decreased for this material from r = 6 to r = 5. Computational efficiency of the ROM against the full order model show that it is about the same speed as the full order for this highly nonlinear property case.

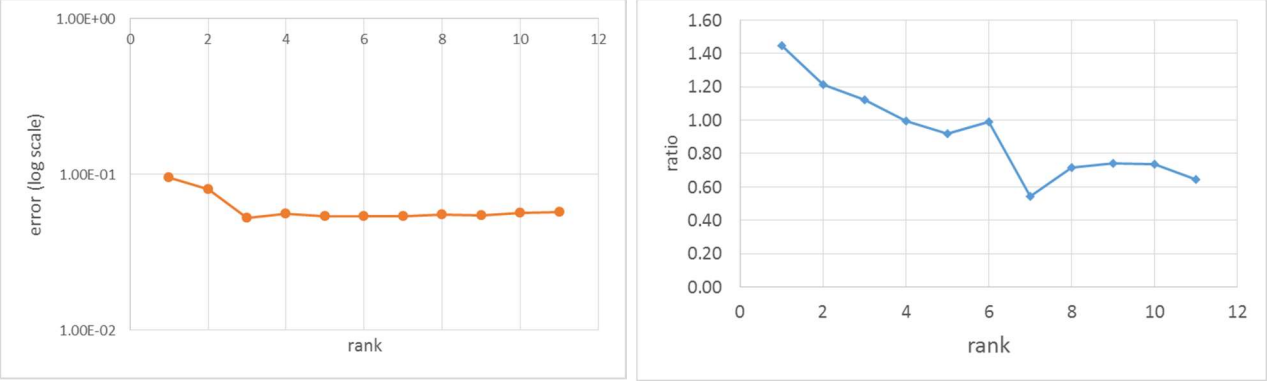

Figure 53. Solution error as a function of rank for Unifrax material (left) and ratio of solution times for the ROM using Unifrax material properties (right).

Using rank r = 5, Figure 54 shows the errors and percent error between the Abaqus results and the ROM plotted across the solution space, arranged by node number. Peak errors correspond to the face parallel to the incident heat flux face, with a maximum temperature delta of 100 K and a maximum 8.1% error across the solution set. Note, the errors peak within the first 100 seconds and then remain constant. While the ROM has some difficulty resolving temperatures at the back face of the cube, at the corners in particular, the Unifrax material is moderately well predicted by this ROM, however the computational speed ups at this mesh density are not realized.

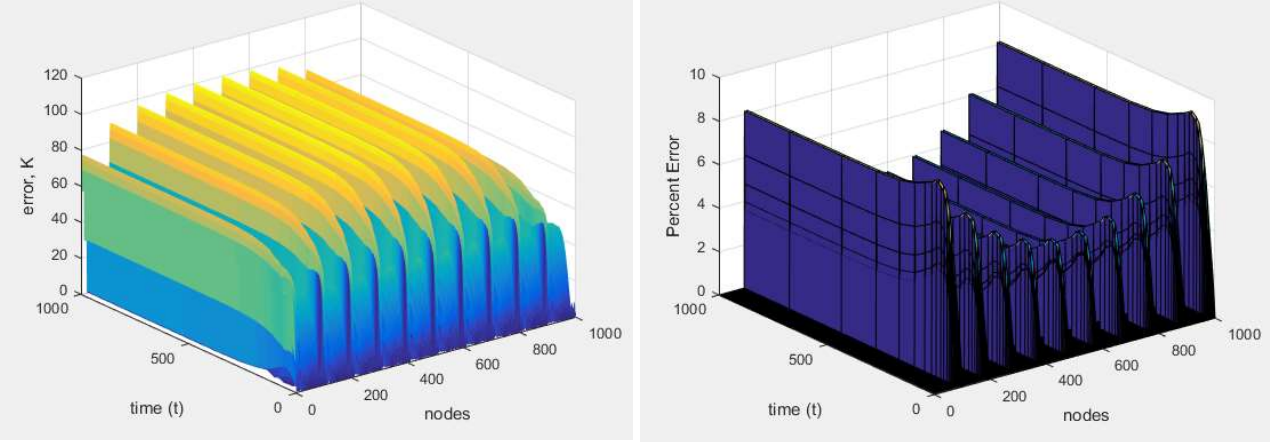

Figure 54. Absolute error (left) and maximum relative error at boundary each node (right) from 3D ROM using Unifrax material properties.

6.4.3 Increased Spatial Discretization

From the results above, good accuracy can be achieved using this ROM approach on temperature dependent nonlinear material properties for the multi-dimensional case. However, the computational speed ups seen in the previously presented 1D cases are not observed. The solvers used in the commercial code are just as efficient as the ROM given this mesh density. An additional study was performed to evaluate the impact of increasing spatial discretization using the temperature independent AA 5083 material properties. The same boundary and initial conditions were applied. Spatial increments of 10, 25, and 50 evenly spaced nodes applied in each direction were investigated while the temporal increment was held constant at 1 second. This resulted in three dimensional mesh densities of 1000, 15625, and 125000 nodes. Full solution snapshot times, POD generation times, ROM solution times, and POD relative error was captured for each increment. Results were plotted as a function of discretized nodes. The ratio of time to produce a full solution versus the time to execute the ROM was plotted against node count. The results provide a sense of scale on how effective a ROM approach might be for other discretized systems with a larger mesh size. Results for the discretization study are presented in Figure 55. The results in Figure 55 (a) demonstrate that the efficiency of the ROM run time increases dramatically with mesh density, while ROM errors remain relatively flat (see Figure 55 (b)).

(a) (b)

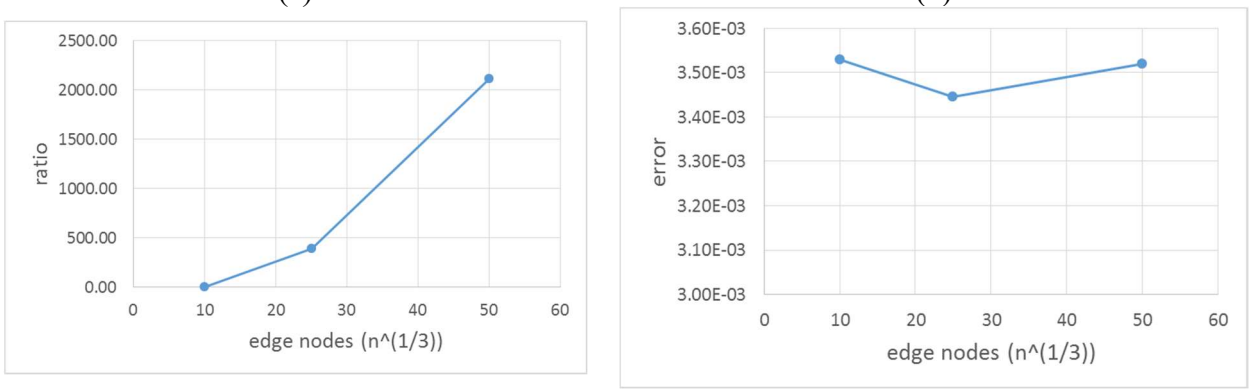

Figure 55. Plots of advanced discretization results for AA 5083 material using the 3D transient ROM (a) ratio of snapshot solution times vs. ROM solution times and (b) Relative Error

6.5 Summary

Multiple dimension heat transfer was added to the 1D ROM. For the constant and lower nonlinear material cases, the eigenvalue distribution with rank was similar to the 1D case at the lower ranks and higher eigenvalues at the upper ranks. For the highly nonlinear material case, the eigenvalue distribution with rank was overall very different from the 1D case. All models used an optimal rank of 4 or 5 despite material property type. These differences between the 1D and 3D eigenvalue distributions for the same material types indicate that complex geometry plays as great or more significant role when using POD to create the ROM. ROMs were able to predict results within 8% and for these simple 3D cubic cases, and computational times were approximately the same as the full order models. However, a study on increased discretization showed that computational efficiency became more significant as mesh density increased, where ROM solution times of 500 and 2000 times faster than the full order model were realized.

7 Conclusions

An approach was developed and demonstrated in this research to treat a variety of nonlinearities within transient heat transfer problems using reduced order modeling (ROM) techniques. A method for determining optimal rank as a function of error was presented and used to determine the optimal ROM size. For speed and accuracy, optimal rank selection is best chosen by looking at how error changes as a function of rank. Previous research has used energy of the eigenvalues as a means to identify optimal rank for use in a ROM, however this research showed that energy content alone is not sufficient to get accurate solutions from the ROM. In order to achieve accurate results combined with computational efficiency, the rank was chosen by evaluating error at several ranks and identifying the rank at which the error stabilizes. Nonlinear material properties were treated directly within the ROM, radiation boundary conditions were linearized in the ROM, and nonlinear source terms were treated by combining DEIM with POD all while increasing computation efficiency. All one-dimensional ROM techniques were then extended to three dimensions for full geometry model approximations. While there is still research to be done, this work has shown that a ROM of heat transfer problems with complex nonlinearities can be used to provide accurate predictions while increasing the computational efficiency by several orders of magnitude.

7.1 Conclusions

A 1D heat transfer problem was initially presented with a variety of nonlinearities. A mathematical model was evolved along with the introduction of several reduced order modeling approaches in order to fully approximate the solution. From this development, several specific advancements were made in reduced order heat transfer modeling.

Nonlinear temperature dependent material properties can be effectively incorporated into a ROM without sacrificing computational efficiency. Previous ROM methods accounted for material properties by using constant time-averaged nodal temperatures. This research showed that the best way to treat nonlinear temperature dependent material properties is by pulling the properties outside of the matrices and associating them with the temperature vector. This resulted in accurate results for highly nonlinear low conductivity material properties over a large temperature range. For this method the material properties were defined using smooth polynomial functions. This allows the temperature dependency to remain in the problem formation so that once the ROM is developed, other input heat flux values could be further investigated. Accuracy will depend on how well the material properties are fitted by a function. However, for well-fitted material property functions, the initial applied heat flux and associated POD became the limiting factor for accuracy instead of the nonlinear temperature dependent material properties.

ROMs are capable of delivering high integrity solutions from the reduced order state, including the estimation of results from an applied heat flux unknown a priori. Previously, ROMs were developed from a unique set of snapshots and had a one-time use. By investigating a variety of input heat flux values, a ROM was identified for use in accurately estimating a wide range of

additional heat flux values unknown a priori. This research showed that a more agile ROM can be developed from a function like the step function defined in this work so that this single ROM can in turn predict a wide range of outputs with a high level of accuracy. This allows for additional computational time savings.

Radiation has typically been ignored in ROM heat transfer problems. In this research, radiation was treated as a linearized term and combined with a collective heat transfer coefficient at the surfaces. As a result, the radiation results did not look very different from the convection cases, likely because it was merged with the convection boundary conditions. The addition of the radiation term typically required an increase of 1 or 2 ranks to achieve accurate results in the ROM, which did not significantly increase computational times.

The computational usefulness of this ROM will depend on the size of the initial system. Low mesh densities in the 1D full order models resulted in moderate computational gains from the ROM (10 – 40 times faster). Moreover, the 3D ROMs were solved in approximately the same times as the full order models. This research showed that real computational gains were made with highly discretized systems where solution times of several thousand orders of magnitude were observed.

7.2 Future Work

Future work includes further development of how the ROM is constructed as well as extending the techniques to other equations. Future research on improving the ROM includes the use of non-smooth material property functions, anisotropic material properties, direct radiation calculation, and nonlinear source term spatial and temporal effects. The ROM techniques could then be applied to other equations that include adding in kinetically driven phenomenon such as phase changes and chemical reactions as well as use in feedback control.

In this research, the ROMs provided the most accurate solutions with properties that can be represented by smooth functions. For example, material properties in the Stainless Steel 302 resulted in a non-smooth functions for thermal diffusivity and volumetric specific heat, and therefore were not as well predicted. Commercial codes typically use a linear interpolation function. For this type of material, properties can be treated as discontinuous functions within the ROM. This is easily done in the MATLAB code. While the increased computational effort might be observed on the full scale model, this will likely result in only a slight rank increase for the ROM.

All properties used in this research were isotropic, but the extension of the ROM into three dimensions permits the investigation of anisotropic material properties. Complex layered materials such as carbon fiber composites typically require a detailed model in order to accurately assess thermal material response. Based on the formulation of the current code, the investigation of composites in a ROM could be easily done.

Domains with radiation boundary conditions and significant temperature changes at the boundaries were predicted within 8% error. The radiation term was linearized, and an average boundary nodal temperature was used in part of the ROM implementation. This likely causes

some loss of accuracy in the more nonlinear material cases. Prediction could be improved if the radiation term was handled directly as a fourth order term in the ROM. Given the nature of the reduced order model, an increase in computational efficiency would still likely be realized.

The source term investigated in this research was temperature dependent only. The source term was applied at all nodes and was effective throughout the entire time domain. Other source terms typically used in heat transfer are localized and may also be a function of time. These spatial and temporal effects need to also be investigated for use in the ROM. The nature of POD is to not distinguish between spatial and temporal domains, therefore similar results would likely be observed.

Additional areas of research would continue to forward the knowledge base for POD-driven ROMs in heat transfer. In this research, an approach was made to incorporate the DEIM algorithm to reduce nonlinear source heating terms. However, source terms can represent kinetically driven phenomenon such as phase changes and chemical reactions. This ROM is ideal for estimating these complex physical processes with both speed and accuracy. The approach provided here provides a basic roadmap for implementation of source terms such as those.

The nature of the ROM as both fast and accurate lends itself to improving the response time and accuracy of control inputs. For this type of research in particular, the model was developed with an independent incident heat flux term that drives temperature response. This work would readily extend to using that heat flux term as the controlling input for achieving a set temperature profile across a domain.

In addition, a robust ROM tuned from snapshots that is both fast and accurate across a wider domain would be particularly suitable for stochastic problems. For these problems, the model is run multiple times and the input variable is subject random variation, resulting in a distribution of outcomes. This work would easily extend to aid that type of problem.

References

[1] Antoulas, A. “Approximation of Large-Scale Dynamical Systems.” SIAM, 2005. Chapters 3, 7, 9, and 12.

[2] Ipsen, I. and Meyer, C. “The Idea Behind Krylov Methods.” American Mathematical Monthly, 1998. V 105, Issue 10, 889-899.

[3] Kosambi, D. D., J. Indian Math. Soc., 1943, 7, 76–88.

[4] Hotelling, H. “Analysis of Complex of Statistical Variables into Principal Components.” J. Educ. Psych., vol. 24, pp. 417–441, 1933.

[5] Karhunen, K. “Ueber lineare Methoden fuer Wahrscheinigkeitsrechnung.“ Ann. Acad. Sci. Fennicae Ser. A1 Math. Phys., vol. 37, pp. 3–79, 1946.

[6] Loeve, M.M. “Probability Theory.” Van Nostrand, Princeton, NJ, 1955

[7] Kirby, M. and Sirovich, L. “Application of Karhunen-Loeve Procedure for Characterization of Human Faces.” IEEE Trans. Pattern Anal. Machine Intell., vol. 12, no. 1, pp. 103–108, 1990.

[8] Atwell, J. A. and King, B.B. “Proper Orthogonal Decomposition for Reduced Basis Feedback Controllers for Parabolic Equations.” Math. Comput. Modell., vol. 33, pp. 1–19, 2001.

[9] Ball, K.S., Sirovich, L., and Keefe, L.R. “Dynamical Eigenfunction Decomposition of Turbulent Channel Flow.” Int. J. Numer. Meth. Fluids, vol. 12, pp. 585–604, 1991.

[10] Algazi, V.R., Brown, K.L., and Reddy, M.J. “Transform Representation of the Spectra of Acoustic Speech Segments with Applications, Part I: General Approach and Application to Speech Recognition”, IEEE Trans. Speech Audio Process., vol. 1, pp. 180–195, 1993.

[11] Zahorian, S.A. and Rothenberg, M. “Principal Component Analysis for Low-Redundancy Encoding of Speech Spectra.” J. Acoust. Soc. Am., vol. 69, pp. 519–524, 1981.

[12] Nenadic, Z., Gosh, B.K., and Ulinski, P.S. “Modelling and Estimation Problems in the Turtle Visual Cortex.” IEEE Trans. Biomed. Eng., vol. 49, no. 8, pp. 753–762, 2002.

[13] Białecki, R.B., Kassab, A.J., and Ostrowski, Z. “Application of the Proper Orthogonal Decomposition in Steady State Inverse Problems.” in M. Tanaka and G. S. Dulikravich (eds.), Proc. Int. Symp. on Inverse Problems in Engineering Mechanics, Nagano City, Japan, 3–12, Elsevier, Amsterdam, Boston, 2003.

[14] Gugercin, A. and Antoulas, A. “A comparative study of 7 algorithms for model reduction.” Proceedings of the 39th IEEE Conference on Decision and Control, 2000. Vol 3, 2367-2372.

[15] Blinov, D.G., Prokopov, V.G., Sherenkovskii, Yu.V., Fialko, N.M., Yurchuk, V.L. “Effective method for construction of low-dimensional models for heat transfer process.” International Journal of Heat and Mass Transfer, 2004, v 47, issue 26, 5823-5828.

[16] Zhou, X., and Sirovich, L. “Coherence and chaos in a model of turbulent boundary layer.” Phys. Fluids A 4 (1992) 2855– 2869.

[17] Liakopoulos, A., Blythe, P.A., Gunes, H. “A reduced dynamical model of convective flows in tall laterally heated cavities.” P. R. Soc. Lond. A. 453 (1997) 663–672.

[18] Gunes, H. “Low-dimensional modeling of non-isotermal twin-jet flow.” Int. Commun. Heat Mass Transfer 29 (1) (2002) 7786–7797.

[19] Sirovich, L. “Empirical eigenfunctions and low dimensional systems.” in: L. Sirovich (Ed.), New perspectives in turbulence, Springer-Verlag, New York, 1991, p. 139.

[20] Deane, A., Kevrekidis, I., Kardiadakis, G., Orszag, S. “Low-dimensional models for complex geometry flows: application to grooved channels and circular cylinders.” Phys. Fluids A 3 (10) (1991) 2337–2354.

[21] Hekmati, A., Ricot, D., and Druault, P. “Aeroacoustic analysis of the automotive ventilation outlets using Extended Proper Orthogonal Decomposition.” 15th AIAA/CEAS Aeroacoustics Conference (30th AIAA Aeroacoustics Conference) May 2009, Miami Florida.

[22] Yu, D., Chakravorty, S. “A Randomized Proper Orthogonal Decomposition Technique.” 2015 American Control Conference (ACC). Chicago, IL. 1-3 July 2015. Pp 1137-1142.

[23] Vidyasagar, M. “Randomized algorithms for robust controller synthesis using statistical learning theory,” Automatica, vol. 37, pp. 1515–1528, 2001.

[24] Tempo, R. et al., “Probabilistic robustness analysis: Explicit bounds for minimum number of samples,” Systems and Control Letters, vol. 30, pp. 237–242, 1997.

[25] Ray, L. and Stengel, R. “A monte carlo approach to the analysis of control system robustness,” Automatica, vol. 29, pp. 229–236, 1993.

[26] Polyak, B. and Tempo, R. “Probabilistic robust design with linear quadratic regulators,” Systems and Control Letters, vol. 43, pp. 343– 353, 2001.

[27] Calafiore, G. and Campi, M. “The scenario approach to robust control design,” IEEE Transactions on Automatic Control, vol. 51, pp. 742–753, 2006.

[28] Campi, M., Garatti, S. and Prandini, M. “The scenario approach for systems and control design,” Ann. Rev. Control, vol. 33, pp. 149–157, 2009.

[29] Berkooz, G. et al., “The proper orthogonal decomposition in the analysis of turbulent flows,” Ann. Rev. Fl. Mech., vol. 25, pp. 539–575, 1993.

[30] Hall, K.C. et al., “Proper orthogonal decomposition technique for transonic unsteady aerodynamic flows,” AIAA Journal, vol. 38, pp. 1853–1862, 2000.

[31] Sirovich, L. “Turbulence and dynamics of coherent structures. part 1: Coherent structures,” Quarterly of Applied Mathematics, vol. 45, pp. 561–571, 1987.

[32] Yu, D. and Chakravorty, S. “A randomized iterative proper orthogonal decomposition technique with application to filtering of pdes,” Proceedings of American Control Conference, pp. 4363–4368, 2012.

[33] Yu, D. and Chakravorty, S. “An iterative proper orthogonal decomposition (i-pod) technique with application to the filtering of partial differential equations,” Journal of Astronautical Sciences, vol. Special issue on J. N. Juang’s 60th birthday, to appear, 2013.

[34] Lefebvre, G. “A general modal-based numerical simulation of transient heat conduction in a one-dimensional homogeneous slab.” Energy and Buildings. 42 (2010) 2309-2322.

[35] Baur, U. and Benner, P. and Haasdonk, B. and Himpe, C. and Martini, I. and Ohlberger, M. “Comparison of methods for parametric model order reduction of instationary problems.” Max Planck Institute Magdeburg. Feb 2015. 1 – 36.

[36] Haasdonk, B. and Ohlberger, M. “Reduced basis method for finite volume approximations of parametrized linear evolution equations.” ESAIM: Math. Model. Numer. Anal., 42 (2008), pp. 277–302.

[37] Waldherr, S. and Haasdonk, B. “Efficient parametric analysis of the chemical master equation through model order reduction.” BMC Systems Biology, 6 (2012), p. 81.

[38] Haasdonk, B. and Ohlberger, M. “Efficient reduced models and a-posteriori error estimation for parametrized dynamical systems by offline/online decomposition.” Math. Comput. Model. Dyn. Syst., 17 (2011), pp. 145–161.

[39] Eftang, J., Knezevic, D., and Patera, A. “An hp certified reduced basis method for parametrized parabolic partial differential equations.” Math. Comput. Model. Dyn. Syst., 17 (2011), pp. 395–422.

[40] Knezevic, D. and Patera, A. “A certified reduced basis method for the Fokker-Planck equation of dilute polymeric fluids: FENE dumbbells in extensional flow.” SIAM J. Sci. Comput., 32 (2010), pp. 793–817.

[41] Haasdonk, B. “Convergence rates of the POD-Greedy method.” ESAIM: Math. Model. Numer. Anal., 47 (2013), pp. 859-873.

[42] Haasdonk, B., Dihlmann, M., and Ohlberger, M. “A training set and multiple basis generation approach for parametrized model reduction based on adaptive grids in parameter space.” Math. Comput. Model. Dyn. Syst., 17 (2011), pp. 423–442.

[43] Gugercin, S., Antoulas, A., and Beattie, C. “H2 model reduction for large-scale dynamical systems.” SIAM J. Matrix Anal. Appl., 30 (2008), pp. 609–638.

[44] Daniel, L., Siong, O., Chay, L., Lee, K., and White, J. “A multiparameter moment-matching model-reduction approach for generating geometrically parameterized interconnect performance models.” IEEE Trans. Comput.-Aided Design Integr. Circuits Syst., 23 (2004), pp. 678–693.

[45] Weile, D., Michielssen, E., Grimme, E., and Gallivan, K. “A method for generating rational interpolant reduced order models of two-parameter linear systems.” Appl. Math. Lett., 12 (1999), pp. 93–102

[46] Wang, Y., Cao, Z. Weizhong, Z., Guojun, Y. “A comparative study of POD interpolation and POD projection methods for fast and accurate prediction of heat transfer problems.” International Journal of Heat and Mass Transfer, 2012, 55, 17-18, p. 4827-4836.

[47] Wang, Y. “Reconstruction & prediction of wind pressure on heliostat.” Acta Aerodyn. 27 (5) (2009) 586–591.

[48] Fic, A., Białecki, R., and Kassab, A., “Solving Transient Nonlinear Heat Conduction Problems by Proper Orthogonal Decomposition and the Finite-Element Method.” Numerical Heat Transfer, Part B: Fundamentals, 2005. Vol 48, issue 2, 103-124.

[49] Białecki, R., Kassab, A., and Fic, A. “Reduction of the Dimensionality of Transient FEM Solutions Using Proper Orthogonal Decomposition.” Proc. 36th AIAA Thermophysics Conf., Orlando, FL, AIAA Paper, 2003–4207, 2003.

[50] Białecki, R., Kassab, A., and Fic, A., “Proper Orthogonal Decomposition and Modal Analysis for Acceleration of Transient FEM Thermal Analysis.” Int. J. Numer. Meth. Eng., vol. 62, pp. 774–797, 2005.

[51] Sirovich, L. “Turbulence and Dynamics of Coherent Structures, Part I: Coherent Structures.” Q. Appl. Math., vol. XLV, pp. 561–571, 1987.

[52] Liang, Y., Lee, H., Lim, S., Lin, W., Lee, K. and Wu, C. “Proper Orthogonal Decomposition and Its Applications—Part I: Theory.” J. Sound Vibration, vol. 252, no. 3, pp. 527–544, 2002.

[53] Krysl, P., Lall, S. and Marsden, J. “Dimensional Model Reduction in Non-linear Finite Element Dynamics of Solids and Structures.” Int. J. Numer. Meth. Eng., vol. 51, pp. 479–504, 2001.

[54] LeGresley, P.and Alonso, J.J. “Investigation of Non-linear Projection for POD Based Reduced Order Models for Aerodynamics.” AIAA Paper 2001-0926, presented at 39th AIAA Aerospace Science Meeting & Exhibit, Reno, NV, January 8–11, 2001.

[55] Ahlman, D., Soderlund, F., Jackson, J., Kurdila, A., and Shyy, W. “Proper Orthogonal Decomposition for Time-Dependent Lid-Driven Cavity Flows.” Numer. Heat Transfer B, vol. 42, pp. 285–306, 2002.

[56] Guha, P. and Nabi, M. "Model Reduction and Controller Design for a Nonlinear Heat Conduction Problem Using Finite Element Method." International Journal of Automation and Computing. 9 (5) Oct. 2012, p. 474 – 479.

[57] Guha, P. and Nabi, M. "A control law for a nonlinear heat conduction problem on nontrivial domains using FEM." In Proceedings of the 17th Mediterranean Conference on Control and Automation, IEEE, Washington, DC, USA, pp. 320– 323, 2009.

[58] Curtain, R.F. "Model reduction for control design for distributed parameter systems." In Research Directions in Distributed Parameter Systems, SIAM, Philadelphia, PA, pp. 95–121, 2003.

[59] Rudnyi, E., Korvink, J. "Model order reduction for large scale finite element engineering models." In Proceedings of European Conference on Computational Fluid Dynamics, Delft, The Netherlands, 2006.

[60] Chatterjee, A. "An introduction to the proper orthogonal decomposition." Current Science, vol. 78, no. 7, pp. 808–817, 2000.

[61] Rowley, C.W. "Model reduction for fluids, using balanced proper orthogonal decomposition." International Journal of Bifurcation and Chaos, vol. 15, no. 3, pp. 997–1013, 2005.

[62] Singler, J.R. "Approximate low rank solutions of Lyapunov equations via proper orthogonal decomposition." In Proceedings of American Control Conference, IEEE, Seattle, USA, pp. 267–272, 2008.

[63] Ding, P. "Application of the reduced order model in the on-line control of glass thickness and solution of heat transfer inverse problems." Ph.D .Thesis, Xi'an Jiao Tong University, Xi'an, China, 2009.

[64] Ostrowski, Z., Białecki, R., Kassab, A. "Solving inverse heat conduction problems using trained POD-RBF network inverse method." Inverse Problems in Science and Engineering, 2008. Vol 16, issue 1, 39-54.

[65] Bialecki, R.A., Kassab, A.J. and Ostrowski, Z. "Application of the proper orthogonal decomposition in steady state inverse problems." In: M. Tanaka (Ed.) Inverse Problems in Engineering Mechanics IV (Amsterdam: Elsevier BV), 2003. pp. 3–12.

[66] Zhang, X., Xiang, H. "A fast meshless method based on proper orthogonal decomposition for the transient heat conduction problems." International Journal of Heat and Mass Transfer. 84 (2015) pp. 729-739.

[67] Li, S. Liu, W. "Meshfree Particle Methods." Springer, Berlin, 2004.

[68] Belytschko, T., Lu, Y.Y., Gu, L. “Element free Galerkin methods.” Int. J. Numer. Methods Eng. 37 (2) (1994) 229–256.

[69] Vinh, P., Timon, R., Stéphane, B., Marc, D. “Meshless methods: a review and computer implementation aspects.” Math. Comput. Simul. 79 (2008) 763–813.

[70] Atluri, S., Zhu, T. “A new meshless local Petrov–Galerkin (MLPG) approach in computational mechanics.” Comput. Mech. 22 (1998) 117–127.

[71] Liu, G, Gu, Y. “An Introduction to Meshfree Methods and their Programming.” Springer, Netherlands, 2005.

[72] Liu, G. “Mesh Free Methods: Moving Beyond the Finite Element Method.” CRC Press, USA, 2002.

[73] Atluri, S., Shen, S. “The Meshless Local Petrov–Galerkin (MLPG) Method.” Tech Science Press, Encino, 2002.

[74] Barbieri, E., Meo, M. “A fast object-oriented Matlab implementation of the reproducing kernel particle method.” Comput. Mech. 49 (2012) 581–602.

[75] Khosravifard, A., Hematiyan, M., Marin, L. “Nonlinear transient heat conduction analysis of functionally graded materials in the presence of heat sources using an improved meshless radial point interpolation method.” Appl. Math. Modell. 35 (2011) 4157–4174.

[76] Chen, L., and Liew, K. “A local Petrov–Galerkin approach with moving Kriging interpolation for solving transient heat conduction problems.” Comput. Mech. 47 (2011) 455–467.

[78] Holmes, P., Lumley, J., Berkoz, G. “Turbulence, Coherent Structures, Dynamical Systems and Symmetry.” Cambridge Monographs on Mechanics. Cambridge University Press, 1996.

[79] Cusumano, J. P., Sharkady, M. T. and Kimble, B. W., Philos. Trans. R. Soc. London, Ser. A, 1994, 347, 421–438.

[80] Feeny, B. F. and Kappagantu, R., J. Sound Vibr., 1998, 211, 607–616.

[81] Koditschek, D., Schwind, W., Garcia, M. and Full, R., 1999.

[82] Ruotolo, R. and Surace, C., J. Sound Vibr., 1999, 226, 425– 439.

[83] Pinnau, R. “Model Reduction via Proper Orthogonal Decomposition.” Model Order Reduction: Theory, Research Aspects, and Applications, 2008. 95-109.

[84] Modest, M.F.” Radiative Heat Transfer.”.McGraw-Hill, 1993.

[85] Walters, M., Garcia, E., Miller, K., Griffith, T. "Identification of Structural Nonlinear Behavior using Singular Value Decomposition Methods." 50th AIAA/ASME/ASCE/AHS/ASC structures, Structural Dynamics, and Materials Conference. May 2009. Palm Springs Florida.

[86] Allison, T. C., "System Identification via the Proper Orthogonal Decomposition," Ph.D. dissertation, Department of Mechanical Engineering, Virginia Polytechnic Institute, Blacksburg, VA, 2007.

[87] Galbally, D, Fidkowski, K., Willcox, K., and Ghattas, O. "Non-linear model reduction for uncertainty quantification in large-scale inverse problems." Internat. J. Numer. Methods Engrg., 81 (2010), pp. 1581–1608.

[88] Chen, Y. "Model order reduction for nonlinear systems." Master's Thesis, MIT, Cambridge, MA, June 1999.

[89] Rewienski, M, White, J. "A trajectory piecewise-linear approach to model order reduction and fast simulation of nonlinear circuits and micromachined devices." IEEE Transaction on Computer-aided Design of Integrated Circuits and Systems 2003; 22(2):155–170.

[90] Bos, R., Bombois, X., van den Hof, P. "Accelerating large-scale nonlinear models for monitoring and control using spatial and temporal correlations." Proceedings of American Control Conference, Boston, U.S.A., 2004.

[91] Astrid, P., Weiland, S., Willcox, K., Backx, T. "Missing point estimation in models described by proper orthogonal decomposition." IEEE Transactions on Automatic Control 2008; 53(10):2237–2251.

[92] Barrault, M., Maday, Y., Nguyen, N.C., Patera, A.T. "An 'empirical interpolation' method: application to efficient reduced-basis discretization of partial differential equations." Comptes Rendus Math´ematique Acad´emie des Sciences. Paris 2004; I:339–667.

[93] Grepl, M.A., Maday, Y., Nguyen, N.C., Patera, A.T. "Efficient reduced-basis treatment of nonaffine and nonlinear partial differential equations." Mathematical Modelling and Numerical Analysis (M2AN) 2007; 41(3):575–605.

[94] Astrid, P. "Reduction of Process Simulation Models: A Proper Orthogonal Decomposition Approach." Ph.D. thesis, Department of Electrical Engineering, Eindhoven University of Technology, Eindhoven, The Netherlands, 2004.

[95] Chen, Y. "Model Order Reduction for Nonlinear Systems." Master's thesis, Massachusetts Institute of Technology, Cambridge, MA, 1999

[96] Chen, Y. and White, J. "A quadratic method for nonlinear model order reduction.",in Technical Proceedings of the 2000 International Conference on Modeling and Simulation of Microsystems, 2000, pp. 477–480.

[97] Phillips, J.R. “Projection frameworks for model reduction of weakly nonlinear systems.”,in DAC ’00: Proceedings of the 37th Annual Design Automation Conference, ACM, New York, 2000, pp. 184–189.

[98] Bai, Z. “Krylov subspace techniques for reduced-order modeling of large-scale dynamical systems.” Appl. Numer. Math., 43 (2002), pp. 9–44.

[99] Dong, N. and Roychowdhury, J. Piecewise polynomial nonlinear model reduction,in Proceedings of the Design Automation Conference, IEEE Computer Society, Los Alamitos, CA, 2003, pp. 484–489

[100] M. A. Cardoso and L. J. Durlofsky, Linearized reduced-order models for subsurface flow simulation, J. Comput. Phys., 229 (2010), pp. 681–700.

[101] M. J. Rewie´nski, A. “Trajectory Piecewise-Linear Approach to Model Order Reduction of Nonlinear Dynamical Systems.” Ph.D. thesis, Massachusetts Institute of Technology, Cambridge, MA, 2003.

[102] Rewienski, M, and White, J. “Model order reduction for nonlinear dynamical systems based on trajectory piecewise-linear approximations.” Linear Algebra Appl., 415 (2006), pp. 426–454.

[103] Feng, L., Rudnyi, E., and Korvink, J. THERMINIC 2004, 10th International Workshop on THERMAL INVESTIGATIONS of ICs and Systems, 29 September - 1 October 2004, Sophia Antipolis, pp. 281-285.

[104] Barrault, M., Maday, Y, Nguyen, N.C., and Patera, A.T. “An “empirical interpolation” method: Application to efficient reduced-basis discretization of partial differential equations.” C. R. Math. Acad. Sci. Paris, 339 (2004), pp. 667–672.

[105] Grepl, M., Maday, Y, Nguyen, N.C., and Patera, A.T. “Efficient reduced-basis treatment of nonaffine and nonlinear partial differential equations.” M2AN Math. Model. Numer. Anal., 41 (2007), pp. 575–605

[106] Nguyen, N.C., Patera, A.T., and Peraire, J. “A “best points” interpolation method for efficient approximation of parametrized functions.” Internat. J. Numer. Methods Engrg., 73 (2007), pp. 521–543

[107] Nguyen, N.C., Peraire, J. “An efficient reduced-order modeling approach for non-linear parametrized partial differential equations.” Internat. J. Numer. Methods Engrg., 76 (2008), pp. 27-55.

[108] Chaturantabut, S. and Sorensen, D. “Nonlinear Model Reduction via Discrete Empirical Interpolation.” SIAM Journal on Scientific Computing, 2010, Vol 32, Iss 5, 2737-2764.

[109] Verhoeven, A. "Redundancy Reduction of IC Models by Multirate Time-Integration and Model Order Reduction." Ph.D. thesis, Department of Mathematics and Computer Science, Eindhoven University of Technology, Eindhoven, The Netherlands, 2008.

[110] Ly, H. and Tran, H. "Proper Orthogonal Decomposition for Flow Calculation and Optimal Control in a Horizontal CVD Reactor." Quart. J. Appl. Math. Quart. J. Appl. Math. 2002. V 60, Issue Sept, 631-656.

[111] Klimanek, A., Bialecki A., Ostrowski, Z. "CFD two-scale model of a wet natural draft cooling tower." Numerical Heat Transfer, Part A: Applications. 2010 57 2, p. 119-137.

[112] Press, W., Teukolsky, S., Vetterling, W. and Flannery, B. "Numerical Recipes in C." pp. 753–784, Cambridge University Press, New York, 1992.

[113] Ostrowski, Z., Białecki, R., and Kassab, A. "Solving Inverse Heat Conduction Problems using Trained POD-RBF Network Inverse Method." Inverse Problems in Sci. and Eng., vol. 16, no. 1, pp. 39–54, 2008.

[114] Biglari, A., Sutherland, J. "An a-posteriori evaluation of principal component analysis-based models for turbulent combustion simulation." Combustion and Flame 162 (2015) pp. 4025-4035.

[115] Sutherland, J., Parente, A. Proc. Combust. Inst. 32 (1) (2009) 1563–1570.

[116] Parente, A., Sutherland, J., Dally, B., Tognotti, L., Smith, P., Proc. Combust. Inst. 33 (2) (2011) 3333–3341.

[117] Parente, A., Sutherland, J., Tognotti, L., Smith, P. Proc. Combust. Inst. 32 (1) (2009) 1579–1586.

[118] A. Biglari, J.C. Sutherland, Combust. Flame 159 (5) (2012) 1960–1970.

[119] Sutherland, J., Parente, A. 5th US Natl. Combust.Meet. (2009).

[120] Parente, A., Sutherland, J. Combust. Flame 160 (2) (2013) 340–350, doi:10.1016/j.combustflame.2012.09.016.

[121] Chen, H., Reuss, D., and Sick, V. "On the use and interpretation of proper orthogonal decomposition of in-cylinder engine flows." Measurement Science and Technology. 23, 8, 2012. 1-14.

[122] Email from B. Lattimer to J. Free containing experimentally confirmed material properties and references to published values. Oct. 2015.

[123] Incropera, F. and DeWitt, D. "Fundamentals of Heat and Mass Transfer." 5th Ed. Wiley, 2002, Table A.1.

Appendix A

Table of coefficients for AA5083-H116

$x(\mathbf{T}) = a \cdot \mathbf{T}^2 + b \cdot \mathbf{T} + c$

	a	b	c
Thermal conductivity, k(T) [W/m·K]	-	-	117
Specific heat capacity, $c_p(T)$ [J/kg·K]	-	-	900
Density, ρ [kg/m^3]	-	-	2666
Thermal diffusivity, α(T) [m^2/s]	-	-	4.8762e-5
1/Volumetric heat capacity, $\frac{1}{\rho c_p}$(T) [(m^3·K)/J]	-	-	4.1677e-7

Lattimer [122]

Table of coefficients for AA6082-T651

$x(\mathbf{T}) = a \cdot \mathbf{T}^2 + b \cdot \mathbf{T} + c$

	a	b	c
Thermal conductivity, k(T) [W/m·K]	-	7.0e-2	151.79
Specific heat capacity, $c_p(T)$ [J/kg·K]	-	0.41	679.17
Density, ρ [kg/m^3]	-	-	2696
Thermal diffusivity, α(T) [m^2/s]	2.9266e-12	-9.9672e-9	8.2618e-5
1/Volumetric heat capacity, $\frac{1}{\rho c_p}$(T) [(m^3·K)/J]	8.1669e-14	-2.7815e-10	5.3832e-7

Lattimer [122]

Table of coefficients for Stainless Steel 302

$x(\mathbf{T}) = a \cdot \mathbf{T}^2 + b \cdot \mathbf{T} + c$

	a	b	c
Thermal conductivity, k(T)	-3.9267e-6	1.9428e-2	9.8485

[W/m·K]			
Specific heat capacity, $c_p(T)$ [J/kg·K]	-1.8626e-4	4.1751e-1	373.49
Density, ρ [kg/m^3]	-	-	8055
Thermal diffusivity, α(T) [m^2/s]	4.7327e-14	1.7248e-9	3.4268e-6
1/Volumetric heat capacity, $\frac{1}{\rho c_p}$(T) [(m^3·K)/J]	1.0094e-13	-2.0492e-10	3.0962e-7

Incropera [123]

Table of coefficients for MACOR

x (**T**) = a·**T²** + b·**T** + c

	a	b	c
Thermal conductivity, k(T) [W/m·K]	6.0073e-7	-6.7663e-4	1.8086
Specific heat capacity, $c_p(T)$ [J/kg·K]	-8.4507e-4	1.6768	388.65
Density, ρ [kg/m^3]	-	-	2520
Thermal diffusivity, α(T) [m^2/s]	1.0758e-12	-1.6933e-9	1.2144e-6
1/Volumetric heat capacity, $\frac{1}{\rho c_p}$(T) [(m^3·K)/J]	5.1073e-13	-8.6548e-10	6.9796e-7

Lattimer [122]

Table of coefficients for Marinite

x (**T**) = a·**T²** + b·**T** + c

	a	b	c
Thermal conductivity, k(T) [W/m·K]	-	-	0.17
Specific heat capacity, $c_p(T)$ [J/kg·K]	-	0.7566	894.62
Density, ρ [kg/m^3]	-	-	961
Thermal diffusivity, α(T) [m^2/s]	3.0906e-14	-1.1376e-10	1.8865e-7
1/Volumetric heat capacity, $\frac{1}{\rho c_p}$(T) [(m^3·K)/J]	1.8180e-13	-6.6920e-10	1.1097e-6

Lattimer [122]

Table of coefficients for Unifrax

$$x\,(\mathbf{T}) = a\cdot\mathbf{T}^2 + b\cdot\mathbf{T} + c$$

	a	b	c
Thermal conductivity, k(T) [W/m·K]	1.2007e-7	-2.0958e-5	6.0607e-2
Specific heat capacity, $c_p(T)$ [J/kg·K]	-	0.3312	737.82
Density, ρ [kg/m^3]	-	-	272
Thermal diffusivity, α(T) [m^2/s]	2.6233e-13	4.2593e-11	2.4158e-7
1/Volumetric heat capacity, $\frac{1}{\rho c_p}$(T) [(m^3·K)/J]	3.7411e-13	-1.8344e-9	4.8968e-6

Lattimer [122]

Appendix B

trans_diff_prelim.m

diffusion_1D_bd.m

generate_pod.m